

***AN AIR-COUPLED ULTRASONIC
ARRAY SCANNING SYSTEM FOR
RAPID THROUGH TRANSMISSION NDT***

Stephen P. Kelly

***Submitted in May 2000
for the degree of Doctor of Philosophy***

***Centre for Ultrasonic Engineering
Department of Electronic and Electrical Engineering
The University of Strathclyde
204 George Street, Glasgow, G1 1XW
Scotland, UK***

The copyright of this Thesis belongs to the author under the terms of the United Kingdom Copyright as qualified by the University of Strathclyde Regulations 3.49. Due acknowledgement must always be made of the use of any material contained in or derived from this thesis.

LIST OF CONTENTS

<i>Acknowledgements</i>	(x)
<i>Abstract</i>	(xi)
<u>Chapter1 – Introduction</u>	1
<i>1.1 Overview of Thesis</i>	1
<i>1.2 Aims and Contributions of Thesis</i>	5
<i>1.2.1 Aims of Thesis</i>	5
<i>1.2.2 Contributions to the Field of Non Destructive Testing</i>	6
<i>1.2.3 Publications to Date Arising from the Work of this Thesis</i>	7
<i>a) Journal Publications</i>	7
<i>b) Conference Proceedings</i>	7
<u>Chapter 2 - Review of Ultrasonic NDT in the Aerospace Industry</u>	8
<i>2.1 Introduction</i>	9
<i>2.2 NDT Considerations in the Aerospace Industry</i>	10
<i>2.2.1 Materials and Defects</i>	10
<i>2.2.2 Different NDT Requirements</i>	11
<i>a) Introduction</i>	11
<i>b) In-Service Testing</i>	11
<i>c) Production Inspection</i>	12
<i>2.3 Development of Water-Jet Systems</i>	14
<i>2.3.1 Introduction</i>	14
<i>2.3.2 Difficulties and Advantages</i>	14
<i>2.3.3 Design Considerations</i>	15
<i>a) Introduction</i>	15
<i>b) Modelling Approach</i>	16
<i>c) Model Verification</i>	16

2.3.4	<i>Conclusions</i>	17
2.4	<i>State of the Art</i>	17
2.4.1	<i>Introduction</i>	17
2.4.2	<i>Current Capabilities</i>	17
2.5	<i>Conclusions</i>	19
 <u>Chapter 3 - The Scanning System - An Overview of Constraints</u>		20
3.1	<i>Introduction</i>	21
3.2	<i>System Requirements</i>	22
3.3	<i>Problems of Air-Coupling</i>	24
3.3.1	<i>Introduction</i>	24
3.3.2	<i>Specific Acoustic Impedance Mismatches</i>	25
3.3.3	<i>Air Attenuation</i>	29
3.4	<i>Mode of Operation</i>	31
3.5	<i>Propagation Channel Investigation</i>	33
3.5.1	<i>Introduction</i>	33
3.5.2	<i>Transducers/Matching</i>	34
3.5.3	<i>Air-gap Investigation</i>	35
3.5.4	<i>Frequency Content of Multiple Reflections</i>	39
3.5.5	<i>Sample Transit Time</i>	41
3.5.6	<i>Conclusions</i>	44
3.6	<i>Scan Rate Analysis</i>	45
3.6.1	<i>Introduction</i>	45
3.6.2	<i>Original System Design Concept</i>	45
3.6.3	<i>Method of Horizontal Scanning</i>	47
3.6.4	<i>Minimum Practical Transmitter PRT</i>	48
a)	<i>Multiple Reflections</i>	49
b)	<i>Transducer Material Limitations</i>	51
3.6.5	<i>Scan rate Calculations</i>	57
3.6.6	<i>Results of Analysis</i>	60
a)	<i>Pulse Repetition Time</i>	61
b)	<i>Number of Averages</i>	61

c)	<i>Air-gap Sizes</i>	62
d)	<i>Number of Serial Array Elements</i>	63
e)	<i>Parallel Approach</i>	64
3.6.7	<i>Further System Design Considerations</i>	65
3.6.8	<i>Final Proposed Design Concept</i>	67
3.6.9	<i>Conclusions</i>	68
3.7	<i>Conclusions</i>	69

Chapter 4 - Selection of Transducer Technology **70**

4.1	<i>Introduction</i>	71
4.2	<i>1-3 Connectivity Piezocomposite Transducer Technology</i>	72
4.2.1	<i>Introduction</i>	72
4.2.2	<i>Basic Design Theory</i>	74
4.2.3	<i>Volume fraction</i>	76
4.2.4	<i>Constituent Materials</i>	78
a)	<i>Ceramic phase</i>	78
b)	<i>Passive phase</i>	79
4.2.5	<i>Aspect Ratio and Pillar Geometry</i>	81
4.2.6	<i>Backing and Matching Considerations</i>	82
4.2.7	<i>Array Considerations</i>	83
4.2.8	<i>Summary</i>	84
4.3	<i>Electrostatic Transducer Technology</i>	85
4.3.1	<i>Introduction</i>	85
4.3.2	<i>Membrane Considerations</i>	87
4.3.3	<i>Backplate Considerations</i>	88
a)	<i>Random</i>	88
b)	<i>Grooved</i>	89
c)	<i>Micro-machined</i>	92
4.3.4	<i>Bias Voltage Effects</i>	94
4.3.5	<i>Array Considerations</i>	95
4.3.6	<i>Summary</i>	95

4.4	<i>Experimental Evaluation</i>	96
4.4.1	<i>Introduction</i>	96
4.4.2	<i>Transducer Manufacture</i>	97
	a) <i>Composites</i>	97
	b) <i>Electrostatics</i>	98
4.4.3	<i>Experimental Arrangement</i>	100
4.4.4	<i>Wideband Characterisation</i>	103
	a) <i>Transmission Response Using PVDF Membrane Hydrophone</i>	104
	b) <i>Reception Response Using PVDF Transmitter</i>	105
	c) <i>Pulse-Echo Response from a Flat Reflector</i>	106
4.4.5	<i>Narrowband Characterisation</i>	108
4.4.6	<i>Pitch-Catch Insertion Loss</i>	108
4.4.7	<i>Robustness and Environmental Considerations</i>	111
4.4.8	<i>Focusing Performance</i>	112
4.5	<i>Conclusions</i>	117
 <u>Chapter 5 - Development of a Novel Air-Coupled Matching Layer</u>		119
5.1	<i>Introduction</i>	120
5.2	<i>Background</i>	121
	5.2.1 <i>Evaluation of Standard Matching Layer Theory</i>	121
	5.2.2 <i>Review of Air-Coupled Matching Techniques</i>	123
5.3	<i>Introduction to the Proposed New Matching Layer</i>	124
	5.3.1 <i>Basic Novel Matching Layer Concept</i>	124
	5.3.2 <i>Cavity Resonance Hypothesis</i>	125
	5.3.3 <i>Design Requirements</i>	135
5.4	<i>Microscopic Characterisation of the Matching Layers</i>	136
	5.4.1 <i>Introduction</i>	136
	5.4.2 <i>Scanning Electron Microscope (SEM) Analysis</i>	136
	5.4.3 <i>Optical Microscopy Analysis</i>	137
	5.4.4 <i>Summary of Results</i>	139

5.5	<i>Acoustic Characterisation of the Matching Layers</i>	140
5.5.1	<i>The Characterisation Approach</i>	140
a)	<i>Introduction</i>	140
b)	<i>Material Characterisation Using Transmission Coefficient Calculations</i>	140
c)	<i>Biot's Theory</i>	144
5.5.2	<i>Acoustic Characterisation</i>	145
a)	<i>Silicone Rubber</i>	145
b)	<i>Porous Filter</i>	147
c)	<i>Matching Layer</i>	148
5.5.3	<i>Conclusions</i>	151
5.6	<i>Development of the Matching Layer Design Strategy</i>	152
5.6.1	<i>Introduction</i>	152
5.6.2	<i>Transducer Considerations for Model Verification</i>	152
a)	<i>Matching Layers Manufactured</i>	152
b)	<i>Transducers Used in Testing</i>	153
c)	<i>Influence of Perspex Lenses on Design</i>	154
d)	<i>Design of the Perspex Lenses</i>	156
5.6.3	<i>Transmission Response</i>	157
a)	<i>Modelled Variation of the Thickness of the SR Layer</i>	157
b)	<i>Theoretical and Experimental Frequency Responses</i>	159
c)	<i>Experimental Narrowband Behaviour</i>	161
5.6.4	<i>Reception Responses</i>	163
a)	<i>Modelled Variation of the Thickness of the SR layer</i>	163
b)	<i>Theoretical and Experimental Frequency Responses</i>	164
c)	<i>Experimental Narrowband Behaviour</i>	165
5.6.5	<i>Electrical Impedance Profiles</i>	166
5.6.6	<i>Pitch-Catch Performance Investigation</i>	169
5.6.7	<i>Design Graphs and Guidelines</i>	169
a)	<i>Introduction</i>	169
b)	<i>Transmitter Design Guidelines</i>	170
c)	<i>Receiver Design Guidelines</i>	174

d)	<i>Pitch-Catch Design Example</i>	178
5.6.8	<i>Summary</i>	179
5.7	<i>Conclusions</i>	179
<u>Chapter 6 - Results and Evaluation of Prototype Systems</u>		180
6.1	<i>Introduction</i>	181
6.2	<i>Prototype Transducers</i>	181
6.3	<i>The Electronic Receive System</i>	184
a)	<i>The Pre-Amplifiers</i>	184
b)	<i>The Analogue Processing Unit</i>	185
c)	<i>Parallel Data Acquisition</i>	185
6.4	<i>Laboratory Testing</i>	186
6.4.1	<i>Initial Testing</i>	186
6.4.2	<i>Test and Scan Capability</i>	187
6.4.3	<i>Test Samples</i>	189
6.4.4	<i>Scan Results</i>	190
a)	<i>Comparison with Water-Coupled Inspection</i>	191
b)	<i>Investigation of Capabilities and Limitations</i>	195
c)	<i>Honeycomb Inspection</i>	198
d)	<i>Lamb Wave Scanning</i>	201
6.5	<i>Industrial Scanning</i>	204
6.5.1	<i>Introduction</i>	204
6.5.2	<i>Industrial Scanning Results</i>	205
6.5	<i>Conclusions</i>	207
<u>Chapter 7 Conclusions and Suggestions for Further Work</u>		208
7.1	<i>Conclusions</i>	208
7.1.1	<i>General Overview</i>	208
7.1.2	<i>The Scanning System</i>	209
7.1.3	<i>Selection of Transducers</i>	209
7.1.4	<i>The Matching Layer</i>	209

7.1.5	<i>The Results</i>	210
7.2	<i>Suggestions for Further Work</i>	212
7.2.1	<i>Potential Future Developments</i>	212
7.2.2	<i>Further Matching Layer Investigations</i>	213
	References	215
	Appendix A - Matching Layer Materials and Manufacturing Method	

ACKNOWLEDGEMENTS

Firstly, I would like to express my thanks to my supervisor Professor Gordon Hayward for giving the assistance, encouragement and time that were gratefully received during the completion of this Thesis. The fact that he gave me the chance to do this work in the first place is also greatly appreciated.

There are several other people that I would also like to thank for their generous assistance throughout the course of my work. Tony Gachagan: for laying a solid foundation in the design of the piezocomposite transducers for operation in air, and for assistance with the transducer comparison work. Roger Farlow: for not only developing the reception electronics but also for providing a commendable product support service in times of difficulty and earth loop hunting. Tomas Gomez: for his unquestionable expertise with all things relating to porous materials and Biot's Theory, and for guiding the way in the matching layer model development. Walter Galbraith: for hydrophone assistance and help in the BAe. industrial Labs. Graham Benny: for assistance with the calibration scanner. John Smith and Kevin Taylor from BAe. are also due special thanks for their support throughout this work, for providing me with samples and data, and for assistance with the integration of the air-coupled system with the commercial scanner.

Technical assistance has been an important part of this work and a big thanks must go to all those involved. Tommy McCunnie and George Brown manufactured many transducers that were required, and Alex Ward produced many other mechanical parts that were necessary. Thanks also to David Skillen for production of all the reception electronics and expert soldering in the connection to the arrays.

In the time that I have been involved with the group at Strathclyde I have encountered many changes of personnel and I would now like to thank them all for their friendship, chat and for making the Tea Room the special (and sometimes strange) place that it is.

I would like thank my mum and dad for all the assistance and enduring support they have given me throughout my life. I would finally like to extend a special thank you to my wife, Lynne, for her help, encouragement and patience throughout the work of this Thesis. I could not have completed it without her (literally).

ABSTRACT

Within the aerospace industry there is an increasing requirement to investigate the structural integrity of the new composite materials that are now being used frequently in the manufacture of aircraft. The complexity of the material manufacture necessitates that evaluation is required prior to final production and it is the development of a novel approach to this testing that constitutes the focus for the work of this Thesis. Existing techniques frequently utilise ultrasonic signals to interrogate the sample under investigation, however, these are cumbersome and scan speed is invariably slow when testing of large samples is considered. This is because large samples are normally tested using a through transmission approach, where narrow jets of water are used to couple the ultrasonic signal through the propagation channel. The fundamental basis of the proposed approach is the removal of the water couplant, enabling a receiver array to be employed, and thus scan large areas more quickly. Flexibility would also be increased with this technique due to a capability to scan moisture sensitive parts.

In order to achieve this, however, the considerable problem of the acoustic impedance mismatch at each solid/air boundary would have to be overcome. Firstly, a narrowband, relatively low frequency approach is selected. It is concluded however, that in order to maximise the scan speed benefit, parallel data acquisition from the receiver array elements must be achieved and no signal averaging must be performed. A small array element pitch and focussing are deemed necessary in the pursuit of adequate defect detection resolution. It is important to select the most appropriate transducer technology for coupling in air and a comprehensive comparison of two relevant technologies (piezocomposite and electrostatic) is carried out. Piezocomposites are found to be superior in terms of sensitivity, robustness and focusing capability. A novel acoustic matching layer is developed to improve coupling from the transducers to the air load. This is investigated microscopically and acoustically and a linear model is developed to enable the design for the most successful operation. Prototype air-coupled systems are produced and scan results compared favourably with the results using water-coupled techniques.

CHAPTER 1

INTRODUCTION

1.1 Overview of Thesis

Chapter 2: Review of Ultrasonic NDT in the Aerospace Industry

This Chapter is included to give an appreciation of the different types of testing that are employed within the aerospace industry. In particular, the water-jet technology that is currently used for the scanning of large aircraft sections to perform pre-production investigation is considered. The proposed air-coupled system that will be developed throughout this Thesis is intended to provide an alternative to these systems. Comparison between the two technologies will therefore be required to judge the success of the new air-coupled system. The potential advantages and disadvantages of the water-jet and air-coupled systems will be presented in this Chapter and the current state of the art in each case will be discussed.

Chapter 3: The Scanning System – An Overview of Constraints

The main design concepts for the new air-coupled scanner are introduced and explained in this Chapter. It is concluded that in order to meet the requirements within the aerospace industry there are a number constraints that must be considered in the system development. The proposed concept for the air-coupled scanning array system is presented. A model to investigate the scan rates as key system parameters are varied is used as an aid to the design process. It is concluded that one efficient system could consist of a single large transmitter and a thirty two-element receiver

array, with a combination of parallel and serial data acquisition being used to acquire data. This decision is shown to be influenced by the fact that the transmitter excitation repetition rate is limited to around 1kHz due to material limitations and the potential for interference from signals reverberating in the air gaps. A linear systems model is used to investigate the signal reverberations within the air propagation channel and close correlation between theory and experiment is demonstrated. It is also noted that signal averaging cannot be performed and it is concluded that focussing of both the transmitter and the receiver is required in order to meet the resolution requirements. A narrowband approach at 600kHz centre frequency is proposed, with bandpass filtering and envelop detection being performed in reception to improve signal to noise ratio and to simplify data acquisition.

Chapter 4: Selection of Transducer Technology

There are two transducer technologies that are known to possess the most potential for development of an air-coupled NDT application: piezoelectric composite transducers (also known as piezocomposite transducers for convenience) and electrostatic transducers. This Chapter considers these technologies in detail, both theoretically and experimentally, in order to make the most appropriate choice for the air-coupled scanner development. A comprehensive literature review of the two approaches is presented in order to consider important aspects of design and manufacture as well as the advantages and disadvantages that have been reported in each case. A wide range of transducers of each type for transmission and reception were manufactured and used to perform characterisation in both narrowband and wideband operation. Wideband responses are measured using calibrated piezopolymer transducers that are designed to operate in both transmission and reception modes. Two way pitch-catch insertion losses are measured in order to provide further comparison and the composite transducers are found to be significantly superior in terms of sensitivity for both transmission and reception. The important capability to perform focussing to improve resolution is investigated by manufacturing a focussed probe of each type and performing a beam profile analysis in each case. The composite technology is again found to be superior and also the robustness of the electrostatics is believed to be questionable. Finally, the difficulty

of realising an array structure at the desired operational frequency is also noted from relevant literature to be more problematic with the electrostatic technology. Selection of the composite technology over the electrostatics for the continuation of the Thesis is considered to be the obvious choice.

Chapter 5: Development of a Novel Air-Coupled Matching Layer

It was accepted that in order to complete the development of the air-coupled scanner successfully, it would be necessary to develop an efficient matching layer to improve the energy coupling between the transducers and the air load. This Chapter explains the difficulties of this design problem and presents the novel matching layer concept that is developed as a solution. The constituent materials include microporous membrane filters (in contact with the air load) and silicone rubber (in contact with the transducers). The filter has very low specific acoustic impedance due to the large percentage of air within them and so coupling to air is potentially very good. The silicone rubber provides a method of attaching the filter to the transducers and is also critical in achieving designs for efficient performance at a specific frequency. This is done by selecting the total matching layer thickness, by controlling the thickness at which the silicone rubber cures. In order fully understand and achieve a design capability for this matching layer technology, a detailed program of characterisation is carried out. Firstly, the microscopic characteristics of a cross section of a matching layer are studied with both optical and scanning electron microscopes. The acoustic properties are then determined by studying the wideband transmission coefficients through the constituent materials alone and then through a matching layer, once the silicone rubber and the filter are combined. This material information leads to the development of a four layer linear model for the matching layer that is combined with the linear systems model to provide a valuable tool in the development of a design strategy. The model is validated by the very close correlation between theoretical and the demonstrated experimental performance. The matching layer designs achieved using this model for the transmitter and the receiver array operating at 600kHz are then presented. A through transmission improvement of 30dB is shown to be provided with the attachment of the matching layers. Finally, design

guidelines and 'lookup' graphs and tables are given to assist in the design of these matching layers for different frequencies in other potential air-coupled applications.

Chapter 6: Evaluation of Prototype Systems

Once development of the prototype systems was completed, a number of scans were performed in order to evaluate the success and the potential of the air-coupled technology. This Chapter presents the results of this evaluation. In a number of cases these results were compared directly with water-coupled scans of the same samples. The results of these comparisons were very encouraging since the resolution and defect detection capabilities were shown to be more than adequate. An eight-channel prototype system was also integrated with an industrial scanner in a British Aerospace (BAe.) test facility. Rapid scanning was achieved here with adequate resolution. A potential scanning technique by converting between through transmitted longitudinal signals and Lamb wave signals is also discussed.

Chapter 7: Conclusions and Suggestions for Further Work

The conclusions reached for each Chapter within the Thesis are briefly reviewed in this Chapter and synopses of the major results of the work will be given. Although every attempt has been made to cover the aspects of the work presented in this Thesis as fully as possible, there are certain cases where further work would be of benefit. Suggestions of where this work could be most usefully directed are made within this Chapter.

1.2 Aims and Contributions of this Thesis

1.2.1 *Aims of This Thesis*

The aims of this Thesis were:

- To develop an air-coupled through transmission scanning system for operation in an industrial aerospace environment as a potential alternative to existing technologies and provide improvements in terms scan speeds and flexibility.
- To determine the most suitable transducer technology for this test application and then optimise performance in terms of sensitivity, resolution and defect detection capability.
- To devise the most appropriate scanning procedure in order to optimise the benefit of the new technique while still satisfying the constraints of the industrial environment and enabling simple implementation on existing scanning equipment.
- To produce prototype scanning systems with the new air-coupled approach and test performance on industrial samples compared with the performance of the existing technology.

1.2.2 Contributions to the Field of Non-Destructive Testing

- Successfully developed an air-coupled scanning system with adequate resolution and sensitivity for many realistic applications in the aerospace industry. This system was compared with the water-coupled systems that are currently in use at a British Aerospace (BAe) test facility and demonstrated adequate resolution. Initial testing of the system on the industrial scanner at BAe in Preston has been completed successfully. Substantial improvement in the test scan rate was achieved by adopting an eight-element receiver array approach that covers a larger area of the test specimen with each scan. In order to achieve this, the data was acquired in parallel from the eight elements of the array and no signal averaging was performed.
- Developed a novel air-coupled matching layer to improve the coupling of energy to and from the transducers in reception and transmission respectively at specific narrowband frequencies of operation. A linear mathematical model for the technology was produced and close correlation between theoretical and experimental operation is demonstrated. This model was used to design the matching layers for the new air-coupled scanner prototype transducers and to provide 'lookup' graphs and tables to enable definitive designs for a range of applications to be found. This technology currently has a patent application pending.
- The two main contenders for air-coupled applications were compared experimentally, based on a novel two-way insertion loss measurement. These two technologies were 1-3 connectivity piezocomposite transducers and electrostatic transducers. The composites were found to be superior in terms of sensitivity, thus providing increased through transmission potential. Improved robustness to avoid damage, and ease of focussing to improve resolution were also important factors.

1.2.3 Publications to Date Arising From the Work of this Thesis

a) Journal Publications

Kelly SP, Farlow R and Hayward G, 'Applications of through-air ultrasound for rapid NDE scanning in the aerospace industry', IEEE Transactions on Ultrasonics Ferroelectrics and Frequency Control, 1996, Vol 43(4), pp581-591.

Gachagan A, Hayward G, Kelly SP, Galbraith W, 'Characterisation of air-coupled transducers', IEEE Transactions on Ultrasonics Ferroelectrics and Frequency Control, 1996, Vol 43 (4), pp678-689.

Whitley S, Girma D, Hayward G, Kelly S, Smith G, 'Non-contact ultrasound and wireless telemetry – a step forward in remote NDT', Insite, Vol42, No 1, Jan 2000

b) Conference Proceedings

Farlow R, Kelly SP and Hayward G, 'Advances in air-coupled NDE for rapid scanning applications', Proceedings of IEEE Symposium, Cannes, 1994.

Kelly SP and Hayward G, 'Real time through transmission inspection of aircraft composites using air-coupled composite arrays', Proceedings of IEEE Symposium Seattle, 1995

CHAPTER 2

REVIEW OF ULTRASONIC NDT IN THE AEROSPACE INDUSTRY

Abstract

This Chapter presents and discusses existing technologies used within the aerospace industry to achieve non-destructive testing of aircraft components. Primarily, this discussion considers an ultrasonic system where ultrasound is coupled between transducer and test specimen using jets of water. This is the main production test technique that is used to investigate the integrity of large carbon fibre and honeycomb sections after manufacture prior to attachment to the aircraft. The development and design of this technology is explained and the advantages of this technique over other methods highlighted. The current state of the art is presented with an analysis of currently available product data and the limitations are explained to provide evidence of the requirement for an improved system. It is proposed that such an improvement could be realised by developing an ultrasonic air-coupled array system.

2.1 Introduction

The introduction of carbon fibre reinforced polymer (CFRP) composite materials began in the manufacture of aircraft more than twenty years ago. Since then, efforts have been ongoing to develop the most suitable and flexible technology to perform non-destructive testing of the material both during pre-production and subsequently during in-service testing. Non-destructive testing (NDT) is the process of investigating the structural integrity of a material using an inspection technique that does not interfere with the structure itself. The objective is to detect irregularities within the material that would be detrimental to safety and/or performance of the aircraft.

Although the CFRP material is extremely strong and lightweight, and so ideally suited for manufacture of aircraft, the use is at the expense of additional test requirements. The materials have posed new challenges due to the nature of the constituent materials and the resulting potential defects that necessitate rigorous inspection after material manufacture prior to attachment to the aircraft. Also, periodic in-service testing is required due to the possible introduction of serious defects that would go unnoticed otherwise, since visual inspection can rarely reveal the extent of any damage.

There are many technologies that are used within the aerospace industry in order to fulfil all test requirements, including shearography [1], eddy current [2] and laser/ultrasound [3]. The most widely used technology however is ultrasound [4, 5]. Ultrasound is used in different ways to deal with particular testing requirements, and the technique used depends on the component to be tested. Factors such as size, geometry, material, and the safety importance of the component can all influence the method of testing selected. Ultimately, however, the objective of the NDT engineer must be to investigate all components as quickly and cheaply as possible without compromising safety and meeting all defect detection criteria.

2.2 NDT Considerations in the Aerospace Industry

2.2.1 Materials and Defects

There are two different methods of utilising the CFRP material. The choice of method used depends on the particular component, the requirement for weight savings and achieving the required strength in load bearing areas. Firstly, there is the use of solid monolithic plates of CFRP. These are made with thin layers of carbon fibre that are initially laid at varying angles of orientation in order to provide strength in the required directions. The thickness and number of layers (or plies) is altered according to the requirement for strength and this can vary from one or two millimetres up to several centimetres. Between these layers there are layers of uncured epoxy and the shape of the required part is determined using a mechanical tool that provides a mould. Curing is then achieved in an autoclave where pressure and temperature are set to the required levels.

The other method of using CFRP is to make honeycomb structures. In this case, solid carbon fibre plates (manufactured as before) are placed at the front and rear of the part and in-between these there is a honeycomb made from some lightweight material. Typically, the honeycomb is made from a paper like material that is saturated with epoxy to improve strength (Nomex), or Aluminium, and the resulting structure is very strong and very light. The sandwich of the three layers of this structure is bonded using epoxy at the front and rear attachment of the CFRP plates.

In addition to the strength and weight improvements, another advantage of either of these methods of material manufacture is the freedom of component design in the development of the aircraft since very complex structures can be produced. It is also convenient that the material and the part are made simultaneously.

There is, however, a major drawback in that the complexity of the manufacturing process necessitates detailed inspection of every part before incorporation within the aircraft. There are several defects that may be introduced during manufacture that could pose a significant safety hazard. For example, *porosity* can result from insufficient polymer at any point within the solid carbon fibre and would

compromise the inter laminar shear strength. *Delamination* is a fabric discontinuity, or the separation between two or more adjacent plies of the layup. This can be mechanically induced by an impact or distorting or can be due to insufficient epoxy in bonding a honeycomb structure. The presence of some foreign body (such as the polythene that the individual layers of carbon fibre are packet in) must also be detected and this is referred to as an *inclusion*. The acceptable size of any defect is specific to each test object.

2.2.2 Different NDT Requirements

a) Introduction

Two distinct NDT requirements exist in the aerospace industry to deal with both pre-production and in-service testing. Although the technologies used in both cases are similar, there are obvious requirements for different approaches due to changes in accessibility of the components.

b) In-Service Inspection

In-service testing generally provides access to only one side of the test material. In general, there is a requirement for manual testing and automation is very difficult. There is therefore a need for the instrumentation to be as compact and lightweight as possible. Pulse-echo (PE) techniques are normally used where an ultrasonic signal is transmitted into the material under test and the echo from within the material is received with the same probe. Analysis of the properties of the signal in terms of amplitude, frequency content and time of flight can enable characterisation of the internal structure of the material and so determine structural integrity. An array of elements can be used to increase scan area coverage and so increase scan speed.

The ultrasound is coupled between the ultrasonic probe and the test specimen either with direct contact using a coupling gel or by using a constant flow of water. The presence of air in the propagation channel between the transducer and the test sample is a major consideration of this Thesis and will be considered in detail in subsequent Chapters. For the moment, however, it is sufficient to note that the high acoustic impedance mismatch between solid and air means that the presence of any air would

significantly compromise test results when using conventional ultrasonic techniques and therefore must be avoided.

c) Production Inspection

The other NDT requirement is that of pre-production testing of components before attachment to the aircraft structure. This is the test problem that is considered throughout the remainder of this Thesis, where an alternative to existing technology is proposed. In this case, access to both sides of the test sample is provided and automated rapid scanning is a realistic proposition. Automated ultrasonic pre-production testing can be separated into two common techniques and the selection of which one depends largely on the type of sample to be tested. The first technique to be developed involves the complete immersion of both the transducers and the test specimen. This was first used in the early 1940s but in the 1980s the use of immersion tanks increased substantially with the development of rapid automated scanning systems [6]. This sometimes involves PE testing where a reflecting glass plate is used behind the sample under test [7]. Using this PE technique is desirable where characterisation of any defects is required, since depth information is included due to the time of flight details of any reflections.

Another, less informative technique is the through transmission (TT) technique where the transmitter and a receiver are placed on opposite sides of the test object in a water tank. In this case, received signal amplitude is the main source of information and so only an indication of the presence of a defect is provided. The presence of a defect is usually indicated by a reduction in signal amplitude. This is normally due to the presence of pockets of air, which either disperse or reflect the signal.

In either the PE or the TT technique, however, there are obvious restrictions to the use of the complete immersion methods. First of all, some of the samples that require to be tested cannot easily be immersed as they are lighter than water and consequently would require measures to prevent floating. An example of this is the honeycomb structures that contain large amounts of air. In this case the materials used to form the honeycomb are also often porous and elaborate measures would be

required to avoid water ingress as this would result in structural damage in addition to compromising test results. Finally, many of the test objects are too large for convenient immersion, such as the skin of an aircraft wing.

At present, the most widely used and successful method of overcoming the difficulties in ensuring adequate coupling is the use of a through transmission water-jet technique as demonstrated in Figure 2.1.

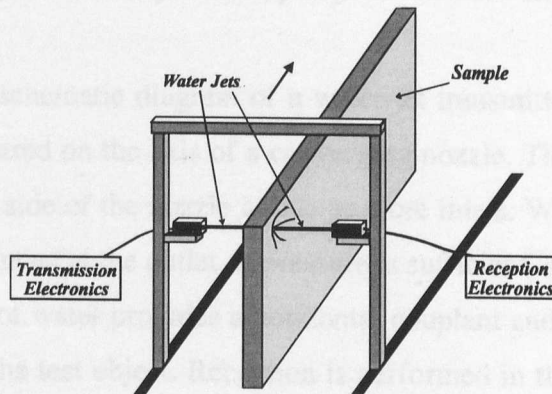


Figure 2.1 Typical water-jet scanner configuration with dimensions 12m horizontally by 9m in height and a water-jet diameter of 5mm.

Figure 2.1 details the basic structure of a water-jet system which scans the transmitting and receiving devices over the surface of the sample in through transmission mode, following a raster pattern with the primary scanning performed along the horizontal axis. Columns of water are used on the transmission and reception sides that act both as waveguides and as impedance adapters. Although far from perfect and still requiring care to be taken in many cases to avoid water ingress, this is currently the most widely used technique in the aerospace industry in the testing of large specimens. Consideration of the development and design of this technology is given in the next Section. It is this technology that is used as the benchmark for measuring the potential improvements by adopting an air-coupled approach.

2.3 Development of Water-Jet Systems

2.3.1 Introduction

The water-jet (squirter, or local immersion) technique was first developed in 1976 in light of the increasing test requirements with the introduction of the CFRP materials, and the practical limitations of the previously well established immersion techniques. Although the introduction of CFRP materials to the manufacture of aircraft has been slow, attempts to improve water-jet test capabilities has been an ongoing process.

Figure 2.2 shows a schematic diagram of a water-jet transmitter probe. In this case the transducer is centred on the axis of a converging nozzle. The water is introduced at pressure from the side of the nozzle at one or more inlets. When the cavity is full, a jet of water is produced at the outlet. If pressure is sufficient, and the distance is not too great, a column of water provides a horizontal couplant and wave guide between the transmitter and the test object. Reception is performed in the same way with the water providing a path between the other side of the test object and the receiver.

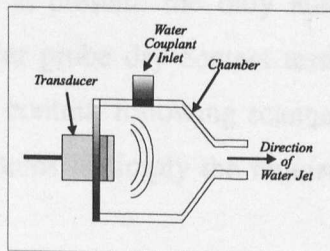


Figure 2.2 Schematic diagram of a water-jet transmitter probe.

2.3.2 Advantages and Difficulties

Water-jet systems have the advantage that they can inspect samples that cannot be immersed due to either a floatation capability or potential damage to the sample caused by water ingress. It is also more convenient for scanning of very large samples or samples that are irregular or curved in shape.

It must be accepted, however, that the water-jet technique has a number of drawbacks. Firstly, the accuracy and repeatability of the full immersion system cannot be matched due to the unavoidable turbulence within the water path. Excessive turbulence and splash back at the point of contact also makes it very

difficult to adopt the PE technique. The water-jet systems are also very slow due to the very small area coverage. This may be appreciated when it is noted that the area that may require to be scanned can be up to 12m by 9m, while the size of the water-jet diameter is around 5mm and a scanner vertical step size of 0.5mm is often employed. Even when a typical scanner travels at full speed of 0.5ms^{-1} , it is clear that the time to perform a scan can be considerable, and times of 24 hours are not uncommon. It has been noted that simultaneous use of up to four pairs of transducers has been achieved [8] but this has great difficulties, both in terms of set-up times and the avoidance of interference from water splash-back. Attempts have been made to produce uniform water curtains [7] to enable this to be simplified and an array of elements to be used. This, however, has yet to be developed into a commercial product. Scan set-up times are generally large due to the requirement for protection of honeycomb or other porous materials from any contact with the water. This is often the case because many test samples include both solid carbon fibre and honeycomb sections. Also, there are some samples that cannot tolerate any contact with water and, at present, the only automated alternative is the very slow and cumbersome roller probe dry contact testing. This method also requires expensive and complicated contour following scanner capabilities. One final inconvenience of the water-jet systems is simply the requirement for irrigation of the water used for the jets.

2.3.3 Design Considerations

a) Introduction

Although development of water-jet systems has been ongoing since the technology was first introduced, there have been few publications of the research findings. This may be due to the highly competitive nature of the aerospace industry and the desire always to preserve any technical advantage. Some available relevant material was found however and the references are provided in [8-12].

The major difficulty facing the designers of a water-jet system is to achieve laminar flow of water in the jet, and thus eliminate the disturbing effects of turbulence or air

bubbles. Careful design, using hydrodynamic considerations, has been performed to achieve this. The key design parameters considered are as follows :-

- The converging nozzle shape, material acoustic impedance and outlet diameter.
- The number of fluid inlets and their positions and angles.
- The size, frequency and angle of the probes.
- Focusing of the probes.
- The water pressure, temperature and filtering.

b) Modelling Approach

In order to study the variation of many of these parameters it has been shown to be valuable to develop a mathematical model based on a two dimensional geometrical approximation. The works presented by Tretout and Violette et al [8-10] were motivated by a lack of commercially available and optimised water-jet systems. The objective of the work was to develop a computer code to determine the optimal water squirter system that could be adapted to given transducers. The modelling approach was based on a ray tracing technique and was achieved in three stages. First of all the beam profile of the transducer was computed with the transducer represented by a line source. Then the ray tracing principle was used to take account of the multiple reflections caused by the presence of the walls of the nozzle. Finally, the acoustic properties of the nozzle walls, and their influence on energy transmitted along each ray, were taken into consideration.

c) Model Verification

In order to verify this model and to provide additional information about the acoustic field due to the nozzle, two different visualisation techniques have been employed. First, the field within the nozzle was visualised by means of the Schlieren optical method, which uses the diffraction of light by density gradients induced by the propagation of the acoustic waves. This however requires that the nozzle is fully immersed and the walls of the nozzle are two dimensional to enable visualisation. A photograph of the ultrasonic field obtained using this method is provided where the

interference fringes are clearly visible. Reasonable correlation with the modelled field was shown.

The acoustic field in the water-jet cannot be investigated in the same way due to the requirement for complete immersion. In order to investigate this, a scanned miniature hydrophone was used. The dimension of the active area of the hydrophone used was 0.2mm in diameter. This was used to provide a scan of the beam profile of the field in a 5mm diameter water-jet. The calculated variations of the field on the axis of the water-jet were shown to be very accurate.

d) Conclusions

Although correlation between theory and experiment have been shown to be reasonable, there is an absence in this literature of any statement of definitive design rules arising from the reported works. It should be emphasised however that the literature considered here is 10-15 years old. When the state of the art of the water-jet systems that are currently available is considered in the next Section, it is clear that many improvements have been made that have not been reported in the public domain literature.

2.4 State of the Art

2.4.1 Introduction

As explained previously, there is a lack of published material on the recent developments in the ultrasonic water-jet technology. The state of the art, therefore, has been established with analysis of current commercial literature. In particular, the existing products available from the three companies Panametrics, Meccasonics and Ultrasonic Sciences [13,14,15] were considered.

2.4.2 Current Capabilities

The capabilities of water-jet technology have clearly progressed since the work described in the previous sections. The water-jet system product lines of the three companies considered are similar although it is suggested that Panametrics have the

most advanced and comprehensive capability. Advanced laminar flow squirters have been developed by Panametrics and this utilises automated vacuum lines for purging of air bubbles from the squirter cavity. Claims are made by Panametrics of an ability to perform pulse echo testing with four separate channels using four separate transducers on a single manipulator. It is also noted that a four channel through transmission system is available using eight transducers, with four transducers each on two separate manipulators.

Both of these techniques could increase sample area coverage with each scan and so could reduce scan times. In order to achieve this, a highly specialised and complex scanning system called the Automated Robotic Gantry Ultrasonic Scanning (ARGUS) system is used. Complex geometry samples can be tested by achieving contour following capability using a “teach and scan” method where every part of the sample is scanned first using an automated mechanical probe to learn the exact position of every part. Collision avoidance sensors are also used to prevent damage to either the ultrasonic probes or the samples under test. The complexity and expense of the systems will undoubtedly be substantial, however, and the system set-up time must also be excessive.

The large time required to set such a system up for scanning would be due to:

- Learning the exact position of the sample under test,
- Alignment of each probe pair,
- Arranging that water splash back from adjacent probes do not interfere with one another,
- Avoiding water ingress to sensitive sample areas.

Operational probe frequencies of the water-jet transducers (at 500kHz to 5MHz) are lower than those for the complete immersion systems (at 5MHz to 30MHz) and indicate that control and monitoring of the water-jets is still unclear. It is also evident from the fact that some completely water free systems have been developed that the water-jet systems are far from ideal. Some test samples are intolerant of any moisture. As mentioned in Section 2.3.2, the only option for scanning of such samples has been the dry contact roller probe approach. This is a PE technique where

the transducer is housed within a fluid filled rubber wheel. It is accepted that the ultrasonic energy coupled into the specimen with this technique is substantially less than that associated with conventional water-coupled testing and that scan times are excessive. However, enough energy is coupled between the probe and the sample to enable successful scanning and, until recently, there has been no alternative.

In the last three years there have been reports on developments of a single channel through transmission air-coupled system that has recently become commercially available [16] from QMI (Quantitative Measurement Instruments). Excitation of the transmitter is performed using high voltage tone bursts at 400kHz. Probes are spherically focussed and matched, and are manufactured using solid ceramic material. Signal to noise ratio is improved by employing signal averaging and using a high gain, low noise amplifier in reception. Although still in its infancy and not providing any improvement over the water-jet systems in terms of scan time reduction, this technology has been given an enthusiastic welcome in the aerospace industry.

2.5 Conclusions

Water-jet ultrasonic scanning is now an important part of the test capabilities within the aerospace industry. Large samples and samples that cannot easily be immersed are almost exclusively tested using the technique. However, recognition of the problem of long scan times is evident from the importance that has been placed on the development of a multi-channel system. Although a four channel system is now available, it is believed that the set-up times for such a system would partially offset effectiveness in reducing overall scan times. In addition to this, another significant limitation of the water-jet technique is that some samples cannot tolerate any contact with water. Although an air-coupled system has been developed in order to address this, it is a single element system and offers no improvement in scan rate. From this, it is suggested that there would be a clear opening for a system that combined air-coupled operation with large sample area coverage by adopting an array approach. It is the development of such a system that has formed the basis for the research that is reported within this Thesis.

CHAPTER 3

THE SCANNING SYSTEM - AN OVERVIEW OF CONSTRAINTS

Abstract

This Chapter explains the main design concepts of the air-coupled NDT array scanning system developed during the course of this work, in an attempt to provide a viable alternative to existing water-jet based systems used in the aerospace industry. An insight into the thoughts and considerations in the design process is given, and all the main design decisions are justified and explained through the presentation of theoretical and experimental results. The practical difficulties associated with achieving air-coupled ultrasonic NDT, and details of the strict requirements for the system are discussed. An explanation of the influence these considerations had on the overall approach is also provided. This is aimed at gaining a fuller understanding of the interactions within the system, and also provides an indication of the possible limits of performance of the proposed approach. It includes a detailed investigation into the influence of multiple reverberations within the propagation channel on system performance and also addresses the importance of maximising the potential advantages of the air-coupled approach.

3.1 Introduction

The ultimate goal of the work that has been undertaken is to provide a useful alternative to the existing water-jet NDT system discussed in Chapter 2. This is the scanning system currently in use at a British Aerospace (BAe) test facility for the pre-production scanning of large carbon fibre composite and honeycomb aircraft sections. Specifically, the impetus behind the funding of this work was the impending requirement to scan the wing skins of the new Euro Fighter Jet, which are to be manufactured in single composite sections of dimensions 6m by 4m. Although water-jet systems have several obvious deficiencies, these have partly been overcome through a period of use and continued development. As a consequence, any alternative system would have to present some significant advantage to the users in order to justify changing from the current equipment. Any new system must also be compatible with the existing water-jet scanner hardware and satisfy certain constraints in order to fulfil successfully the strict requirements of the aerospace industry.

Air-coupled ultrasound provides a potential means of avoiding some of the limitations with the water-jet technique that are outlined in Chapter 2. The subsequent implementation of array technology will create improved inspection rates, and constitutes the basis of the proposed approach. The main aims of the initial phase of the work were to produce a prototype system to prove that an air-coupled array approach is feasible and hence provide an indication of the possible performance limits of such a system. Assuming a successful conclusion, the design decisions for the development of a full scale operational system would be made on the basis of the information gained from the initial research phase.

The first requirement in the development of the new air-coupled system was to evaluate the system constraints and identify any limitations that are imposed by the technology. In order to achieve this, a theoretical modelling approach was adopted, supported by experimental verification where appropriate. Initial work concentrated on an investigation into the influence of the propagation channel characteristics on

the system performance. This included an analysis of the effect of varying the air-gap size and sought to identify any possible influences, detrimental or otherwise, relating to interference of signals reverberating in either the sample or the air-gaps.

The importance of the achievable inspection rate with the new air-coupled system required recognition from the early stages of the research. Although there were never any strict guidelines as to what would constitute an acceptable improvement to merit full scale implementation of the new technology, it was assumed that the most economic and effective solution should be sought. However, an indication of the possible limits of performance should also be provided. To this end, software was written in order to facilitate investigation of scan rate variations as a function of key system parameters. The results of this analysis, and their bearing on the proposed system design, will be presented and explained.

3.2 System Requirements

The system had to meet certain defect detection criteria that are dependent on the nature of the test specimen and had a significant influence on the allowable array element pitch. Resolution requirements with honeycomb samples are generally related directly to a number of honeycomb cells, resulting in a relatively coarse resolution requirement. With solid carbon fibre samples, however, the requirements are much more stringent and are determined by the density of the fibres within the material. The minimum resolution requirement for defect detection imposed by the aerospace industry for carbon fibre composite samples is 4mm by 4mm. In order to achieve this, however, the existing water-jet systems have imposed a vertical step size limit of no greater than 2mm, thus providing a degree of detection overlap and enhancing the system reliability. In the absence of any evidence to indicate the resolution capabilities of an air-coupled system, the decision was taken at the outset to aspire towards achieving similar resolution to that of the water-jet technology. This decision set the array element pitch to 2mm for initial testing and system analysis, and was taken in the knowledge that larger acoustic aperture dimensions,

resulting in greater sensitivity, could be employed depending on developments as the work progressed. This was believed to be a realistic starting point for prototype development.

It should also be noted that the possible test samples, ranging from honeycomb samples of up to 50mm in thickness, to many different thicknesses of solid carbon fibre, pose a wide range of defect detection difficulties. It is generally accepted that through transmission of honeycomb samples has the highest insertion loss, since the energy must be coupled through the outer carbon fibre skin, into and through the cell walls of the honeycomb, and then through a second carbon fibre skin. This is particularly difficult when highly attenuative cell materials are used. In general, carbon fibre samples offer improved transmission, however difficulties are introduced with the more stringent resolution requirements. The decision to proceed with 2mm element pitch for initial prototype development was therefore a compromise, where solid carbon fibre samples were the main consideration. In deciding this, it was accepted that testing of honeycomb samples with initial prototypes would be difficult. Again, this was done with the understanding that resolution requirements could be met with significantly larger, more sensitive elements when testing of honeycomb samples was considered. This problem is discussed in more detail in Chapter 6 where a potential alternative technique is presented.

There is a requirement for any new system to be compatible with the existing scanning rig since only the front end transducers and the associated transmission and reception electronics would be replaced. These components must therefore be sufficiently compact and lightweight to enable attachment to the scanning rig which may move at up to 0.5ms^{-1} . Also, since the final application will involve pre-production testing of safety critical aircraft components, the reliability and robustness of the system will be of paramount importance. It is understood that these attributes will be thoroughly tested in the relatively harsh aerospace production environment.

It must also be emphasised that the new system must be economically viable. The success or failure of the project will depend ultimately on whether or not BAe decide to proceed with the development of a full scale production system. This means that the cost of the system, and any necessary disruption to the manufacturing process during commissioning, must be minimised.

This alone, however, would not be sufficient. Any change to the testing technique must constitute an attractive proposition so that any disruption and expense are outweighed by the resulting benefits. As stated in Chapter 2, there are certain limitations of the water-jet technique that can in theory be solved if a successful array based air-coupled system were to be developed. Most of these are problems are tolerated with the existing system, which is now well established in the aerospace industry.

The major potential of an air-coupled system was the opportunity to produce a linear array of receiving elements. This is simplified compared to the water-jet technique since there is no requirement for monitoring and control of the water coupling across the aperture. Significant improvement in inspection rates could therefore be achievable, with the final improvement depending on the size of the array used.

3.3 Problems of Air-Coupling

3.3.1 Introduction

Historically, air coupling of ultrasound for NDT applications has been avoided for a number of very valid reasons. If the potential advantages of an air-coupled system are to be realised, therefore, it is clear that there are a number of serious difficulties that must first be overcome. At the centre of most of the problems is the large mismatch in specific acoustic impedance between air and the other elements in the system, namely: transmitting and receiving transducers and the sample under test. Further constraints are imposed by the highly frequency dependent attenuation experienced

by ultrasonic waves propagating in air. These problems, their implications for system design, and proposed solutions will now be discussed.

3.3.2 Specific Acoustic Impedance Mismatches

Large boundary acoustic impedance mismatches result in large reflections at each boundary, with very little acoustic energy passing from the transmission to the reception devices in a through transmission system. The extent of this can be appreciated by considering the pressure reflection and transmission coefficients for normal incidence, which are related to the material acoustic impedances by the following Equations [17]:

$$\text{Reflection Coefficient} \quad R_P = \frac{P_r}{P_i} = \frac{Z_L - Z_M}{Z_L + Z_M} \quad \text{Equation 3.1}$$

$$\text{Transmission Coefficient} \quad T_P = \frac{P_t}{P_i} = \frac{2Z_L}{Z_L + Z_M} \quad \text{Equation 3.2}$$

where Z_L is the specific acoustic impedance of the load medium, Z_M is the specific acoustic impedance of the transmission medium, and P_i , P_t and P_r are the incident, transmitted and reflected pressures respectively, as shown in Figure 3.1.

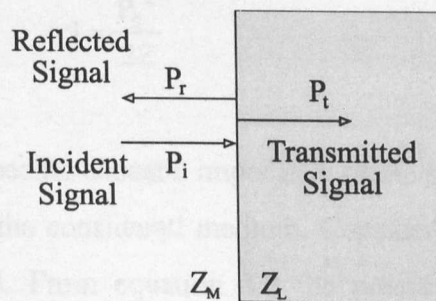


Figure 3.1 Pressures and impedances used in the calculation of transmission and reflection coefficients.

<i>System Element</i>	<i>Acoustic Impedance</i>
Transducer	$33 \times 10^6 \text{ kgm}^{-2}\text{s}$
CFRP Sample	$8 \times 10^6 \text{ kgm}^{-2}\text{s}$
Air	$0.00043 \times 10^6 \text{ kgm}^{-2}\text{s}$
Water	$1.5 \times 10^6 \text{ kgm}^{-2}\text{s}$

Table 3.1 Typical specific acoustic impedances of system elements.

Considering typical acoustic impedances for the main elements in the system as shown in Table 3.1, the extent of the mismatch in air is immediately obvious, and clearly much more severe than a water-coupled system. Based on these typical values, the pressure reflection coefficient at the air/sample boundary is calculated as 0.9999, indicating a very close approximation to total reflection. For the same boundary, the pressure transmission coefficient is calculated as 1.9999. This value is greater than 1 since sound wave *pressure* in the media, and not the sound wave *intensity*, is being considered. Analysis of the intensity transmission coefficient reveals that the signal intensity in the solid is a fraction of what it is in the air. The relationship between peak particle pressure (P_0 atmospheres) and signal intensity (I , which describes the energy that travels through unit area in unit time) is dependent on the specific acoustic impedance in the medium, and is given by [17]:

$$I = \frac{P_0^2}{2Z} \quad \text{Equation 3.3}$$

where $Z = \rho c$ and is the specific acoustic impedance of the medium, ρ is density and c is the wave velocity in the considered medium. Consider an acoustic pressure P in air, incident on a solid. From equation 3.2 the pressure in the solid would be approximately equal to $2P$. If the intensities in air and the solid are I_A and I_S respectively, and Z_S is the specific acoustic impedance of the solid then,

$$I_A = \frac{P^2}{0.0008} \quad \text{and} \quad I_S = \frac{2P^2}{Z_S}$$

The intensity transmission coefficient (I_T) when transmitting from air into a solid can be calculated from:

$$I_T = \frac{I_s}{I_A} = \frac{0.0016}{Z_s} \quad \text{Equation 3.4}$$

For the sample in Table 3.1 this would result in $I_T = 0.0002$, or a factor of 5000 reduction in signal intensity in the sample.

Therefore, it can be concluded that the overall effect of the large specific acoustic impedance mismatches that exist in the system is to cause energy entrapment within each phase of the propagation channel as shown in Figure 3.2, and extremely high insertion loss from transmission to reception (Table 3.2).

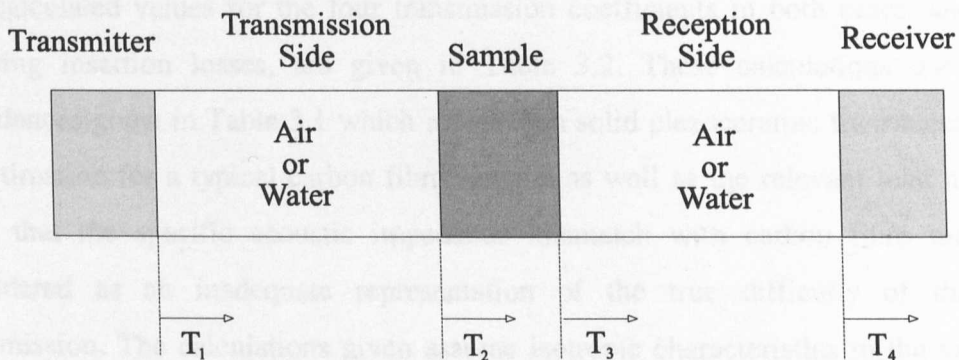


Figure 3.2 Transmission coefficients used to determine the insertion loss in a through transmission system.

The through transmission insertion loss between transmission and reception of a signal through a sample suspended in some load medium can be calculated by multiplying the pressure transmission coefficients at the four boundaries as shown in Figure 3.2. It is appropriate to draw a comparison with the insertion loss in a water-jet system, and that in the same system when the water has been removed, as an indication of the gulf in signal to noise ratio (SNR) that must be bridged in order to develop a successful air-coupled system.

<i>Coefficient</i>	<i>Air load</i>	<i>Water load</i>
T ₁	2.42e-5	0.0868
T ₂	1.9999	1.684
T ₃	0.0001	0.316
T ₄	1.9999	1.913
Total	9.68e-9	0.0884
Insertion loss	-160.3dB	-271.1dB

Table 3.2 *Transmission coefficients and calculated insertion losses in through transmission systems for air and water loading.*

The calculated values for the four transmission coefficients in both cases, and the resulting insertion losses, are given in Table 3.2. These calculations used the impedances given in Table 3.1 which represent a solid piezoceramic transducer, and an estimation for a typical carbon fibre sample, as well as the relevant load media. Note that the specific acoustic impedance mismatch with carbon fibre may be considered as an inadequate representation of the true difficulty of through transmission. The calculations given assume isotropic characteristics in the various phases of the propagation channel. Carbon fibre, however, is by nature anisotropic, and this will increase signal attenuation and make surface penetration more difficult than suggested by these calculations. Quantification of this factor would be extremely complex and would be highly dependent on the many different possible lay-up structures and material components of the samples to be considered. For this reason, the assumption of an isotropic sample is made, with an acoustic impedance value chosen in an attempt to reflect the expected difficulties of through transmission in a carbon fibre sample. Transmission coefficient T₁, T₂, T₃ and T₄ were calculated using Equation 3.2.

These calculations indicate a reduction in system signal to noise ratio of 138.9dB when the water coupling is removed. In order to provide equal performance with air and water-coupled systems, an air-coupled system must somehow recover this loss. However, comparisons of an air-coupled pulse-echo system with an equivalent water-coupled system, conducted by Farlow and Hayward [19], indicated that total recovery is not strictly required since existing water-coupled systems generally exhibit a surplus of system SNR. Experimental investigations of a typical wideband water-coupled system by Farlow and Hayward showed that echo signal recovery was still adequate when 40dB of attenuation was introduced. This work is equally relevant to the present system, since similar air/solid boundaries must be overcome, suggesting that approximately 100dB of SNR enhancement must be generated if an air-coupled system is to possess sufficient sensitivity to achieve successful through transmission testing. In this context, sufficient sensitivity may be defined as the ability to transmit an acoustic pressure wave of the desired characteristics across the two solid/air boundaries at the sample, and convert the incident pressure at the receiver into an easily identifiable electrical signal.

3.3.3 Air Attenuation

Ultrasonic energy transmitted in any medium will eventually be lost through conversion into some form of heat energy. In the atmosphere, however, the absorption process is accelerated as a result of complex molecular interactions, and is determined by the classically recognised mechanism of molecular kinetic energy redistribution, and the more recently defined molecular relaxation losses. Bass *et al* [20] have developed an approach for the calculation of acoustic attenuation in air which incorporates all the relevant considerations.

The pressure P at an observation point a distance Z from the source is calculated from the following expression,

$$P = P_0 e^{-\alpha Z} \quad \text{Equation 3.5}$$

where P_0 is the pressure at the source and α is the attenuation (or absorption) coefficient calculated from Equation 3.7.

$$\alpha = f^2 \left\{ 1.84 \times 10^{-11} \left(\frac{P_0}{P} \right) \left(\frac{T}{T_0} \right)^{\frac{1}{2}} + \left(\frac{T_0}{T} \right)^{\frac{5}{2}} \left[\left(1.278 \times 10^{-2} \frac{e^{-\frac{2239.1}{T}}}{f_{r,o} + \left(\frac{f^2}{f_{r,o}} \right)} \right) + \left(1.068 \times 10^{-1} \frac{e^{-\frac{3352}{T}}}{f_{r,N} + \left(\frac{f^2}{f_{r,N}} \right)} \right) \right] \right\}$$

Equation 3.6

where f is the frequency in Hz, T is the temperature in K, $T_0 = 293.15$ K, P is the atmospheric pressure in Nm^{-2} , $P_0 = 1.01325 \times 10^5 \text{ Nm}^{-2}$ and $f_{r,o}$ and $f_{r,N}$ are the rotational relaxation frequencies in Hz for oxygen and nitrogen respectively.

The most significant observation to be made from this relationship is that attenuation increases with the square of the frequency of the propagating energy. At ultrasonic frequencies, the attenuation in air can therefore have a significant influence on performance of the system, and will vary across the frequency spectrum. Indeed, it could be concluded that air is an inherently narrowband medium with respect to ultrasonic propagation and acts on transmitted ultrasonic pressure as a low pass filter. This becomes more significant as the propagation distance increases and limits both the useful ultrasonic frequency range and the distance over which useful measurements can be made. The problems associated with attenuation in air-coupled ultrasonics may be appreciated when it is noted that at 1MHz, the absorption coefficient is 1.62dB/cm in air for atmospheric pressure, 40% humidity, and 23°C temperature, as compared with 0.0022dB/cm for the same signal propagating in water.

3.4 Mode of Operation

In light of the highly frequency dependent nature of acoustic signal attenuation in air, careful consideration is necessary in deciding the most appropriate frequency characteristics for system operation. Conventional pulse-echo water-coupled systems generally adopt a high frequency (>5MHz) wide bandwidth approach. As mentioned in Section 2.2.2, this produces a scan with information about the type and location of any defects. Most of this data is not available with the through transmission water-jet testing and it is therefore clear that in many cases it is often sufficient to identify the presence of a defect with the required minimum size. The frequency content of the signals received during a through transmission scan is therefore less important. A successful air-coupled system must therefore reach a compromise, enabling attenuation and SNR difficulties in air to be minimised, yet still providing adequate spatial defect detection resolution.

There are a number of reasons that make the adoption of a narrowband approach particularly suited to the proposed application. Firstly, the selected transducer technology which proved to be the most sensitive for air-coupled operations is highly resonant in nature, and performance is optimised under narrowband conditions. This is discussed further in Chapter 4. Secondly, narrowband signals contain more energy and so are more likely to overcome the large impedance mismatches in the system, and provide adequate penetration the sample under test. Thirdly, adopting a narrowband approach enables band pass filtering techniques to be employed in reception. Air-coupled pulse echo experiments performed by Farlow and Hayward [19] have shown that transmitting a signal with at least 20 cycles duration and performing bandpass filtering in reception can improve the system SNR by 35dB.

Finally, as noted in Section 3.3.3, air has been shown to be a naturally narrowband propagation medium and will act as a low pass filter to any wideband transmitted signal. This would severely reduce the frequency content of any through transmitted wideband signal, and so limit, or even eliminate, the intended effect of adopting a wideband approach. Transmitted signal energy content would also be reduced

significantly because of this frequency selectivity, casting further doubt over the ability of wideband signals to overcome the four air/solid boundaries. All of this leads to the conclusion that a narrowband approach would provide the most realistic opportunity to overcome the problems discussed in Section 3.3 by regaining some of the SNR lost with the removal of the water coupling. It is discussed in Section 3.6.6, and it is important to note here, that low SNR is of particular concern since scan rate requirements dictate that operation must be real-time and no signal averaging can be performed.

A narrow band approach having been selected, it then remained to determine the most appropriate operational centre frequency. Considering the rapid increase in attenuation with signal frequency, it is important in this selection process to strike the correct balance between system resolution and the ability of the signal to propagate through the air and the sample. To date, only empirical evidence exists to indicate the resolution capabilities in an air-coupled system at particular operating frequencies. Theoretical analysis is particularly complicated when the acoustic energy is focused (i.e. non-planar), causing a variety of wave modes to be coupled into the sample. In addition to the desired through transmitted longitudinal waves, mode conversion to Rayleigh and Lamb waves can also occur, depending on the relationship between the nature of the sample under test and the spread of incidence angles and frequency of the acoustic energy.

Careful consideration was therefore given to the existing attempts at air-coupled NDT, and the detection resolution and performance reported at the various frequencies used. In most cases these employed technologies other than that chosen by the author, so this information was coupled with the experience of the author from initial testing to reach the final decision. Feasibility studies conducted at Strathclyde prior to the current research [21,22] were applicable in that they employed the same transducer technology. These demonstrated a successful through transmission scan of a honeycomb sample at 500kHz. They also indicated that successful through transmission results had been achieved in air as high as 1.5MHz. This work was used

as a valuable indication of the possible sensitivity performance of the technology, however testing was unfocussed and the resulting resolution was therefore coarse. A more applicable system in terms of resolution was developed and reported by Rivera and Vitale [23], which employed focusing. Rivera suggested that a lateral resolution of approximately 1.5 mm could be obtained with a frequency as low as 400kHz. However this depended on the careful alignment of the focal spot to the test specimen, a procedure that could be time consuming and unreliable, and would limit the flexibility of the system. A higher frequency would therefore appear to be preferable. Rogovsky [24] described a dry contact system with which a range of centre frequencies from 200 to 700kHz had been investigated. Defects ranged in size from 5mm to 15mm, and it was found that flaw detection was more reliable when frequencies between 600 and 700 kHz were used.

On the basis of this information, and initial testing performed by the author, a centre frequency of 600kHz was anticipated to represent a good compromise between resolution and attenuation in the air channel. As is seen later in Chapter 6, initial results confirmed that both through transmission sensitivity and adequate resolution are achieved at this frequency. Indeed these results suggest that an even lower centre frequency could be used with a successful outcome where sensitivity requirements are increased.

3.5 Propagation Channel Investigation

3.5.1 Introduction

Relatively little is known about the propagation of an ultrasonic signal in an air-coupled through transmission system compared with equivalent water-coupled and contact systems. It was considered appropriate, therefore, to conduct a theoretical and experimental investigation into the behaviour of the transmitted signal in the propagation channel, as a function of key system parameters, in order to identify any system limitations or performance enhancement possibilities.

The various stages of the propagation channel through which the acoustic signals must pass are illustrated in Figure 3.2. It has been established that transmitted signals must possess sufficient energy to overcome four air/solid boundaries in order to achieve reception with adequate SNR, and that close to 100% of the energy is reflected at each boundary. Signal frequency has also been selected as a compromise between attenuation and resolution. Consequently, transmitted signals tend to reverberate in each of the propagation channel phases for some time before being completely lost through attenuation. In a system such as this, which adopts a normal incidence approach, the resulting signal reverberations have the potential to influence the performance of the system. This influence is clearly evident in the case of single transducer pulse echo NDT, which has been eliminated as an option with air-coupled systems. Existing pre-amplification systems are incapable of recovering sufficiently quickly from the large initial reflection from the sample surface to process any reflection data from within the material. The effects of reverberating signals in each phase of the propagation channel were thus investigated and the results are discussed in the following Sections.

3.5.2 Transducer/Matching

It is only at each of the transducer/air boundaries that the system designer has control over the energy that is coupled between media by modifying the specific acoustic impedance of the devices. Significant advances have been made in air-coupled transducer technology in recent years and there are two technologies that have shown most potential. Detailed appraisal of these two technologies was conducted in relation to the proposed application and the results are presented in Chapter 4. It is appropriate to note at this stage that in light of the results of this work, the decision was taken to proceed with a piezoelectric composite technology and this is assumed for the remainder of this Chapter. One of the basic principles of the technology is the reduction of the transducer acoustic impedance over conventional ceramic transducers with the introduction of a passive polymer phase. This achieves a closer match to low impedance load media, however when the load medium is air, there is

still a significant mismatch resulting in the prolonged reverberation of energy within the transducer.

Improved acoustic matching to an air load medium can also be achieved with the attachment of suitable passive mechanical matching layers. The aim of these layers, which can be single or multiple, is to act as a mechanical transformer to assist coupling of energy from one medium to another, and again optimum performance relies on the constructive interference of internally reverberating signals. A full description of the design and operation of mechanical matching layers is presented in Chapter 5.

3.5.3 Air-gap Investigation

It has been shown that maximum through transmission can be achieved at an oblique angle of incidence by matching the emergence of the through transmitted component with that of a plate wave mode [25]. Although a potential use of this technique will be discussed in Chapter 6, and a normal incidence approach has been adopted for most of this research. It is also desirable to keep the transmission and reception side air-gaps to a minimum to limit the effects of signal attenuation and air currents. Reduction of the air-gaps, however, must not be at the expense of system reliability due to the interference of reverberating signals. To this end, the effect of varying the air-gap size was investigated theoretically and experimentally in order to determine the extent to which reduction is possible whilst ensuring conservation of flaw detection integrity.

The direct signal received across an air-gap between two transducers was initially modelled and verified with experiment in order to provide a solid platform from which to proceed with the theoretical investigation. All theoretical data presented in this work was obtained using a linear systems modelling technique [26] which makes the approximation of 1-D transducer operation in the thickness polarised dimension. The influence of the frequency dependent attenuation of ultrasound in air, as reported by Bass [20], has also been incorporated into this model which has been verified

experimentally by Hayward and Gachagan [27]. Figure 3.3 shows the result, where the close correlation between the theoretical and experimental signals is evident.

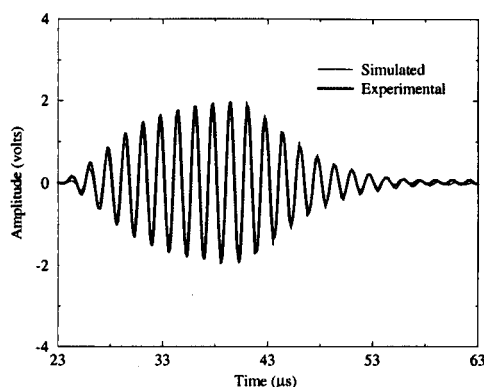


Figure 3.3 Signal received across an 8mm air-gap between two transducers after excitation with a 10 cycle 600kHz tone burst.

The variation of the peak to peak amplitude of this signal as the separation between two transducers in air is increased was then examined and the theoretical and experimental results are presented in Figure 3.4. In practice, a precision manipulator was used to increase transducer separation in steps of $27\mu\text{m}$. The transducers used had 30mm square apertures, and were a matched pair of piezocomposites that operated at 600kHz. The excitation signal was a 10 cycle, 600kHz tone burst, obtained from a Hewlett Packard arbitrary function generator, and the signal amplitude was 10 volts peak to peak. Enclosed within the transducer assembly, the receiver included a pre-amplifier with $7\text{k}\Omega$ input impedance and approximately 60dB gain [28]. Experimental data was obtained by storing the peak to peak amplitude of the received signal after each step of the manipulator. Close correlation between theory and experiment has again been achieved. However, as the air-gap is reduced, the influence of imperfections in transducer alignment and surface finish become more apparent and the theoretically predicted peaks in amplitude are not realised. Fluctuations in the received signal amplitude occur in the region where the air-gap is less than half the transmitted pulse length. In this region, the start of the transmitted tone burst is reflected and interferes with the remainder of the signal from the transmitter. The air-gap length determines the phase relationship between the waves

and hence whether constructive or destructive interference occurs. Constructive interference occurs when the transducer separation is equal to an even number of half wavelengths. Destructive interference occurs when separation is equal to an odd number of half wavelengths. Separation between a peak and a trough is therefore equal to a quarter wavelength due to the resulting half wavelength change to the reflected signal path. In the example shown here, where the system is operating at 600kHz, a quarter wavelength in air is equal to 0.14mm.

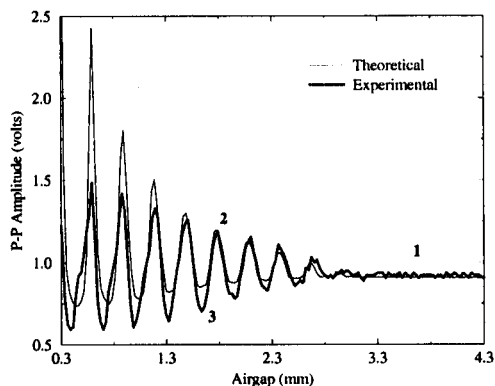


Figure 3.4 Variation of peak to peak received voltage as the air-gap between two transducers is varied.

Examples of the experimental signals received at points one, two and three in Figure 3.4 may be seen in Figures 3.5, 3.6 and 3.7 respectively. Note that in Figure 3.5 there is no overlap between the transmitted pulse and the first reflection and, consequently, there is no influence on the signal amplitude. Figure 3.6 clearly demonstrates the area of overlap between multiple reflections and shows the resulting constructive interference when the air-gap is equal to an even number of quarter wavelengths and is less than half the transmitted pulse length. In Figure 3.7 it can be seen that, although the transducer separation is less than in Figure 3.5, the signal amplitude is slightly lower and the multiple reflections are no longer apparent. This indicates that the air-gap is equal to an odd number of quarter wavelengths, and that the resulting destructive interference has significantly reduced the reflections and lowered the amplitude of the later part of the transmitted signal.

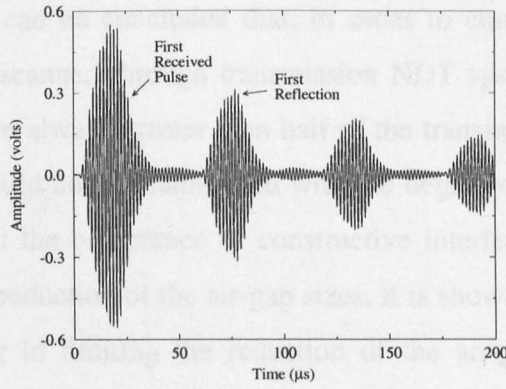


Figure 3.5 Multiple reflections of a 10 cycle 600kHz signal transmitted across a 3.5mm air-gap.

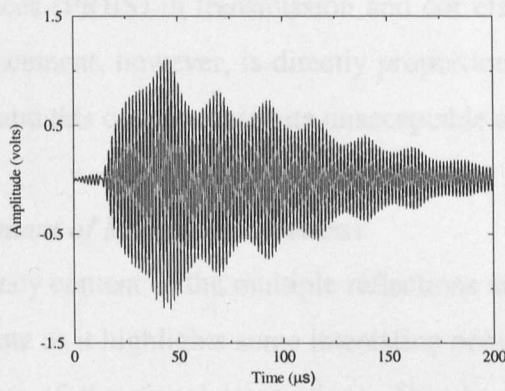


Figure 3.6 Constructive interference of multiple reflections when the air-gap is 1.68mm.

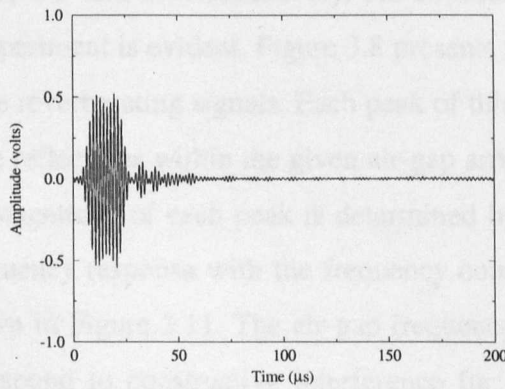


Figure 3.7 Destructive interference of multiple reflections when the air-gap is 1.54mm.

From these results it can be concluded that, in order to conserve defect detection integrity in a rapidly scanned through transmission NDT system, it is necessary to ensure that air-gaps are always greater than half of the transmitted pulse length. The transducer position could not be maintained with the degree of accuracy required to operate consistently at the occurrence of constructive interference. This appears to impose a limit on the reduction of the air-gap sizes. It is shown later, however, that a more dominant factor in limiting the reduction of the air-gaps proved to be the minimum practical focal distance of the transducers. These air-gap conclusions, however, would have a bearing on a possible SNR enhancement technique suggested in the feasibility study prior to this work [21]. This work proposed the use of pseudo random binary sequences (PRBS) in transmission and correlation in reception. The achievable SNR enhancement, however, is directly proportional to the length of the sequence transmitted, and this could necessitate unacceptable air-gap size increase.

3.5.4 Frequency Content of Multiple Reflections

Analysis of the frequency content of the multiple reflections as the air-gap sizes vary is considered appropriate as it highlights some interesting points and provides a more complete understanding of the signal interactions. This has been performed both theoretically and experimentally and Figures 3.8, 3.9 and 3.10 illustrate the relative frequency content of the multiple reflections shown experimentally in the time domain in Figures 3.5, 3.6 and 3.7 respectively. As expected, a close correlation between theory and experiment is evident. Figure 3.8 presents the case where there is no overlap between the reverberating signals. Each peak of this response represents a frequency at which the reflections within the given air-gap arrive at the receiver with the same phase. The magnitude of each peak is determined by the multiplication of the air-gap cavity frequency response with the frequency content of the transmitted tone burst that is shown in Figure 3.11. The air-gap frequency response peaks at all frequencies that correspond to constructive interference for acoustic reverberation within the gap. If the air-gap size was reduced, therefore, the separation between the peaks would increase due to the change to the air-gap frequency response.

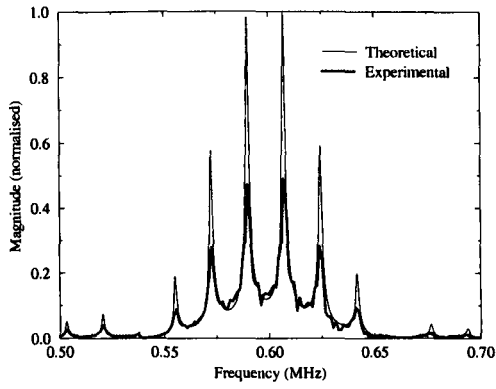


Figure 3.8 Frequency response of the multiple reflections in Figure 3.5.

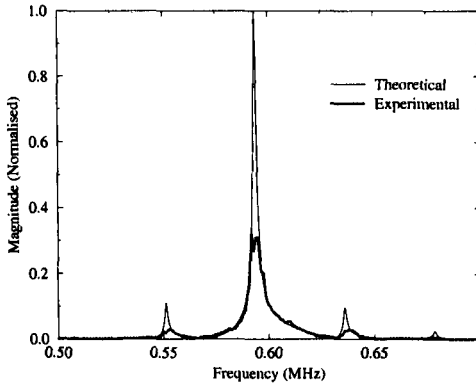


Figure 3.9 Frequency response of the multiple reflections in Figure 3.6.

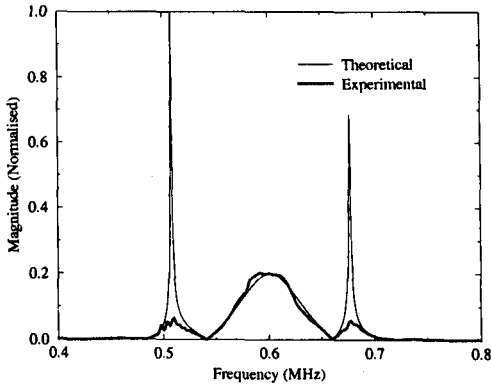


Figure 3.10 Frequency response of the multiple reflections in Figure 3.7.

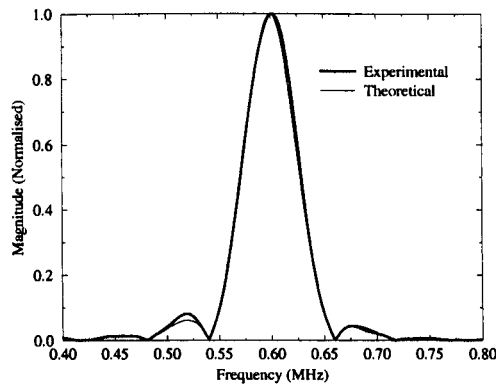


Figure 3.11 *Frequency response of the first received pulse as shown in Figure 3.3.*

Figures 3.9 and 3.10 demonstrate the resulting effect on frequency response when the air-gap provides the correct conditions for constructive and destructive interference of the overlapping reverberations respectively. It can be seen that constructive and destructive interference occur as the tone burst centre frequency corresponds with the peaks and nulls of the air-gap frequency response.

It has been noted that analysis of the frequency response of multiple reflections in an air-gap could provide an accurate air-gap distance measurement method. As with many ultrasonic measurement techniques, however, the accuracy of this method would be largely dependent on the accuracy with which the speed of sound is known. In air, this would constitute a problem because of variations in temperature, humidity and air currents.

3.5.5 Sample Transit Time

It became apparent that a possible system sensitivity enhancement technique exists in the use of similar resonance effects within the sample under test. At particular operating frequencies, maximum through transmission of energy would take place when constructive interference of the transmitted signal occurred within the sample itself. It could be possible to perform a frequency scan for each sample and hence identify the most sensitive operating conditions. In order to investigate this experimentally, the more wideband electrostatic transducer technology, as discussed in Chapter 4, was employed. Initially, a wideband signal was received between two

electrostatic transducers across an air-gap of approximately 15mm. This signal and the frequency response obtained from FFT analysis, are shown in Figures 3.12 and 3.13 respectively.

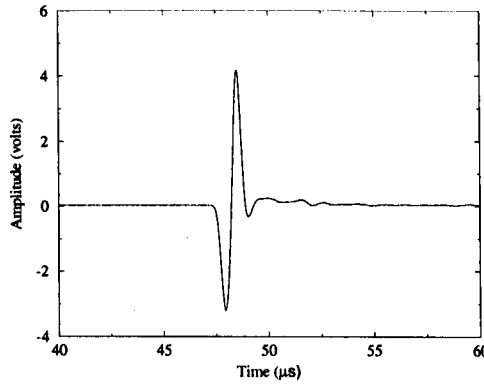


Figure 3.12 *Wideband reference signal transmitted across a 15mm air-gap.*

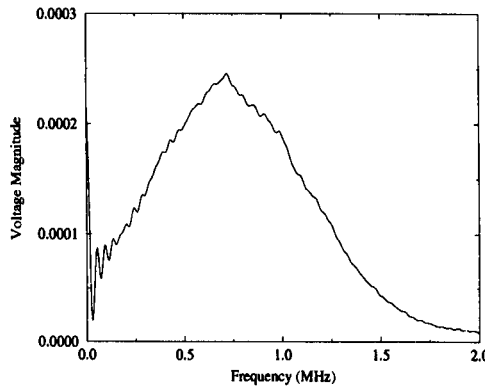


Figure 3.13 *Frequency spectrum of reference signal.*

A carbon fibre sample of 1.5mm thickness was then introduced between the two transducers. The received signal was amplified using a high gain (60dB) low noise amplifier and was continuously averaged in a digital storage oscilloscope. This enabled detection of the wideband signal received through the sample that is shown in Figure 3.14. The frequency response of this signal is given in Figure 3.15. From this Figure it is clear that only a very narrow band of frequencies, corresponding to signal resonance within the sample, has successfully achieved sample through transmission. This has occurred at 1.07MHz, a frequency which is considerably removed from the peak frequency response of the transmitted signal, and emphasises

well the significant influence that energy entrapment and signal resonance can have in an air-coupled system. Knowing the sample thickness to be 1.5mm, this frequency can be used to deduce that the longitudinal wave velocity within the sample is 3210ms^{-1} , by assuming the thickness of the sample to be equal to a half wavelength at this frequency.

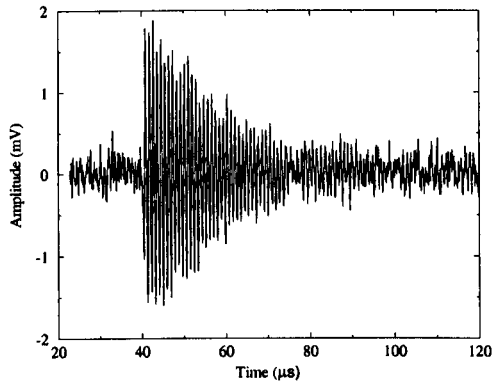


Figure 3.14 Signal received after transmission through a 1.5mm thick composite sample.

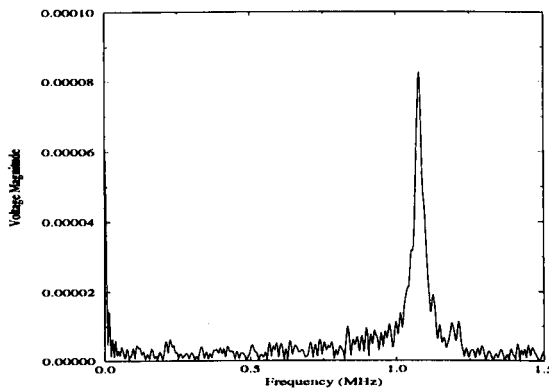


Figure 3.15 Frequency spectrum after transmission through sample.

In order to investigate this phenomenon under narrowband conditions, the electrostatic transducers were again employed by sweeping the centre frequency of a 20 cycle excitation tone burst from 400Hz to 1.5MHz, and noting the amplitude of the received signal. The tone burst was from a signal generator and was 200mV in amplitude prior to amplification through a 50dB power amplifier. The resulting measured peak to peak values are plotted against tone burst centre frequency in

Figure 3.16. Predictably, the response has again peaked at exactly 1.07MHz, and the considerable increase in signal through transmission at this frequency is apparent.

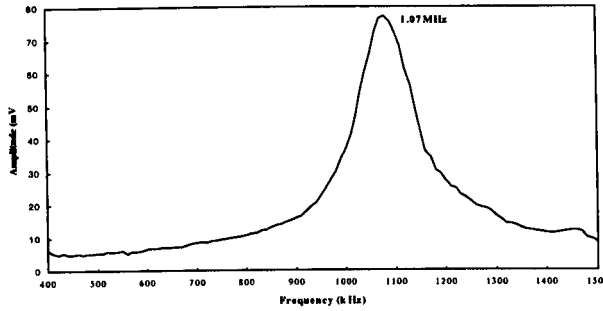


Figure 3.16 Received peak to peak voltage as the narrowband through transmitted frequency is varied from 400 to 1.5MHz.

It is therefore apparent that air-coupled through transmission could be enhanced by sweeping the centre frequency of the excitation signal to correspond with the resonance frequency of the sample. Clearly, however, this would be ineffective if even slight variations in sample thickness were to be tolerated. It is also extremely doubtful that such testing enhancements could be applied to honeycomb samples. System complexity and expense would also be increased and the overall flexibility of the system would be reduced. It seems advisable, therefore, to avoid reliance on this technique alone to achieve sufficient air-coupled through transmission sensitivity, and consequently it is given no further consideration.

3.5.6 Conclusions

The propagation channel has considerable potential to influence the through transmission system performance in air, primarily because of the specific acoustic impedance mismatches that result in prolonged signal reverberation in each phase of the channel. The possible detrimental effect of reverberating signal interference limits the air-gap reduction to a maximum of half of the transmitted pulse length. It is recognised that through transmission sensitivity could be enhanced by selecting air-gap sizes and transmission frequencies to correspond with constructive interference in the air-gaps and the sample. However, the small wavelengths in air of the selected

frequency range result in very small frequency shifts between constructive and destructive interference. In order to ensure the integrity of the system defect detection, this technique should therefore be avoided.

3.6 Scan Rate Analysis

3.6.1 Introduction

As previously explained, the main area of improvement to be provided by the new air-coupled system over the existing water-jet technology is the rate with which scanning of large test samples can be performed. Achievement of this, however, must not be at the expense of system efficiency with respect to hardware requirements. Initially, it was considered that the time required to scan a sample would be primarily related to the number of receiver array elements connected in series through a multiplexer under computer control. This would have the attraction of minimising the hardware requirement for signal amplification and subsequent data acquisition and storage. It is evident, however, that the extent to which scan rate improvement could be achieved would be limited with this approach. The following Sections discuss various possible scanning and data acquisition approaches. They describe a straightforward system calculation that was used to examine the achievable inspection rate improvements as various system parameters were modified. Results of an experimental investigation into the limits of transmitter excitation speed and amplitude are presented, and the implications of this for system design are made clear. The initial system design concept and the final proposal for the system on the basis of the scan rate calculations and transmitter limitations are also presented.

3.6.2 Original System Design Concept

A diagram of the original system design concept is shown in Figure 3.17. This consists of a single large transmitter element of the same dimensions as the receiver array that has a number of elements with 2mm element centre to centre pitch. The orientation of the array should be vertical since scans will be performed in a raster pattern with the main scanning direction along the horizontal axis. This would

provide greater test sample area coverage with each horizontal scan. Since a narrow band approach was selected, the transmitter is excited with a tone burst at the centre frequency of the transducer that has been amplified through a power amplifier. Each receiver array element has a dedicated pre-amplifier enclosed within the screened transducer housing in order to minimise extrinsic noise. These pre-amplifiers should possess high gain and ultra low input spectral noise density in order to accommodate the inevitably very low signal conditions. Both transmission and reception devices require the application of linear focusing in order to meet the spatial resolution requirements. This was based on initial experiments and previous experience, which suggested that the 2mm square element sizes required without focusing would not possess sufficient sensitivity. Also, even if this were possible with regard to sensitivity, the resolution performance would be degraded due to the increased directivity of the smaller receiver elements and the increased beam divergence of the transmitter. The receiver array elements are then multiplexed onto a single line under computer control before a further stage of amplification. In addition to the amplifier, the narrowband nature of the system should be exploited by performing band pass filtering on the incoming signals and in so doing, eliminating much of the system noise. Also, since only the peak value of each transmitted signal is required, envelope detection can be performed in order to simplify the data acquisition process. Note, however, that this processing must all be performed in real-time in order to avoid unnecessary system delay, as is shown later. Signals are then serially acquired and digitised and the peak values are stored in C scan format to enable data visualisation and defect identification.

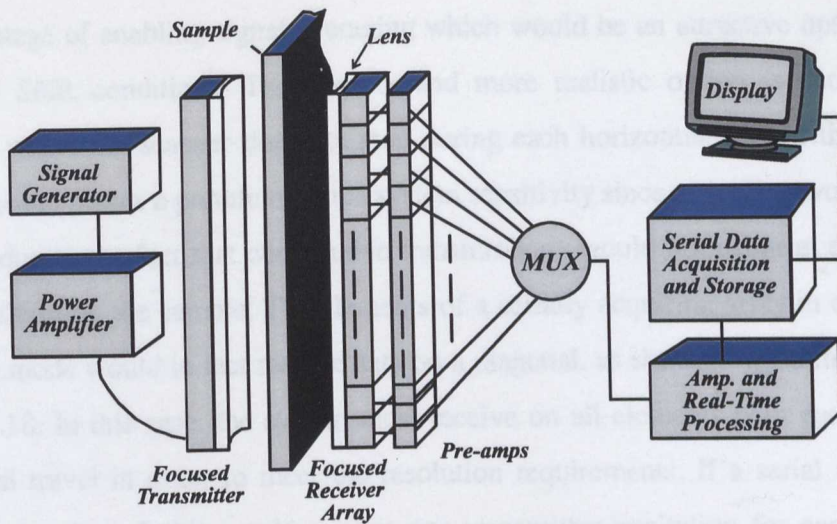


Figure 3.17 Original design concept for the air-coupled through transmission NDT system.

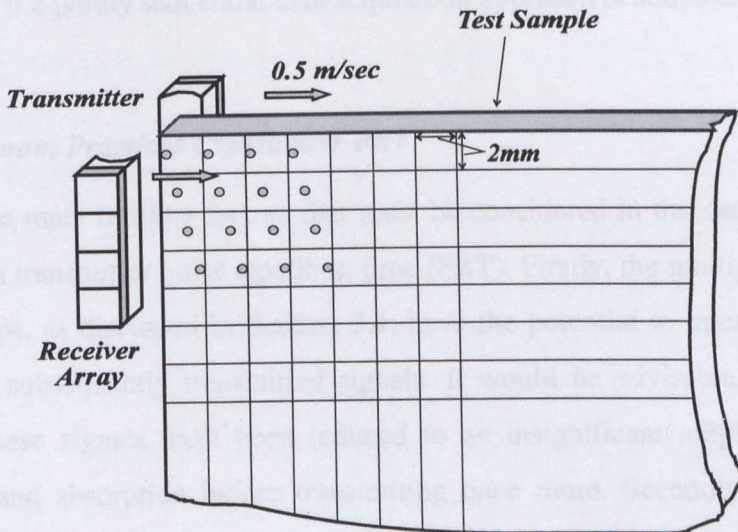


Figure 3.18 Small circles denote the positions of transmitter excitations required with a four element receiver array acquiring data in series for a resolution requirement of 2mm by 2mm.

3.6.3 Method of Horizontal Scanning

There are two possible approaches to the method of horizontal scanning which are considered. The first of these is "intermittent" scanning, where the scanner stops after each 2mm travel for the duration of each array acquisition. This approach would have

the advantage of enabling signal averaging which would be an attractive option in the very low SNR conditions. The second, and more realistic option is “continuous” scanning where the scanner does not stop during each horizontal scan of the sample. This approach places a premium on the system sensitivity since averaging would not be possible due to the fact that consecutive transmissions would not occur at exactly the same position on the sample. The elements of a serially acquiring array in continuous scanning mode would in fact receive data on a diagonal, as shown diagrammatically in Figure 3.18. In this case, the system must receive on all elements with each 2mm of horizontal travel in order to meet the resolution requirements. If a serial acquisition approach is adopted, this would require one transmitter excitation for each receiver array element in the time taken to travel 2mm. It became clear that this requirement could have a dominating influence on the achievable system performance enhancement if a purely sequential data acquisition approach is adopted.

3.6.4 Minimum Practical Transmitter PRT

There are two main limiting factors that must be considered in the determination of the minimum transmitter pulse repetition time (PRT). Firstly, the multiple reflections in the air-gaps, as discussed in Section 3.4, have the potential to interfere with and thus disrupt subsequently transmitted signals. It would be advisable, therefore, to wait until these signals have been reduced to an insignificant amplitude through attenuation and absorption before transmitting once more. Secondly, the physical limitations of the transmitter materials result in limiting both the speed with which excitation can be performed, and the maximum voltage that can be applied successfully, primarily because of the temperature increase as the applied electrical power is dissipated. The influences of both multiple reflections and transducer material limitations have been investigated experimentally in order to establish an estimate for the allowable minimum PRT, and the results are presented in the following Sections.

a) Multiple Reflections

The time taken for the reflections of a signal received through a typical sample in air to be attenuated to what was believed to be an insignificant level was investigated. A matched pair of prototype transducers (which are described in greater detail in Chapter 6) was used. At present it is sufficient to note that the operational frequency was 600kHz and focusing had been achieved with the attachment of Perspex lenses. The test sample, in position between the transmitter and the receiver, was a 5mm thick carbon fibre composite section. The received signal and the resulting reflections are shown in Figure 3.19. Signal reverberation occurs between the transmitter and the sample, as well as between the receiver and the sample, and both of these air-gaps were approximately equal to 40mm. Since the transmission side air-gap is relatively small, signal attenuation between consecutive reflections is not excessive (0.6dB/cm @600kHz for atmospheric pressure, 40% humidity and 23°C), and the first few reflections in this air-gap result in another detectable through transmitted signal. The number of reflections achieving this will depend on the strength of the transmitted signal, the sample under test, the atmospheric conditions, and precise system alignment. The relative signal attenuation, however, should be the same on either side of the air-gap. Note, therefore, that because the two air-gaps are the same, and the sample transit time is negligible, each received reflection is a combination of the reflections in the two air-gaps. Indeed, under ideal conditions, these signals would destructively interfere and reflections would therefore decay more quickly, but on the basis of results presented in Section 3.5.3, it is clear that the small signal wavelengths in question make the occurrence of this extremely unlikely.

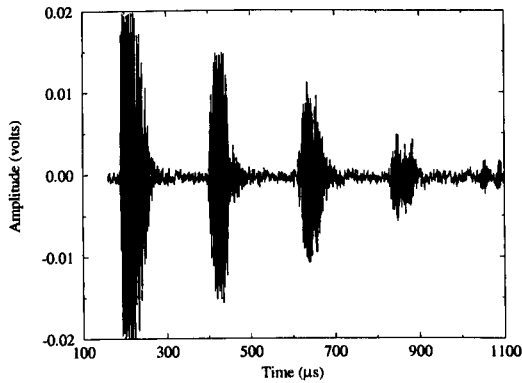


Figure 3.19 *Multiple reflections after transmission through a 5mm thick carbon fibre sample using a pair of prototype focused transducers.*

From Figure 3.19 it is concluded that the first four reflections would all have the potential to influence system reception reliability. Taking into account the time taken from signal transmission to reception of that signal, the next signal could be transmitted any time after the third reflection is received without fear of interference with the fourth reception side reflection. This would result in a minimum reliable PRT of around 1ms. It should be noted that, although the first received pulse is relatively immune to minor adjustments in either the transmitter or the receiver angle of incidence, the amplitudes of the reflections vary significantly with very slight misalignment. This is believed to be due to the nature of the interference between the two signals that make up each reflection, as well as the effect of reflection from the lens faces.

It could be possible to partially avoid the limiting effect of the reverberating signals on the PRT. When focusing is employed, the air-gaps are sufficiently large to enable the transmitted signals to be interlaced with the reflections of previously transmitted signals. In this case however the PRT would have to vary in order to avoid interference with the reflections of up to four previously transmitted signals. The timing of this would be highly dependent on maintaining consistent air-gap transit times at both the transmitter and the receiver sides, and would also assume negligible sample transit times. In the present system it would not be possible to guarantee the air-gap sizes with sufficient confidence to consider proceeding with this approach. It

is also attractive to be able to knowingly vary the air-gaps in order to enable scanning of slightly curved surfaces.

b) Transducer Material Limitations

The previous example investigation sets a lower limit for the PRT of about 1ms. Whether or not it will be possible to use this value depends on the ability of the transducer material to cope with the associated electrical energy dissipation and temperature increase. In the case of the favoured composite transducer technology temperature increase can soften the polymer phase, resulting in increased internal loss and reduced transduction efficiency. Performance is further degraded if the temperature rises beyond the first glass transition temperature of the polymer. At this point the polymer approaches a liquid state and the ceramic rods become decoupled from the polymer.

The effect of increasing the transmitter pulse repetition frequency (PRF) on transducer temperature, and the associated transduction performance was investigated experimentally. A composite transmitter possessing similar characteristics to the previously mentioned prototype, and with a calibrated thermocouple embedded within the epoxy, was used in order to monitor the device temperature under variable operating conditions. The glass transition temperature of the epoxy depends on the curing process adopted, although for the epoxy and curing process employed it is estimated to occur at around 60°C.

The excitation signal used throughout this experiment was a 20 cycle tone burst maintained at the centre frequency of the device (610kHz), and was supplied from an arbitrary function generator via a 50dB power amplifier. The peak to peak voltage directly across the transducer (V_{pp}) was measured using the 1M Ω input channel of a digital oscilloscope. The output peak to peak voltage of the tone burst from the signal generator (V_{SG}) was then varied until V_{pp} equalled 75 volts. This occurred when V_{SG}

was set to 210mV and was typical of the excitation voltage used in through transmission prototype transducer testing. An electrostatic transducer was used to monitor the transmitted signal amplitude, form, and stability, by performing air-coupled reception throughout the experiment at a distance of 50mm. The transducer temperature prior to excitation and system set-up had been noted to be constant at 21.4°C. The excitation toneburst PRF was increased from 100Hz to 3kHz in the steps shown in Table 3.3. Between each step the transducer was left for approximately half an hour to enable any temperature variation, as a consequence of the increase in PRF, to reach equilibrium. Temperature and received peak to peak voltage measurements were then made from the thermometer attached to the thermocouple in the transducer, and the oscilloscope display of the signal received by the electrostatic transducer respectively.

It was also possible to calculate the expected power dissipation in the transducer for the applied voltage and the PRF in each case. The real power (P_{real}) generated by the applied voltage is calculated as follows:

$$P_{real} = \frac{V_{pp}^2}{R_T} \quad \text{Equation 3.7}$$

where R_T is the real part of the transducer impedance at the operating frequency and $V_{pp}=75$ volts. R_T was measured using an impedance analyser and found to be 20.0Ω. This meant that the calculated real power dissipation was:

$$P_{real} = 281 \text{ W}$$

This, however, would be the power dissipated for continuous excitation at this frequency and excitation voltage, and does not take into account the mark to space ratio (MSR) of the different PRFs where,

$$MSR = T_{TB} * PRF \quad \text{Equation 3.8}$$

T_{TB} is the duration of the individual tone bursts, and for 20 cycles at 610kHz $T_{TB}=32.8\mu\text{s}$. Then,

$$\text{Actual real power} = P_{real} * MSR \quad \text{Equation 3.9}$$

Measured temperature and received voltage, in addition to calculated MSR and actual power dissipated, are included in Table 3.3 for each PRF. The most important observation to be made from this experiment was that a 1kHz PRF does not unduly affect the performance of the transducer, and the temperature increase is well within the expected glass transition temperature of the epoxy in use. When the previous experiment on the multiple reflections is considered, this effectively sets the confidently usable PRT minimum at 1ms. The first two received transmissions and associated reflections, when the PRT equals 1ms, are shown in Figure 3.20. The signals that are evident just before 1.0ms and 2.0ms are the electromagnetic detection of the excitation signal. These occur at the time of the excitations. This is not present for the first excitation because triggering was set to the falling edge of the excitation signal.

<i>PRF</i> (Hz)	<i>Temperature</i> (°C)	<i>Received Signal</i> (mV)	<i>MSR</i>	<i>Actual Real Power</i> (W)
0	21.4	0	0	0
100	23.1	22.2	0.0033	0.927
400	27.2	24.2	0.0131	3.681
600	29.8	24.4	0.020	5.620
1000	32.0	24.5	0.033	9.27
1500	34.1	24.9	0.049	13.769
2000	38.5	26.3	0.066	18.546
2500	40.3	27.0	0.083	23.323
3000	44.6	26.5	0.099	27.819
3500	50.2	22.2	0.115	32.315
4000	56.6	19.0	0.132	37.092

Table 3.3 *Important system parameter variation as the transmitter PRF is increased (PRF test).*

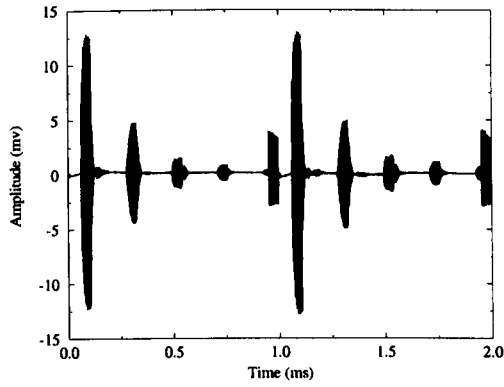


Figure 3.20 First two signals and multiple reflections received across an air-gap when the PRT is set to 1ms.

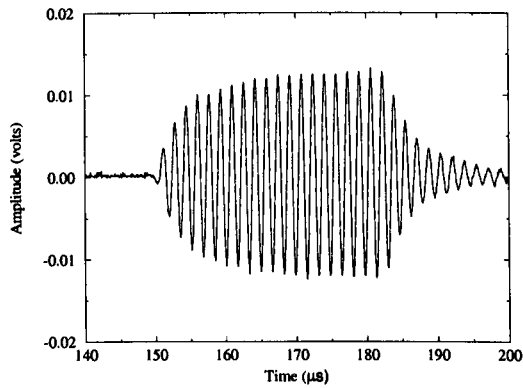


Figure 3.21 Typical signal received before signal loss of stability (PRF=1000Hz).

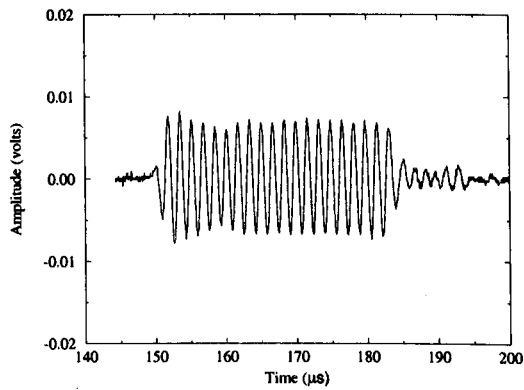


Figure 3.22 Typical signal received after signal loss of stability due to air currents and polymer softening (PRF=4000Hz).

It was informative to note the point at which performance degradation began due to the temperature increase, as the power dissipation in the transducer increases with PRF. The exact point at which degradation begins is difficult to pinpoint due to the long term nature of the experiment and the gradual change in conditions, however it was noticeable that after 3kHz PRF, the signal received on the electrostatic transducer began to reduce in amplitude. More importantly, the signal shape began to change slightly, and as the temperature increased beyond around 45°C, the signal became quite unstable, with large fluctuations and even complete loss of signal on occasion. This was understood to be the point at which thermal gradients in the transmitter air-gap began to influence the received signal. Another possible cause of the loss of signal is the fact that the epoxy was beginning to soften, and the bond with the ceramic was changing, thus influencing both the vibrational characteristics and the internal damping effect. This could have caused an intermittent antiphase relationship between the vibration of the epoxy and the ceramic. Typical signals before and after temperature increase beyond 45°C are shown in Figures 3.21 and 3.22. Note from Figure 3.22 that an improvement in bandwidth is evident as a result of the softening of the epoxy.

V_{pp} (Volts)	Temp (°C)	Received Signal (mV)	Actual Real Power (W)
0	21.6	0	0
50	27	17.5	4.10
75	31.7	24.6	9.27
100	35	32.0	16.5
125	40	36.6	25.8
150	46	40.1	37.1
175	55	41.0	50.5
200	65.5	40.4	66.0

Table 3.4 Important system parameter variation as the applied voltage is increased. (PRF=1kHz and MSR=0.033)

The minimum PRT having been established at 1ms, it was considered worthwhile to extend this investigation to identify the performance trends as the dissipated power is increased by increasing the applied voltage level. In this case, the PRF was maintained at 1kHz and V_{pp} was increased from 50 to 200 volts. The transducer was first left to recover from the PRF testing, and the pre-excitation temperature was measured at 21.6°C. A similar test procedure to the above was adopted, and all measured and calculated results as the voltage is increased are presented in Table 3.4. In this Table, power is the calculated power prior to adjustment for MSR (0.033). Note that the case for $V_{pp}=75$ volts has the same conditions as that for PRF=1kHz in Table 3.3.

A number of interesting observations were made from this testing. It was noted that transmission performance began to degrade beyond $V_{pp}=150$ volts. A similar loss of signal stability was observed at around the same temperature. The received signal amplitude was measured on the occasions between fluctuations, and this was noted to remain quite constant as the voltage and temperature were further increased. This can be explained by the fact that, although the epoxy becomes softer and contributes less to the force output of the device, the drive of the ceramic is increasing to compensate. Finally, it was noticed that the temperature achieved at the various actual powers was greater with the PRF test results than for similar actual powers with the V_{pp} test results. For example in PRF test, 37.092W achieves 56.6°C, whereas in V_{pp} test, 37.1W achieves only 46°C. This can be explained by the fact that actual power, particularly for the higher PRF cases, is slightly underestimated, and can be understood with analysis of an actual excitation signal measured across the transducer, as seen in Figure 3.23. The peak to peak voltage measurements were made in the middle section of this pulse and so did not take account of the peaks caused by the loading effect of the transducer, therefore each transmitter excitation will dissipate more power than anticipated from this measurement.

The influences of multiple reflections and transducer temperature increase on the minimum transmitter PRT could both be reduced if multiplexed excitation of an array of transmitter elements were used. However, this option was discarded for prototype development, due to the considerable additional system expense and complexity. It is also that it is unlikely that sufficient transmission sensitivity to overcome the problems discussed in Section 3.3, would be provided with smaller elements. Much smaller transmitting elements would also possess inferior directivity characteristics, and system resolution would be reduced. Multiplexing of a number of transmitter elements, similar in size to the prototype transmitters currently being tested, may be a worthwhile consideration in the future development of the much larger, fully operational system.

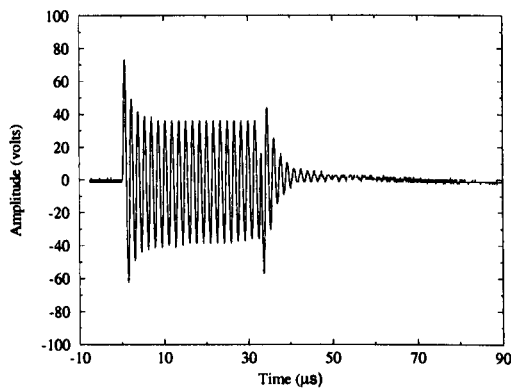


Figure 3.23 Tone burst measured across the transmitter for $V_{pp}=75$ volts.

3.6.5 Scan Rate Calculation

In order to enable assessment of the most efficient system in terms of development cost while still achieving a satisfactory inspection rate improvement, scan rates were analysed theoretically as key system parameters were modified. The calculations considered the time taken for each phase of the through transmission system and the data acquisition as well as variations due to the method of scanning being implemented. The following details explain the theoretical calculations that constitute the basis for scan rate analysis.

The system parameters used in the calculations and the default values used in the analysis are presented in Table 3.5.

<i>Parameter</i>	<i>Description</i>	<i>Default Value</i>
T_{Xag}	Transmission side air-gap	20mm
R_{Xag}	Reception side air-gap	20mm
Y	Test sample thickness	5mm
C_a	Speed of sound in air	344m/s
C_s	Speed of sound in sample	2500m/s
DCT	Data conversion time	10ms
A	Number of averages	1
PRT	Transmitter excitation pulse repetition time	1.0 msec
N	Number of array elements connected in series	100
H	Horizontal width of the test sample	1m
H_{step}	Horizontal resolution requirement	2mm
V	Vertical height of the test sample	1m
N_a	Number of serial arrays connected in parallel	1
M	Element centre to centre spacing	2mm
V_{hs}	Average horizontal array speed	0.5m/sec

Table 3.5 System parameters and default values used in the calculations.

Firstly, the time taken for a single transmission to be stored in memory (T_m) was calculated as,

$$T_m = \frac{T_{X_{ag}} + R_{X_{ag}}}{C_a} + \frac{Y}{C_s} + DCT \quad \text{Equation 3.10}$$

The time to perform 'A' averages (T_a) would then given by :

$$T_a = T_m + (A - 1)PRT \quad \text{Equation 3.11}$$

In this case, only the time T_m of the first transmission has any influence since each subsequent transmission that is required for the averaging would be stored in memory

after a time PRT, independently of T_m . It should be remembered that the ability to perform averaging is dependent on the method of horizontal scanning being employed.

The same argument is applied when calculating the time to receive with averaging on all the elements of the array. i.e.,

$$T_v = T_m + (A - 1)PRT \quad \text{Equation 3.12}$$

When calculating the total time to scan one horizontal line (T_h) of the sample, consideration must be given to the method of scanning as shown below. Note that, for simplicity, the times due to acceleration and deceleration at the beginning and end of each line have been omitted from both calculations.

a) Intermittent

In intermittent mode, the time to move between stationary positions, as well as the time to vertically scan the array, must be taken into account when calculating the total time to scan a single horizontal line. The resulting equation is :

$$T_h = \frac{H}{H_{step}} * \left[\frac{H_{step}}{V_{hs}} + T_v \right] = H * \left[\frac{1}{V_{hs}} + \frac{T_v}{H_{step}} \right] \quad \text{Equation 3.13}$$

b) Continuous

For continuous operation, a similar approach to the calculation of T_v is taken. First of all, the total number of excitations required in one full horizontal scan of the sample (E_h) must be calculated. This is dependent on the width of the sample as well as the number of array elements receiving in series and the required horizontal resolution.

$$E_h = \frac{N * H}{H_{step}} \quad \text{Equation 3.14}$$

then,

$$T_h = T_m + (E_h - 1)PRT \quad \text{Equation 3.15}$$

Note that this calculation is independent of A , the number of averages, since averaging cannot be performed with any accuracy if the scanner is moving continuously.

In both cases, the calculation of T_h must also take into account the limiting speed of the scanner. That is, even when the time required to receive on all array elements is small, the scanner can still only travel at a maximum horizontal speed of 0.5ms^{-1} .

As the time for each horizontal scan is now known, the total time to scan a complete test sample may be calculated as follows:

The number of horizontal scans required to fully test the sample (N_h) must be calculated. It is dependent on the number of serial array elements, the array element centre to centre spacing, and the number of serial arrays connected in parallel. Note that this provides the capability to calculate the scan rates depending on whether data acquisition is performed in series, parallel or a combination of both. When parallel acquisition is adopted, only one transmitter excitation for all elements connected in parallel is required. This is an important consideration that is discussed in more detail at a later stage.

First,

$$N_h = \frac{V}{M * N * N_a} \quad \text{Equation 3.16}$$

then,

$$T_{\text{tot}} = N_h T_h + (N_h - 1) \left[\frac{M * N * N_a}{V_v} \right] \quad \text{Equation 3.17}$$

If only one scan is required then T_{tot} is simply equal to T_h

3.6.6 Results of Analysis

These equations were then coded in order to facilitate investigation of the scan times as key parameters were modified. The findings from this study are now described, where the default values given in Table 3.5 were assigned to parameters unless otherwise stated.

a) Pulse Repetition Time

In order to highlight the dominating influence of the achievable PRT on the system inspection rate performance with a serial acquisition approach, the scan times were noted as the PRT was increased from zero to ten milliseconds. As expected, this resulted in a rapid linear increase as may be observed in Figure 3.24. This confirms that a reduction in PRT holds the key to scan time reduction in an air-coupled scanning system when sequential data acquisition is adopted. The unavoidable limits to the reduction of the PRT that were noted previously suggest that an alternative approach may be necessary.

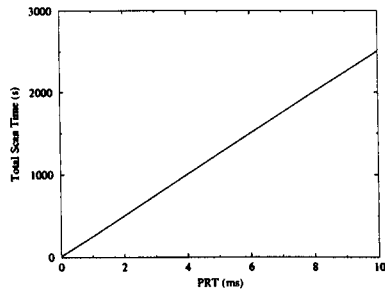


Figure 3.24 *Calculated variation in total scan time as the transmitter pulse repetition time is increased.*

b) Number of Averages

The introduction of a number of averages was investigated and one result is shown in Figure 3.25. The PRT is now assumed to be constant at 1ms. The effect of increasing the number of averages is noted to be closely linked to that of increasing the PRT. This is because each additional average requires a further transmitter excitation and a time delay of PRT in each case. The possibility of performing signal averaging with the new system is therefore virtually ruled out due to the necessity to increase inspection rates, thus placing yet more demands on the sensitivity of the system. Note that this calculation was not performed for continuous horizontal scanning mode as this does not provide the conditions to enable averaging to be performed reliably.

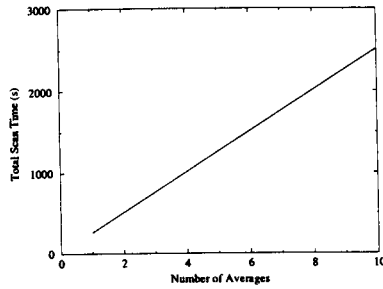


Figure 3.25 Calculated variation in total scan time as the number of averages being performed is increased.

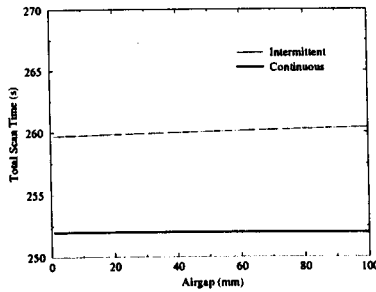


Figure 3.26 Calculated variation in total scan time as the transmission side air-gap is increased.

c) Air-gap Sizes

Initially it was considered that, due to the slow speed of sound in air compared with water, any reduction in the scan times may be largely dependent on the achievable reduction of the air-gap sizes. On the basis of the estimated PRT of 1ms, however, this investigation has refuted these initial concerns, as can be observed in Figure 3.26. This is due to the fact that a PRT of 1ms will be longer than the time spent propagating in the air for any total air-gap sizes less than 344mm, assuming a sound velocity in air of 344ms^{-1} . As long as this is the case, it will make very little difference whether the information arrives in memory immediately after transmission or just before the required PRT has elapsed. In fact, in the continuous scanning case, it will only make any difference on the first transmission of each horizontal scan. It is concluded that the air-gap sizes are of minimal concern with respect to inspection rate improvement. The air-gap sizes could ultimately have an indirect effect on the inspection rates, however, due to the increased effects of air currents limiting the speed with which scanning can

be performed. It must be stressed, therefore, that the air-gap sizes should still be minimised in order to reduce the influence of air currents as well as that of signal attenuation.

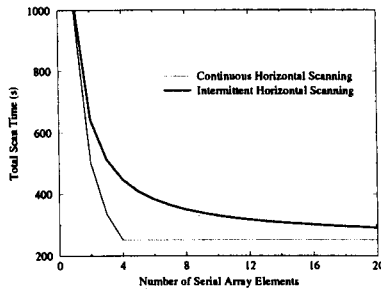


Figure 3.27 Calculated variation in total scan time as the number of receiver array elements receiving in series is increased.

d) Number of Serial Array Elements

The dominating influence of the PRT on the achievable total scan times is evident when the number of array elements receiving in series is increased. This can be seen in Figure 3.27. The time taken with a single array element is equivalent to the time taken with the water-jet system. This graph therefore provides a clear indication of the resulting improvement as the number of serial array elements is increased. It can be seen here that, as expected, the continuous scanning approach is always quicker than the intermittent approach. Since averaging has been eliminated as a possibility, there can be no advantage with the adoption of the intermittent approach. Indeed, it is clear that, due to the size and bulk of the scanning rig, successful implementation of intermittent operation would require complicated and expensive mechanical problems to be overcome. Consequently, the intermittent mode has been discarded as an option and is given no further consideration.

There is a significant reduction in the total scan times as the number of array elements is initially increased. The main point of interest, however, is in the continuous case where there is no noticeable improvement in total scan time as the number of array elements is increased beyond four. The point beyond which there is no improvement in total scan time depends on the relationship between the PRT and the maximum average

horizontal scanner speed. This can be explained as follows on the basis of the assumed maximum scanner speed of 0.5ms^{-1} and minimum horizontal resolution requirement of 2mm. The scanner is capable of travelling each 2mm section in a time of 4ms. This means that, with an assumed PRT of 1ms, only four elements can be received upon in series while the scanner is moving at the maximum speed of 0.5ms^{-1} , if the 2mm resolution requirement is to be met. If any more elements are added to the array, the scanner would have to be slowed down in order to allow time for the extra transmitter excitations that must be accommodated in every 2mm of horizontal travel. The reduction in speed, therefore, cancels out any advantage due to the requirement for fewer horizontal scans.

This highlights a difficulty in achieving sufficient inspection rate improvement with a purely sequential acquisition system. The best possible improvement in scan time on the basis of these parameters would be a four fold reduction. This led to the realisation that there is a requirement for some element of parallel data acquisition.

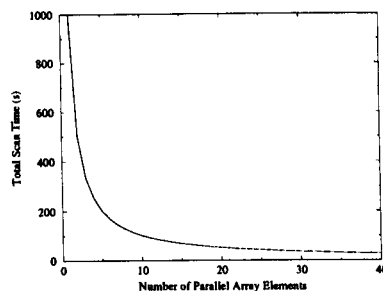


Figure 3.28 Calculated variation in total scan time as the number of receiver array elements receiving in parallel is increased.

e) Parallel Approach

The variation in scan time as the number of array elements receiving in parallel is increased was investigated and the results are shown in Figure 3.28. In this case, the number of elements which can be employed effectively with the system is independent of the PRT since only one transmitter excitation is required for reception on all of the array elements. With this approach, the PRT could only limit the maximum speed with which the scanner could move although it is much more likely that this will be

restricted due to the mechanical limitations of the equipment. The scan rate, therefore, continues to improve as more array elements are added due to a reduction in the total number of horizontal scans required.

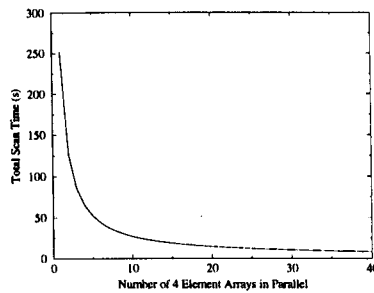


Figure 3.29 Calculated variation in total scan time as the number of four element serial arrays connected in parallel is increased.

Adopting a parallel approach introduces considerable additional expense and complexity to the system due to the requirement for additional real time data processing and acquisition hardware. Since the estimated minimum PRT of 1ms is less than the minimum time to scan 2mm there is still some degree of improvement to scan times achievable by incorporating serial arrays. Further investigation, therefore, looked at the effect of combining serial and parallel data acquisition and using a number of the optimal serial arrays connected in parallel. Figure 3.29 shows the total scan time reduction as the number of four element serial arrays connected in parallel is increased. Again, there is an initial rapid improvement in scan rates that falls off as the number of arrays is increased. If eight parallel arrays of four elements were used the system could offer a thirty two fold improvement over the single element water-jet system. In this way, the additional hardware requirements are kept to a minimum yet significant improvements are still possible.

3.6.7 Further System Design Considerations

With the possibility of averaging ruled out, the sensitivity of the receiver elements becomes even more critical. The water-jet system has a vertical step size of 2mm and in order to simulate this with an array requires element centre to centre spacing of 2mm. This means that the active area of each element is very small which could create

problems in achieving the required sensitivity, particularly with thicker samples. A possible solution to this could be to use larger elements of say 6mm element pitch and then step the array in two 2mm steps prior to one complete array step. This concept is shown diagrammatically in Figure 3.30. Note that the number of transmitter excitations per 2mm cell would still be one and the overall scan time will be similar to before, although the active area for each reception has been tripled in size. This is similar to the water-jet case where a 15mm diameter transducer is concentrated into a 6mm diameter water-jet while the horizontal step size is only 2mm. In both cases there is the same degree of overlap between subsequent horizontal reception lines which may even make flaw detection more reliable. This could be a valuable technique in the scanning of honeycomb samples.

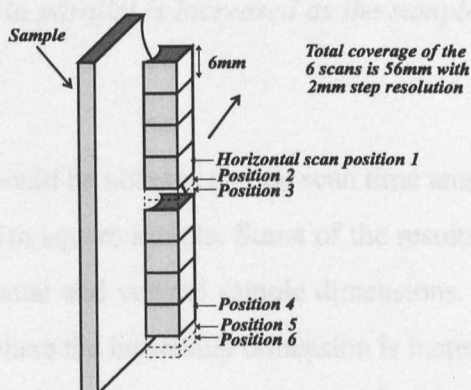


Figure 3.30 Possible scanning procedure that could be used with a larger element array in order still to meet the detection criteria.

Although the previous scan time analysis was based on a maximum scanner speed of 0.5ms^{-1} it is worthwhile considering the possibility of operating at a slower speed, without reduction in inspection rates and with limited additional hardware requirement. The benefits of this could be considerable in terms of potential reduction in air current interference. This could be achieved due to the dependence of the allowable degree of serialisation on the PRT and the maximum speed of the scanner. If the system was scanned at a slower speed, a higher degree of serialisation could be performed on each parallel channel. The speed could be halved and the only additional hardware required to achieve the same inspection rates would be twice the number of receiver elements

and 8-1 multiplexers as opposed to 4-1. There would be little variation in total scan time, however, since each horizontal scan would cover twice the area. This may be a valuable option should the air current interference prove to be too great to enable reliable system performance at maximum speed.

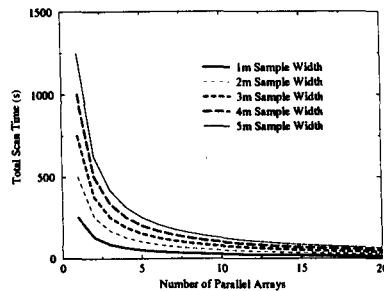


Figure 3.31 Calculated variation in total scan time as the number of four element serial arrays connected in parallel is increased as the sample width to height ratio is altered.

One further point that should be noted is that all scan time analyses were carried out on the basis of scanning a 1m square sample. Some of the results may vary depending on the ratio between horizontal and vertical sample dimensions. An example of this may be seen in Figure 3.31 where the horizontal dimension is increased while the number of parallel arrays performing reception is increased.

3.6.8 Final Proposed Design

In conclusion of this scan rate investigation it is suggested that it is clearly not possible to achieve a sufficient degree of inspection rate improvement by adopting a simple sequential array approach. The most economic and effective method of achieving the required reduction is to develop a system that combines sequential and parallel data acquisition. In light of these findings, the final proposed system design concept is shown in Figure 3.32. This is the same as the original concept in all aspects except the data acquisition phase, which now employs an eight channel parallel data acquisition card. Each channel is supplied by a 4-1 multiplexer under computer control. If implemented successfully, this system would provide a 32 fold improvement in inspection rate over the water-jet system. For the continuation of this research program

however it was proposed to develop an eight element array with 2mm element pitch, and all elements acquiring in parallel, in order to determine conceptual feasibility and provide an eight fold scanning speed enhancement.

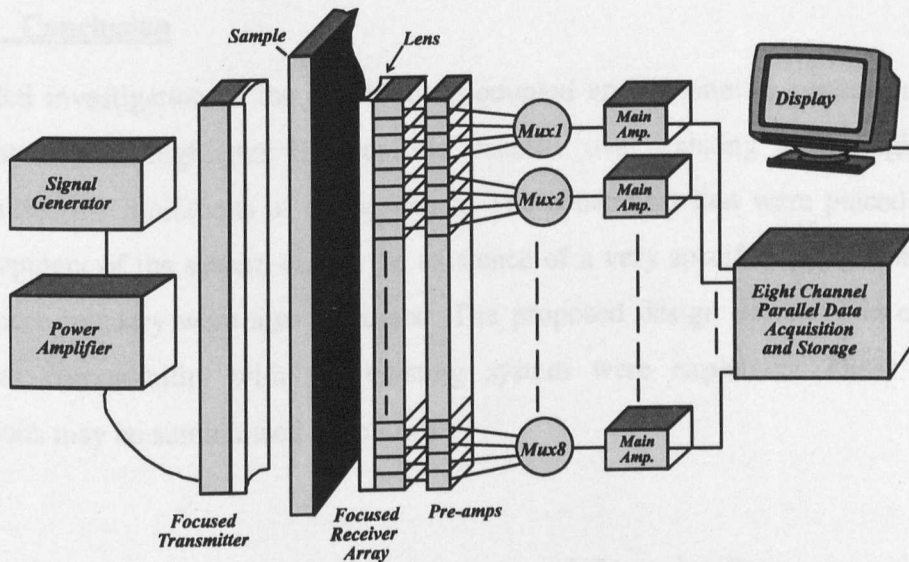


Figure 3.32 Final proposal for the air-coupled scanning array system.

3.6.9 Conclusions

Improvement of system scan rate is of paramount importance in the successful completion of this research. It has been demonstrated that, whilst adopting a purely serial acquisition approach is attractive in that hardware requirements would be reduced, this would severely restrict the possible system scan rate improvement because of the limited allowable transmitter PRT. The rate with which a transmitter can be excited must be restricted for two main reasons. Firstly, multiple reflections in the transmitter side air-gap could interfere and detrimentally influence the integrity of results. The second consideration is the physical limitations of the transducer materials depending on temperature increases as excitation power is dissipated. Scan rate requirements also dictate that data acquisition must be performed in real time without recourse to signal averaging. This is again linked to the limited PRT, and the excessive time between the consecutive transmissions required for averaging. The final design concept was based on the conclusion that the most economic and effective solution

would be realised by adopting an element of multiplexing, and combining serial and parallel data acquisition.

3.7 Conclusion

Detailed investigation of the proposed air-coupled array scanning system has been presented. This highlights the possible benefits over existing technologies, yet recognises the limitations of the approach. The constraints that were placed on the development of the system due to the existence of a very specific application in the aerospace industry were also discussed. The proposed design decisions in order to achieve compatibility with the existing system were explained. These design decisions may be summarised as follows:

- The minimum resolution requirement of 2mm by 2mm, necessitates a maximum receiver element pitch of 2mm.
- A narrowband approach at 600kHz centre frequency has been adopted in order to compensate for the low SNR yet still meet resolution requirements.
- Performing averaging is not possible due to the resulting reduction in scan rate and the inability of the scanning rig to operate in an intermittent mode.
- An air-coupled receiver array and a single large transmitter will be used in order to improve scan rates compared to the existing water-jet system.
- Transmitter material limitations and multiple reflections in the propagation channel limit the minimum PRT to a minimum of 1msec.
- An eight channel array with parallel data acquisition in reception has been selected for prototype development although an element of serial acquisition would be the most efficient approach in the long term.

CHAPTER 4

SELECTION OF TRANSDUCER TECHNOLOGY

Abstract

An essential step in the development of the proposed system was the practical and theoretical assessment of available transducer technologies. This was done with a view to identifying the most suitable approach and paid particular attention to the system requirements outlined in Chapter 3. It has been generally accepted that there are two main contenders for air coupled ultrasonic applications of this nature, but there has been widespread disagreement on which technology would offer the most attractive and practical solution. The two transducer technologies in question are *piezoelectric composite* and *electrostatic*, and as yet the only report of a direct experimental comparison of these devices was performed by the author and colleagues. This Chapter initially presents the theory behind the operation of the technologies in their various forms, extracting information from available literature and outlining the possible advantages and disadvantages in each case. The results of an experimental comparison of their respective attributes, including sensitivity, robustness and focusing capabilities are then highlighted, and the case for the selection of one technology over the other is presented.

4.1 Introduction

For non-contact ultrasonic NDT of both metallic and non-metallic structures, there are two approaches that are of interest for both production and in-service inspection. Firstly, laser generated ultrasound, combined with laser detection, offers the significant advantage of truly remote testing, with the potential for rapid scanning of complex geometrical components. Laser systems have been demonstrated for through transmission scanning [3], plate wave generation [29], and pseudo array imaging [30]. However, current prototype systems are expensive, relatively cumbersome, require safety precautions and can cause damage to the surface of the inspection site. An alternative approach is to use existing scanning methods and NDE (Non Destructive Evaluation) standards, requiring replacement of only the front-end transducer technology and associated electronics. This is a convenient and cost effective solution to the problem of developing an air-coupled test system, but would require significant development of transducer technology in order to overcome the sensitivity problems introduced with the removal of the liquid coupling, as highlighted in Chapter 3. It was noted in Chapter 2 that a commercial air-coupled system has been developed [19]. This system uses solid ceramic transducer technology. Operation is limited to use of a single elements and requires use of signal averaging to achieve sufficient signal to noise ratio. It therefore does not offer any improvement over water-jet technology in terms of scan time reduction.

There are two transducer technologies possessing suitable characteristics that would qualify them as candidates for the array application under consideration without the need for use of signal averaging. These are piezocomposite transducers, comprising a conventional piezoelectric material modified with the introduction of a passive polymer phase, and electrostatic (capacitive) devices. The latter comprise a flexible membrane that vibrates over a conducting backplate under the influence of a D.C. bias field. Although piezocomposites can be made in several different configurations, the devices considered here consist of square section ceramic pillars embedded in a doubly periodic epoxy matrix. Composite transducer design, and the resulting implications for air-coupled performance, will be discussed in detail in Section 4.2 as

a function of several key parameters. Corresponding data on electrostatic devices is discussed with reference to existing literature on the technology in Section 4.3.

The ultimate aim of the work presented in this Chapter was to reach a decision on the selection of transducers for the remainder of the research programme. Therefore, in addition to considering information available in existing literature, it was necessary to conduct a direct experimental comparison of their respective attributes, since the author knew of no existing work of this nature. This was done and consideration was given to all essential requirements for a practical system, including sensitivity, frequency response, robustness, ease and repeatability of manufacture and beam profile under focused conditions.

4.2 1-3 Connectivity Piezocomposite Transducer Technology

4.2.1 Introduction

Piezoceramic transducer technology has found widespread application in its isotropic form in the fields of NDT, biomedicine and sonar. Indeed, the general dominance of the technology over magnetostrictive and other piezoelectric methods (e.g. piezopolymers) has been apparent for many years. Nevertheless ceramic technology suffers from limitations due to the relatively poor acoustic match to low density load media such as air and water, often necessitating the requirement for multiple acoustic matching layers and high power excitation. This can contribute to an inherently narrowband, resonant nature due to energy entrapment within the devices. In many cases, performance can also be reduced due to the existence of lateral acoustic activity operating in competition with the desired thickness mode motion.

These drawbacks have fuelled the continued development of piezoceramic based transducers, in an attempt to broaden the application range and improve performance in existing fields. In the last ten to fifteen years, research effort into the use of composite transducers, combining piezoceramics and passive polymer materials, has eliminated many of the drawbacks. The impetus behind much of the original

pioneering work [31,32,33] came from a requirement for improved acoustic matching in underwater and biomedical applications. The problems of acoustic match, bandwidth, and efficient unimodal thickness operation have all since been addressed with impressive results. Of particular interest to the work in the present project is the acoustic impedance reduction achieved with the introduction of the epoxy phase and the enhancement of thickness mode coupling efficiency. The application of piezoceramic composite technology to the problems of air-coupled NDT has thus become a realistic proposition.

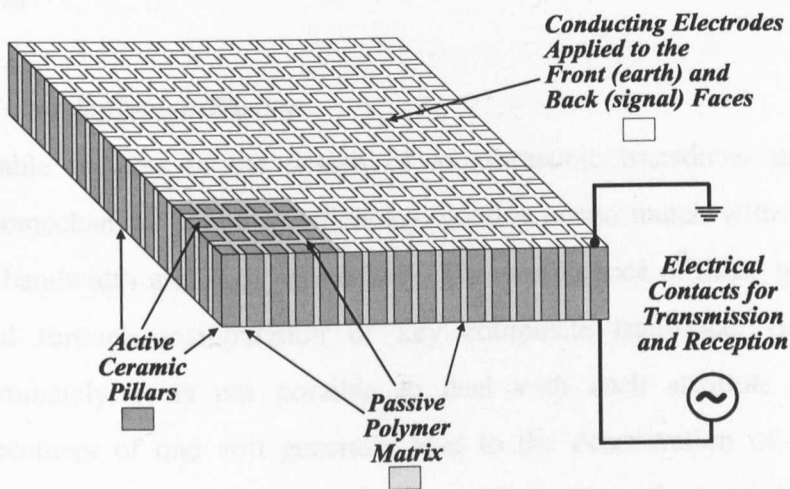


Figure 4.1 Diagram of a doubly periodic 1-3 connectivity square pillar piezocomposite transducer (front left corner of electrode omitted for clarity).

Piezocomposite technology can take several different forms depending on the nature of the geometric relationship between the polymer and ceramic phases. The most versatile and widely adopted form is the 1-3 connectivity structure where active ceramic pillars are embedded in a matrix of passive polymer. The figures '1' and '3' refer to the number of dimensions in which the ceramic and polymer phases respectively are physically connected throughout the device. Figure 1 illustrates one possible form, where the pillar cross section is square and the matrix separation doubly periodic. Optimisation of these devices is very specifically related to the application in question and there are many considerations that must be taken into account, depending on bandwidth, centre frequency and sensitivity requirements.

There is an extensive library of reference material available, detailing the main design considerations and presenting the results of theoretical and experimental investigations into the most influential parameters. Modelling strategies have also been presented and close correlation with experiment has been demonstrated. The results of these works will be considered in Sections 4.2.2 to 4.2.7, and used in explanation of key design parameters. Emphasis will be placed on specific design problems of air-coupled applications, and it will be shown that although practical design decisions inevitably require compromise, a working air-coupled system is possible.

4.2.2 Basic Design Theory

Desirable features in the design of an ultrasonic transducer may include: high electromechanical coupling efficiency, good acoustic match with the load medium, wide bandwidth and high permittivity. The prominence of these qualities can all be altered through manipulation of key composite transducer design parameters. Unfortunately, it is not possible to deal with each attribute in isolation, and enhancement of one will generally lead to the deterioration of another. A major conflict inevitably exists between the optimisation of electrical and mechanical properties of the transducer, and the first task of the designer is to identify the most important characteristics for each individual application.

The introduction of the polymer phase has a number of beneficial consequences. Firstly, there is an obvious reduction in the overall specific acoustic impedance of the structure, thus improving the acoustic match to low impedance load media. Of paramount importance for air operation, however, is that electromechanical coupling efficiency can be improved, despite the absence of electromechanical conversion capabilities within the polymer. This is due to the fact that, in a certain volume fraction range, the ceramic pillars can operate more efficiently because of the reduction of lateral clamping. This effectively means that the expansion and contraction of the pillars is less restricted during vibration when surrounded by mechanically soft polymer rather than hard ceramic. Transducer bandwidth will be

improved with the introduction of the polymer as a result of improved matching and increased internal damping of vibrations, thus reducing the duration of energy reverberation.

Efficient and unimodal thickness mode vibration can also be achieved depending on the damping experienced by laterally propagating energy in the polymer phase. Without careful design, however, lateral resonances within and between the pillars can detrimentally affect performance. Finally, it is possible to produce flexible transducers, and the manufacture of complex shapes can be achieved by moulding at temperatures beyond the glass transition of the polymer. The extent to which the polymer influences performance in each of these ways will be a complex function of the specific mechanical characteristics of the polymer, the percentage introduced, and the geometry of the combination. It is also clear, however, that any reduction in the percentage of ceramic will have a resulting detrimental influence on the electrical properties of the transducer, due to the virtual absence of polymer electrical qualities, thus reducing the efficiency of electrical matching.

In order to aid the design optimisation process, equivalent thickness mode parameters have been calculated [33], describing the basic electrical and mechanical properties of the composite structure as a function of ceramic to polymer volume fraction and constituent material properties. The key equivalent thickness mode parameters include density, specific acoustic impedance, longitudinal wave velocity, electromechanical coupling coefficient, elastic constant and piezoelectric coefficient. These have been incorporated into a linear systems approximation model by Hayward and Hossack [26] to accurately predict transducer behaviour. A limitation of this approach is that the composite lateral dimensions must be significantly smaller than the fundamental thickness mode wavelength in order to enable valid assumption of homogeneous operation, by shifting the lateral modes of resonance beyond the frequency where they would influence the thickness mode drive. This is not considered to constitute a serious limitation, since it is in harmony with the aims of efficient design. Some researchers have found that, where homogeneous operation

cannot be assumed, finite element modelling [34,35] enables accurate prediction of performance with structural and material variations.

4.2.3 Volume Fraction

The most obvious and influential design variable is the ceramic to polymer volume fraction, as this will vary the emphasis between the electrical and the mechanical properties of the transducer. Manufacturing constraints, however, often limit dimensional control at the extremities of the volume fraction range, restricting the ability to shift the frequencies of lateral intra- and inter-pillar resonances, and making it more difficult to meet the requirements for homogeneous operation. This difficulty is exacerbated when high frequency operation is considered, since the wavelength of the thickness mode mechanical resonance is reduced. At very high volume fractions (above 80%), the effect of increased pillar clamping is apparent, and at very low volume fractions (below 20%), increased damping of the ceramic affects sensitivity.

Density and permittivity increase linearly with the ceramic volume fraction, as does the specific acoustic impedance of the device over most of the volume fraction range. Smith [36] has shown this to be the case using his equivalent thickness mode parameters, and accurate experimental verification has been provided by Hayward and Hossack [26]. The relationship between the electromechanical coupling efficiency and volume fraction has also been reported, and both finite element [37] and linear approximation approaches [26,36] have been used to provide valuable theoretical insights into the practical methodologies. In the range of volume fractions between 20% and 80% ceramic, thickness mode coupling efficiency of between 60% and 75% can be achieved. Although this is somewhat short of the effective electromechanical coupling coefficient ($k_{33} = 70$ -80%, calculated for an unclamped ceramic rod) it represents a substantial improvement on the thickness mode coupling coefficient of the component piezoceramic ($k_t = 40$ -50%) and is due to the preferable lateral clamping conditions. At low volume fractions, poor electromechanical coupling is evident due to elastic loading by the polymer adversely influencing performance. Hossack and Hayward [34] showed that accurate modelling of this

trend should take into account the effects of ceramic depolarisation during the frequently adopted 'slice and fill' manufacturing process. This is directly proportional to the amount of dicing performed, and consequently, to the polymer volume fraction. Another consideration at low volume fractions is that, in practice, the low capacitance of the device is easily loaded by cable capacitance thus further degrading the electrical drive performance. At volume fractions above 80%, the pillars again become more severely restricted laterally and thickness mode coupling coefficient reduces until it equals that of the constituent ceramic block at 100% ceramic.

Hayward and Gachagan [27] carried out an investigation that has proven to be invaluable to the work of this research, as it focused on performance variation of composite transducers and design optimisation for operation in air, and considers both transmission and reception characteristics. This work combined unidimensional thickness mode (linear systems) and finite element modelling with experimental verification to highlight the consequences of volume fraction variation under various backing and matching conditions. The linear approximation model included the air attenuation effects reported by Bass [20] as well as external electrical loading conditions in both transmission and reception, according to earlier work by Hayward [38,39].

The pressures produced in air by transmitters of varying volume fraction were measured using a Polyvinylidene Fluoride (PVDF) membrane hydrophone [40]. It was found from experiment and modelling that, in an unbacked, unmatched state, 50% to 70% composites possessed superior drive performance. A PVDF transmitter was used to produce an impulsive pressure to determine the air-coupled receive sensitivity of the transducers. This was found to occur at 20% volume fraction. When a silicone rubber matching layer was introduced, peak performance occurred at 70% and 40% for transmission and reception respectively. It was concluded that this was due to the reduced benefit of improved matching through volume fraction reduction.

These results indicate that the mechanical matching is more critical in reception and electrical characteristics are more important for transmission. This could be explained firstly by the fact that electrical resonance (f_e) is normally selected as the transmission operating frequency. The reason for this is the fact that electrical resonance is defined by the impedance minimum and the resulting maximum current flow and charge deposit that occur at this frequency cause maximum stress at the transducer electrodes. It must also be noted that mechanical resonance (f_m) dominates in reception, which is defined by the thickness and longitudinal velocity of sound within the transducer. Mechanical resonance is therefore the frequency at which a receiver will naturally resonate when subjected to incident acoustic pressure. Hayward *et al* [37] suggested that these specific resonances for transmitter and receiver probes deserve careful consideration, particularly when operating in pitch/catch mode. Conventional theory indicates that the electromechanical coupling efficiency is proportional to the separation of the frequencies of electrical and mechanical resonance [41]. For efficient transducers, therefore, the separation can be quite significant. This must be taken into account, particularly when operating under narrowband excitation conditions and especially in the unavoidably narrowband air medium. Electrical resonance (f_e) of the transmitter should coincide with mechanical resonance (f_m) of the receiver. Hayward and Gachagan [27] also used finite element analysis to predict that a pair of transducers, optimised in relation to suggested volume fractions and centre frequency alignment, would represent a 30dB improvement in sensitivity over a single 30% transducer operating in pulse echo mode from an ideal reflector.

4.2.4 Constituent Materials

a) Ceramic phase

An extensive list of commonly used piezoelectric ceramics and their material properties is presented in [42]. Lead Zirconate Titanate (PZT) ceramics are known to possess the attractive qualities of high relative permittivity (to facilitate electrical matching) and high effective electromechanical coupling factor (k_{33}), which are of value in the manufacture of composite transducers. Although there are a number of

variations of the basic PZT material, PZT-5H is known to possess the most suitable characteristics for composite manufacture. Theoretical data presented by Hayward and Gachagan [27] confirms this for transmission in air but suggests that maximum air-coupled receive sensitivity would be achieved with PZT-5A. The important characteristics of these two materials can be seen in Table 4.1. The lower mechanical quality factor (Q_m) of the PZT-5H would indicate a wider bandwidth characteristic, however in reality this will be dominated by the quantity and properties of the passive filler material that is introduced.

Ceramic	Impedance MRayl	Density kgm ⁻³	V_1 ms ⁻¹	k_t	k_{33}	ξ_r^s	Q_m
PZT5H	34.2	7500	4560	0.50	0.75	1730	65
PZT5A	33.7	7750	4350	0.49	0.70	830	75

Table 4.1 Important characteristics of the two ceramics recommended for thickness mode composite transmitters and receivers operating in air.

b) Passive phase

Two basic properties required of any passive phase material are a low viscosity prior to curing (in order to facilitate pouring into fine ceramic slots) and a high mechanical bond strength. The bond strength is required to ensure that the polymer is well attached to the parent ceramic material. Epoxy resins meet these requirements and are available with a wide range of mechanical and elastic properties, enabling flexibility in design. Both soft and hard setting epoxies are available, and loading of these has been demonstrated to enable further control over acoustic properties. Elastic stiffness is important as it controls the damping experienced by the ceramic, which in turn varies the emphasis between bandwidth and sensitivity enhancement. This also controls damping of laterally propagating modes of vibration, thus influencing the achievement of unimodal thickness vibration.

It is generally acknowledged that using a softer epoxy, with lower elastic stiffness and density, will achieve enhanced coupling efficiency due to the reduction of lateral

clamping and the near independent pillar vibration that results. Softer epoxies could also be considered desirable in air due to the improved impedance match, as they generally possess lower specific acoustic impedance. With soft epoxies, however, thickness mode coupling efficiency is a misleading indication of performance, as it neglects the importance of surface dilation quality. This is highlighted in work presented by Hayward and Bennett [35], where harmonic finite element modelling was used in conjunction with a laser vibrometer system to determine impedance profiles and surface dilation quality with hard and soft setting epoxies. This clearly demonstrates the near unimodal behaviour when soft epoxy is used, but the average relative surface displacement at resonance is shown to be significantly reduced, thus reducing the overall sensitivity of the device. Perfectly uniform surface vibration, where the pillars and the epoxy vibrate in perfect unison, is indicated by a dilation quality of 1.0. Surface dilation qualities of 0.960 and 0.860 at the centre frequency were indicated by the finite element modelling for the hard and soft setting epoxies respectively. Softer epoxies are therefore more applicable when wideband, unimodal operation is more important than sensitivity, since the vibrating pillars will experience a much higher degree of damping. For application in air-coupled NDT, where poor system sensitivity is the dominant factor, it would be advisable to use a hard setting epoxy. Reduced mechanical loss within the epoxy, however, means that additional care must be taken regarding the frequencies of inter pillar modes of vibration.

Another parameter that has been given consideration is the Poisson ratio (σ) [43,44] of the passive filler material. In an isotropic medium, this value is defined as:

$$\sigma = \frac{-\text{LateralStrain}}{\text{LongitudinalStrain}} \quad \text{Equation 4.1}$$

In most cases this results in a positive value since a stress applied along one axis will normally result in strains of opposite sign in the lateral and longitudinal directions. In the passive phase of a composite transducer with an incident pressure, this would relate to the degree of lateral expansion over the thickness contraction or the degree

of lateral contraction over the thickness expansion. It is desirable to minimise this effect since it would be in opposition to the motion of the ceramic pillars. Generally, the lower the Poisson ratio of the passive material used, the more efficient the composite. There is considerable benefit in using a passive material with a Poisson ratio of zero and so provides no resistance to the motion of the pillars. Smith [43] has even suggested that performance could be further enhanced with the introduction of a negative Poisson ratio material, which would provide assistance to the motion of the pillars. Although such materials do exist; theoretical results presented indicate that only very limited additional benefit would be provided with their use. This is a conclusion that has since been reinforced by Hayward *et al* [44], using finite element analysis.

Epoxy	Name	Density kgm ⁻³	Impedance Mrayls	Poisson Ratio	Young's Modulus	V ₁
Hard set	CY1301/	1140	3	0.35	6.0	2631
	HY1300					
Soft set	CY208/	1150	1.9	0.40	2.2	1652
	HY956					

Table 4.2 Characteristics of two epoxies with hard and soft setting properties.

Table 4.2 highlights the important properties of the two epoxies assumed throughout this work for hard and soft setting applications. Note that the hard setting epoxy has a lower value for Poisson ratio, thus further strengthening the case for its use. Hayward showed that this value for the hard set can be reduced further, to around 0.1, with the introduction of glass microballoons. This was also noted to produce a reduction in specific acoustic impedance, however an associated reduction in sensitivity eliminates this approach as an option for an air-coupled NDT application.

4.2.5 Aspect Ratio and Pillar Geometry

In the quest for unimodal operation, careful consideration must be given to the shape and dimensions of the ceramic pillars, as these can have significant bearing on the

strengths of both inter- and intra-pillar parasitic lateral modes of vibration. The requirement for fine lateral dimensions to enable efficient operation and valid assumption of vibrational uniformity, translates to a requirement for tall thin ceramic pillars, or a low pillar aspect ratio (width / height). Manufacturing constraints and the selected volume fraction, however, limit the extent to which this is possible. Two papers known to the author [34,35] use finite element analysis to determine the limiting dimensions for efficient operation including the influences of pillar shape, volume fraction and constituent material parameters. One of these [35], defines a maximum pillar aspect ratio (MPAR) and provides values that are compatible with homogeneous operation for a range of volume fractions and pillar shapes.

Reduction of the pillar aspect ratio is in practice a less demanding manufacturing problem with low volume fraction composites. However, the suggested MPAR values become very much lower as the volume fraction is reduced. This is because a combination of low volume fraction and high aspect ratio results in increased separation of the pillars relative to the transducer thickness. When a polymer with low mechanical loss is assumed for improved dilation quality, strong lateral vibrations can then occur. For a hard setting polymer, the suggested MPAR drops from 0.47 to 0.17 for transducers with 70% and 20% volume fractions respectively, corresponding to the suggested volume fractions for an unmatched composite transducer pair for air-coupled pitch-catch operation.

In addition to square pillars, cylindrical and triangular pillar shapes have also been investigated, again with a view to suppression of lateral resonant activity. Cylindrical pillars have been shown not to possess any significant advantage over square pillars, but triangular pillars do have some potential. Success depends on alignment of the pillars such that no two pillars offer parallel sides. However, in practice, a limited reduction in lateral modes, enabling less stringent MPAR values for low volume fractions, is considered inadequate compensation for the increased manufacturing effort and expense that would be required.

4.2.6 Backing and Matching Considerations

Transducer bandwidth can be increased with the introduction of mechanical damping at the back face of the device. The acoustic match with the transducer is altered in order to vary the amount of energy absorption at the boundary. Reducing the mismatch will increase the amount of energy absorbed, thus shortening the duration of the internal signal reverberations and broadening the bandwidth. The amplitude of the acoustic signal output at the front face, however, is reduced as a consequence. Hayward and Gachagan [27] conducted theoretical investigations under various damping conditions in air and noted a 17dB reduction in sensitivity when undamped and fully damped conditions were compared (where “fully damped” corresponds to a backing specific acoustic impedance equal to that of the transducer). It is obvious that in the present narrowband, low SNR application, no reduction in sensitivity can be tolerated and bandwidth improvement offers no advantage. Mechanical damping would therefore not be a sensible consideration for the current air-coupled system and air backing is selected.

The theory of front face mechanical matching and a novel approach to overcoming the practical problems encountered in air will be presented in Chapter 5. The introduction of a layer (or multiple layers) between the transducer and the load medium can be used to increase the energy coupled to and from the load by acting as an acoustic transformer. This is shown to be a very important consideration in the successful completion of an air-coupled system.

4.2.7 Array Considerations

One important consideration is the ease and success with which an array transducer can be produced for the receiver of the proposed system. Although no air-coupled composite array system is known to the author, composite transducers have long been established as a suitable technology for arrays in biomedical [45] and sonar [46] applications. The main reason for this is that an array can be easily fabricated from a single device by adopting selective electroding. Element acoustic isolation is conveniently achieved by separation of the elements with a row of the epoxy in the passive lattice. Efficient design to eliminate inter-pillar resonances, as discussed

above, should ensure minimal element cross talk. These benefits are thought to be equally applicable to operation as an air-coupled receiving array. A potential problem, however, is sensitivity reduction resulting from the necessarily small active areas to meet resolution requirements.

4.2.8 Summary

In the work of this research, emphasis has been placed on the achievement of sensitivity enhancement at the expense of bandwidth. For this reason, back face acoustic loading should not be included. It is also clear that significant advances could be made if efficient acoustic matching to an air load was achieved. The achievement of favourable transducer mechanical properties has been shown to be more effective in reception than in transmission, the latter benefiting from superior electrical properties that enhance drive capabilities. This is linked to the fact that electrical and mechanical resonances dominate in transmission and reception respectively. Consequently, a compromise between the requirements for electrical and mechanical property optimisation has been shown to be achieved with the use of 20%-40% volume fraction receivers and 50%-70% volume fraction transmitters, depending on the nature of the acoustic matching. Also, f_e of the transmitter should coincide with f_m of the receiver, the ceramic phases of which should be PZT-5H and PZT-5A respectively.

The importance of uniform surface dilation quality must not be overlooked in the process of enhancing the thickness mode coupling efficiency. A relatively hard setting epoxy should therefore be used as the passive phase. Ciba-Geigy CY208/HY956 is known to fulfil requirements. Due to its susceptibility to supporting laterally propagating energy, care must be taken to avoid encroachment of lateral resonances into the frequency band of the thickness mode resonance. In general this necessitates a requirement for tall thin pillars with 0.47 and 0.17 MPAR values for transmitter and receiver respectively.

4.3 Electrostatic Transducer Technology

4.3.1 Introduction

The problem of overcoming the acoustic impedance mismatches between the transmission and reception devices and air is intrinsically linked with the improvement of air-coupled sensitivity. Electrostatic (or capacitive) transducers are well suited to addressing this problem because of the mechanisms and materials defining their operation. Generally speaking, an electrostatic transducer is a capacitor with two conducting electrodes separated by a dielectric material. Figure 4.2 shows a simple schematic representation of the main components.

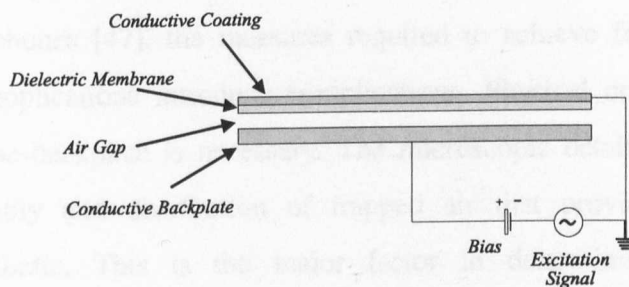


Figure 4.2 Schematic diagram of a simple electrostatic transducer.

A solid conducting plate forms the back positive electrode and serves as the support for the transducer structure. A thin polymer membrane is then stretched in front of this backplate, providing the dielectric separation for a metallic coating on its outer surface that forms the front earth electrode. The membrane is pulled against the backplate under the influence of an electrostatic force provided by a D.C. bias voltage. In transmission, an alternating voltage, which can be either continuous, tone burst or impulsive, is modulated onto the bias voltage. This produces an alternating electrostatic force, resulting in vibration of the membrane at a frequency determined by the excitation signal. This in turn produces longitudinal pressure waves in the load medium. In reception, an incident pressure wave causes motion of the membrane, resulting in a changing capacitance as the distance between the membrane and the backplate fluctuates. If the load impedance is sufficiently large, the charge in the system may be considered constant, so the measured voltage variations are a direct indication of the incident pressure. Transduction is therefore achieved with the vibration of the

metallised membrane, and since these are available down to $2\mu\text{m}$ thickness, an extremely close acoustic match with air is possible due to the low density of the vibrating medium. In addition to improvement of acoustic impedance match, electrostatic technology provides other distinct advantages over piezocomposites for some applications. Close contact between the membrane and backplate results in a high degree of damping and an inherently wideband frequency response. Also, performance has been shown to be essentially reciprocal, thus enabling efficient pulse echo operation.

Although the principles of this technique have long been established in the form of condenser microphones [47], the measures required to achieve frequencies that are useful in NDT applications introduce complications. Physical contact between the membrane and the backplate is necessary. The microscopic details of the backplate control the quantity and distribution of trapped air that provides space for the membrane to vibrate. This is the major factor in determining the transducer characteristics. For this reason, most research effort has concentrated on the development of novel backplate configurations in an attempt to achieve repeatable designs with specific characteristics.

Other design variables that merit consideration include membrane thickness, tension and attachment, as well as bias and excitation voltage effects. The relative importance and interaction of the various design parameters is not fully understood, however, and there have been conflicting reports on the findings by different workers involved in the field. The complexity of the technology has inhibited the successful mathematical modelling of the devices. Although several strategies have been proposed, a definitive solution, successful in both sensitivity and frequency predictions, has not yet been developed for standard designs, and experimental verification has often proved difficult. Promising results have been achieved recently, however, as a result of more precise manufacturing techniques, novel design approaches and finite element modelling.

4.3.2 Membrane Considerations

The most commonly used membrane materials are the commercially available Mylar and Kapton, metallised on one face with either gold or aluminium. At present, these are available in thickness ranging from $2\mu\text{m}$ to $13\mu\text{m}$. The two most comprehensive studies of the membrane effects known to the author were conducted by Carr and Wykes [48] and Hietanen *et al* [49]. Carr concluded that there is a linear relationship between the resonant frequency and the inverse square root of the membrane thickness. Hietanen, however, suggested that the resonant frequency had a linear relationship with the inverse of the mass per unit area of the membrane. Disagreement also exists in relation to the effects of the membrane tension. Carr noted that, although the applied tension had little bearing on the resonant frequency and bandwidth, there was a particular tension at which maximum transmission sensitivity was achieved. In contrast, Hietanen concluded that variation of the tension had no appreciable effect on sensitivity. These contradictions highlight the difficulty of repeatability with electrostatic technology and make for uncertainty regarding the most appropriate design approach.

Although membranes of $2\mu\text{m}$ thickness are available in order to achieve maximum bandwidth and centre frequency, it has been noted that membranes below $5\mu\text{m}$ thickness introduce additional manufacturing complexity due to wrinkling under the bias field, and do not possess sufficient robustness for most practical applications. The dielectric strength of the membrane must also be sufficient to withstand the applied bias voltage without breaking down or allowing the gradual displacement of static positive charge between the electrodes. Hietanen *et al* [49] have shown that failure to comply with this requirement results in the degeneration of the transducer sensitivity performance over time.

The physical contact of the membrane with the backplate has been considered by Rafiq and Wykes [50] who produced a backplate with a convex curve of radius 4m . This measure ensured contact of the membrane with the backplate surface, resulting in more repeatable performance, and was prompted by the realisation that large

bubbles of air were sometimes trapped when the backplate is brought into contact with the membrane. The curve on the backplate provided a path for air to escape.

4.3.3 Backplate Considerations

As mentioned previously, the dimensions and structure of the backplate are known to be the most influential factors in determining the overall characteristics of the device. There have been three separate approaches to the development of backplates. Initially, the two approaches most commonly adopted were the use of randomly rough backplates, where characteristics were altered by the degree of roughness, or grooved backplates, where the size, shape and orientation of the grooves determined performance. The recent application of micro-machining technology, however, has enabled control of the backplate surface structure with a much higher degree of accuracy than was previously possible, and has introduced the possibility for more ambitious design approaches. In all cases, however, the principal aim has been to control and understand the effects of the air trapped between the membrane and the backplate. This determines the degree to which movement of the membrane is restricted and influences the frequency, bandwidth and sensitivity of the transducer.

a) Random

The use of randomly rough backplates is the simplest manufacturing approach to the development of an electrostatic transducer, although the inevitable uncertainty of important parameter values has made quantitative analysis difficult. The membrane is supported by discrete points of contact with the backplate, resulting in a random array of individual resonators or sub-membranes. Each sub-membrane will have unique characteristics depending on the separation of the points of contact, the depth of the air-gap and the tension experienced by the membrane. It can therefore be assumed that the resonant frequency and sensitivity will vary across the active surface of the device and extremely wideband operation is possible.

In order to explain the operation of the random structure at a basic level, Carr and Wykes [48] adopted the idea that a comparison with the theory for a frictionless piston

could be made. This assumed that motion of the membrane is constrained by the spring constant of the air-gaps and indicated that the resonant frequency would be inversely proportional to the square root of the depth of the air-gap (referred to as the 'air-gap model'). Carr noted that an alternative model, considered by Warren [51] and others, suggested that the resonant frequency relied mainly on the horizontal separation of the points of contact (referred to as the 'surface wavelength model'). The resonance of each sub-membrane would then be inversely proportional to the distance between the points of contact, as is the case with a flexible supported membrane.

These models were tested by Carr against experimental data obtained using optical methods. Although it was conceded that measurement of backplate characteristics was difficult, and calculations depended on estimated average values for surface parameters, both models were noted to be reasonably accurate, with the air-gap model performing slightly better. It must be concluded, however, that neither of the proposed models is capable of providing more than just an indication of performance trends associated with various parameters, particularly when random backplates are used. A successful model would have to combine both of these effects, and to consider other factors including randomly varying membrane tension and charge distribution. The effects of randomly rough backplate characteristics could be broadly summarised by noting that the resonant frequency is inversely proportional to the average roughness of the surface. It is evident, however, that the use of random backplates will always have an element of uncertainty and that more detailed control over the structure would be required in order to provide repeatability and enable more accurate modelling of transducer performance.

b) Grooved

The use of grooved backplates presents a more realistic solution to the problems of repeatability and the production of a transducer with specific characteristics. Several different configurations have been considered, including either rectangular or V-grooves with either concentric or parallel orientation, and various possible modelling strategies have been proposed with varying degrees of success. In all cases, the structure consists of an array of equally spaced sub-membranes with similar

characteristics, and effectively reduces the complexity of the problem. Although the performance of these backplates is more controllable than with the random approach, there are still several parameters capable of affecting frequency and sensitivity performance. Frequency response in particular is known to be influenced by a number of surface detail parameters. In common with random backplates, there are surface wavelength and air-gap resonances due to the groove pitch and depth. In the case of rectangular grooves, a random resonance will also exist due to the surface roughness on the rails separating the grooves. Finally, when the grooves are V shaped, the angle of the groove has been noted to have an influence. Regardless of which of these has the greatest effect, it is clear that the frequency response is potentially multi-peaked. As a result, the frequency response is generally more narrowband than the random approach although sensitivity performance would be enhanced if resonances could be made to coincide.

Rafiq and Wykes [50] used the frictionless piston model (later adopted by Carr for random backplates) in order to develop a successful method for the design of V-grooved backplates producing any specified centre frequency in the range 30-200kHz. Although the frequency response was noted in a practical examination to be multi-peaked, it was concluded that groove pitch was the main backplate parameter in determining the resonant frequency. Rafiq also investigated a commercially available rectangular grooved backplate device made by Polaroid. The results in this case suggested that the surface finish on the rails was a crucial parameter, since when these were polished lightly with a cloth, the centre frequency changed from 55kHz to 100kHz. This work was later complemented by Carr and Wykes [48], who considered a rectangular groove structure, and provided experimental evidence that the groove depth and rail width had little bearing on the resonant frequency which was controlled primarily by the groove pitch.

An electrical equivalent circuit for a V-grooved electrostatic transducer was presented by Matilla *et al* [52] and used with considerable success in predictions of both frequency response and transducer sensitivity for resonant frequencies between 20 and

80kHz. The work presented here, however, favoured the use of groove depth rather than groove pitch in the calculation and also considers the problem of designing the electrical interface to the transducer to optimise noise performance and improve sensitivity.

Hietanen *et al* [49,53,54] conducted a series of investigations into the performance of V-grooved backplates. A Helmholtz Resonator model [49] was used in order to predict the performance of a single groove which was considered representative of the whole structure. This approach made the assumption that the sound wavelength is greater than the individual dimensions of the resonator. Again, in contrast to Rafiq's findings, he concluded that the depth of the grooves, in addition to the mass per unit area of the membrane, provides sufficient information to predict the transducer resonant frequency. At a later stage, however, in a purely experimental analysis [53], it was conceded that groove pitch and angle would also have an influence. Most recently [54], he presented methods for predicting electric field and charge distribution in a single groove. This serves as a valuable step towards a more comprehensive understanding of transducer behaviour.

The relatively simple geometrical construction of the V-groove approach indicates that finite element modelling may provide a useful insight into transducer performance. Adamowski *et al* [55] have attempted this, resulting in successful predictions of transducer centre frequency. The calculations, however, did not take into account the damping effect of the air inside the groove, with the consequence that bandwidth was significantly overestimated.

In the light of the various modelling and experimental approaches that have been proposed, and the similar success of fundamentally different suggestions, it is difficult to reach a conclusion regarding the method offering the most potential. Collectively, these studies provide a valuable insight into the various possible performance influences with grooved backplates. It is clear, however, that the microscopic level at which differences evidently occur, result in variations depending on the manufacturing

and test approaches adopted by different workers, even when the devices being considered are nominally identical. Also, repeatability in manufacture, even when the same technique is adopted, has been limited to devices with operating frequencies below 200kHz. This has been due to an inability to achieve sufficiently fine and controllable backplate dimensions in manufacture, thus severely restricting the usefulness of the technology, and further emphasises the requirement for tighter manufacturing control.

c) **Micromachining Techniques**

Recent advances, achieved with the use of micro-machining technology, have gone some way to overcoming the problems of manufacturing repeatability and limited centre frequency, and have extended the useful application range of the electrostatic approach. In particular, the use of electrostatics to achieve air-coupled NDT has been proposed and successfully demonstrated in laboratory conditions. Control of the structure at a microscopic level has also enabled a more successful and comprehensive modelling approach to be formulated for higher frequency operation. Finally, a novel micro-machining approach to produce repeatable operating frequencies up to 11MHz has been developed. This work has been complemented with the development of a successful modelling strategy for the technique.

Schindel and Hutchins [56,57] have used a combination of photolithography and chemical etching to produce a uniform grid of 40 μ m diameter pits in a polished silicon wafer. A conducting layer is then evaporated onto this surface that is then used as the back electrode of the device. Metallised dielectric films are then used as the vibrating membrane in the conventional manner. This approach has been demonstrated to provide excellent repeatability and enable controllable, -6dB bandwidths up to 2.3MHz. The resonant behaviour of the grooved approach has been avoided and control over the bandwidth is exercised through simple alterations of the bias voltage, film thickness and excitation signal [58]. These devices have been shown to possess considerable potential in a number of air-coupled applications, however only empirical verification of the approach has been provided to date, with no attempt to explain the

theory associated with the backplate design variables. Wideband through transmission in air has been demonstrated as a possible resonance method of thickness gauging, and narrowband through transmission has been used in the non-destructive identification of defects including impact damage and inclusions in CFRP plates [56]. Surface profiling and distance measurements have also been investigated using a focused, pulse echo approach [57].

Micro-machining techniques have been adopted by Anderson *et al* [59] in order to produce more conventional grooved structures with finer dimensions and greater accuracy than was previously possible. This has enabled repeatable production of higher frequency devices, and provided a more solid platform from which to proceed with a theoretical study. The electrical equivalent circuit model that is presented considers the groove geometry, membrane mechanical stiffness and the applied tension, as well as all relevant electrical parameters. Predictions of electrical admittance and transmit sensitivity, as a function of frequency, over the range 50 - 500kHz, are made and correlate well with supporting experimental results.

Haller and Khuri-Yakub [60] devised a micro-machining technique that resulted in a 1-3 structure comprising a silicon nitride membrane supported above a heavily doped silicon backplate by a regular array of silicon dioxide posts. This was achieved by performing a time controlled chemical etch of a silicon dioxide sacrificial layer through a grid of 3 μ m diameter holes in the membrane layer. In contrast to Schindel's devices, the frequency response is essentially resonant, with the centre frequency determined by the separation of the pillars, which controls lateral clamping, and 3dB bandwidths were measured at approximately 20%. Again, an electrical equivalent circuit model is proposed, but in this case the fundamental theory was extracted from work performed previously by Mason [61], which assumes a suspended membrane under tension. This was considered to be a good approximation for each sub-membrane, since the restoring force due to the compressed air between the membrane and the backplate is negligible when compared to that of the membrane itself. Experimental measurements of electrical resistance and capacitance, membrane displacement, and insertion loss were

made as a function frequency up to 2MHz and close correlation with the theoretically predicted values was demonstrated. A continuation of this work, reported by Ladabaum *et al* [62], has recently revealed a capability of the technology to produce resonant frequencies up to 11MHz.

It is clear, therefore, that the future of electrostatic transducer production must be directed towards the use of micro-machining techniques. Centre frequencies and bandwidths far beyond those possible with even the random approach have been demonstrated and repeatability in manufacture is ensured to a microscopic degree. This technique could offer other advantages since the integrated circuit technology would make for simple and inexpensive mass production. Integration of control electronics and receiver amplifiers into the backplate silicon would also be possible using normal IC techniques.

4.3.4 Bias Voltage Effects

The effects of varying the bias voltage have been investigated by a number of researchers. The general consensus has been that increasing the bias voltage improves the sensitivity and increases the centre frequency and bandwidth of the device, but only up to a point. Hietanen *et al* [49] concluded from theoretical analysis that the sensitivities in both transmission and reception are directly proportional to the applied bias voltage. He then showed experimentally that the limiting factor on this is the dielectric strength of the membrane, and suggests a guideline of 20 volts per μm thickness of the membrane. Carr and Wykes [48] also noted that the resonant frequency increases with bias voltage, and suggest that this is due to a reduction in the air-gap size as the membrane is pulled tighter. Similar observations by Schindel *et al* [58] point out that the increased frequency with bias voltage could also be due to increased tension in the membrane. Hutchins *et al* [63] have recently reported on an approach that eliminates the requirement for an externally applied bias by using an alternative membrane. He uses an electret film that has been permanently polarised by high temperature application of a large D.C. voltage and suggests that excellent response is achieved in terms of both sensitivity and bandwidth.

4.3.5 Array Considerations

There exists evidence of the ability of electrostatic transducers to operate successfully in air as an array. Higuchi *et al* [64] used micromachining technology to develop a phased array for robotic proximity sensing applications. Selective backplate electrode deposition was used to define 32 linear array elements at 1mm pitch. The use of a membrane with 12 μ m thickness, however, limited operational frequencies to below 200kHz. Elements were shown to possess similar characteristics, although reception sensitivity was poor. More recently, Munro and Wykes [65] also produced a phased electrostatic array for operation in air. Several possible manufacturing approaches were attempted for operation at 100kHz and reasonable performance consistency across the array aperture was demonstrated for the best case. This was used to produce a 2-D range map of an angled 30mm square cube at a distance of 300mm. Schindel *et al* [58] also suggested that a convenient method of defining elements would be to perform selective doping of the backplate silicon when micromachining methods were used.

4.3.6 Summary

Electrostatic ultrasonic transducers are undoubtedly a well matched, potentially wideband, high frequency source or receiver, when operating in the air environment. This is primarily due to the low density membrane used as the electro-acoustic interface and the high degree of damping provided by the close contact with a backplate under the influence of a D.C. bias. Performance is critically dependent on the microscopic surface details of the backplate and the resulting pockets of air that are trapped between it and the membrane. The optimum frequency of operation increases as the horizontal separation between points of contact of the membrane and backplate decreases and the depth of the air-gap is reduced, although precise design guidelines are not available for standard manufacturing techniques, due to the microscopic level at which changes occur. Reducing the thickness of the membrane is known to result in increased sensitivity and higher frequency response. This is also the case when the applied bias voltage is increased. Robustness requirements

restricted the reduction membrane thickness however, and the bias voltage cannot exceed the dielectric breakdown of the membrane.

A limited degree of performance repeatability has been achieved by machining grooves in the backplate, and high frequency wideband performance is possible by using polished backplates. A combination of high frequency, wide bandwidth and repeatability has been achieved only recently, however, by adopting micromachining techniques. The introduction of these methods has significant implications for the range of applications open to electrostatic technology, however caution is required when evaluating the results presented to date. Although it may be possible to produce ultrasonic pressure in air at 11MHz, it is unclear to what practical use this can be put, given that measurements were made within 2mm of the surface. Not only are there limitations due to frequency squared dependence of sound attenuation in air, but obvious practical difficulties are encountered due to the lack of robustness of the membranes required to produce such high frequencies.

4.4 Experimental Evaluation

4.4.1 Introduction

A solid background knowledge of the theory behind each technology having been acquired, it was necessary to conduct a detailed experimental comparison of their respective attributes, in order to enable selection of one technology in preference to the other. For this purpose, a range of devices, including 1-3 connectivity composites with different volume fractions and mechanical loading conditions, and electrostatics with different membrane and backplate characteristics, was manufactured. Although it has been concluded that narrowband operation would appear to be preferable in the application of air-coupled NDT, a comprehensive comparison of the technologies requires consideration of transmission response under wideband excitation conditions and reception response to an incident impulsive pressure. Consequently, a wideband piezopolymer transmitter and a membrane hydrophone receiver, both of which are calibrated for air-coupled operation, were used to achieve through air system impulse

response characterisation. The absolute pressures produced in air for a known transmitter excitation, and voltage responses to a known incident pressure have been compared. Insertion loss details have also been calculated for both technologies under narrowband and wideband conditions. In addition to sensitivity performance, other important considerations exist for the proposed application. Relative focusing capabilities have been compared by making beam profile analyses of the devices under focused conditions. Finally, the suitability of the technologies to operate reliably in the relatively hostile aerospace industrial environment has been assessed.

Mnemonic	Volume Fraction	Ceramic	Matching	Backing	Coupling Coefficient (k_t)
C20	20%	PZT5A	None	None	0.446
C20B	20%	PZT5A	None	3.2MRayl	0.476
C30ML	30%	PZT5A	Double	None	0.612
C40	40%	PZT5A	None	None	0.591
C40MLB	40%	PZT5A	Single	8MRayl	0.577
C60	60%	PZT5A	None	None	0.587
C60B	60%	PZT5A	None	8MRayl	0.586
C70ML	70%	PZT5A	Double	None	0.570
C70	70%	PZT5H	None	None	0.622
PZT5H	100%	PZT5H	None	None	0.470

Table 4.3 Summary of the composite transducers manufactured to perform experimental comparison.

4.4.2 Transducer Manufacture

a) Composite

The doubly periodic square pillar approach shown in Figure 4.1 was adopted for the work of this research. The standard ‘dice and fill’ technique [66] was used in the manufacturing process, where a solid polarised block of ceramic was first diced using a diamond wire saw, and then potted with a low viscosity epoxy prior to curing. Table 4.3 summarises the characteristics of the various composite devices

manufactured, all of which included a hard setting epoxy filler (CY1301/HY1300). A solid (i.e. non composite) PZT5H device is included for comparison. Operational frequencies were measured at $550\text{kHz} \pm 10\%$. Silver paint was used to deposit electrodes, and fundamental thickness mode frequency measurements were performed using an impedance analyser. This enabled the frequencies of electrical and mechanical resonance to be obtained, from which the electromechanical coupling coefficients (k_t) were calculated. The effects of ceramic depolarisation due to the dicing process can be seen by the slightly lower than expected values for k_t . Repolarisation is possible with the application of a high voltage ($\sim 2\text{kV}$), at high temperature, but the limited benefit was thought not to merit the setting up of such a facility. The diameter of all devices was 30mm and the housing comprised a cylindrical screened case made of mild steel, with a BNC connector at one end to facilitate electrical connection to the two transducer electrodes. Composites C30ML and C70ML both included a novel front face matching layer that will be discussed in detail in Chapter 5.

b) Electrostatic

The design of the electrostatic transducers used is shown in Figure 4.3(a) and Figure 4.3(b) shows the electrical circuitry that is required to apply the bias voltage without causing damage to either the excitation equipment in transmission or the amplifier in reception. Commercially available Mylar film, coated on one side with aluminium, was used in all cases to form the vibrating membrane that was pre-tensioned between two aluminium rings. The conducting backplate is electrically isolated from the rest of the transducer assembly by a removable perspex plug. Three tension screws then enable the non conducting side of the membrane to be brought into contact with the backplate and tension to be applied as required. A summary of the various devices manufactured is presented in Table 4.4. A randomly rough approach has been adopted in all cases with a variation in average roughness ($3\mu\text{m}$, $9\mu\text{m}$, $50\mu\text{m}$) achieved using a commercial lapping and polishing machine.

Mnemonic	Membrane Thickness	Backplate	Average Roughness	Bias Voltage
PS-2.5	2.5 μ m	Polished Steel	3 μ m	120V
LA-2.5	2.5 μ m	Lapped Aluminium	9 μ m	120V
RB-2.5	2.5 μ m	Rough Brass	50 μ m	120V
PS-3.5	3.5 μ m	Polished Steel	3 μ m	200V
LA-3.5	3.5 μ m	Lapped Aluminium	9 μ m	200V
RB-3.5	3.5 μ m	Rough Brass	50 μ m	200V
PS-5	5 μ m	Polished Steel	3 μ m	250V
LA-5	5 μ m	Lapped Aluminium	9 μ m	250V
RB-5	5 μ m	Rough Brass	50 μ m	250V

Table 4.4 Electrostatic transducers manufactured to perform experiments.

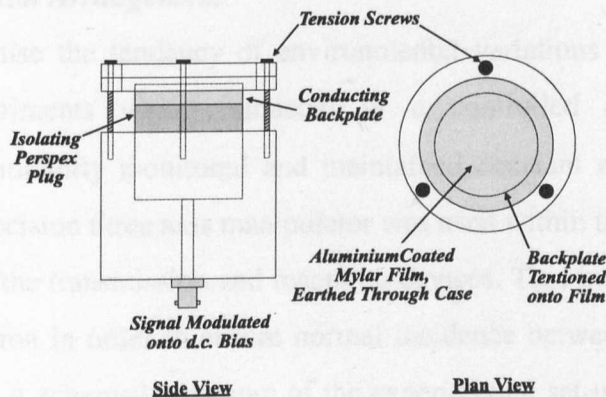


Figure 4.3(a) Construction of electrostatic transducers

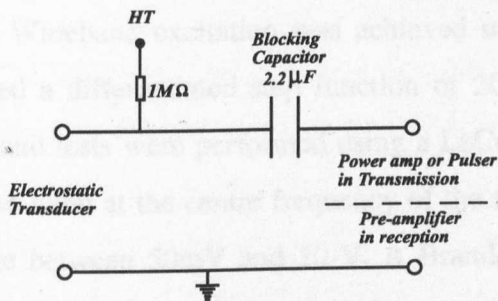


Figure 4.3(b) Electrical decoupling circuitry required for electrostatic operation.

It is not considered a major limitation that a more sophisticated manufacturing method, such as grooved or micromachined backplates, has not been adopted since no significant improvement in sensitivity has been reported, and the main aims of these techniques have been to achieve manufacturing repeatability, wide bandwidth and high frequency performance. Three different thicknesses of membrane were considered (2.5 μm , 3.5 μm , and 5 μm) to enable evaluation of a more comprehensive selection of devices. A BNC connector enabled electrical connection to the backplate and grounded the rest of the assembly, including the aluminium coated front face of the membrane. To ensure valid comparison between the two technologies, circular backplates with 30mm diameter were used to present the same active area as the composites. As expected, the random approach lacked the resonances of grooved backplates, resulting in a relatively wide operational frequency range in all cases. Bias voltages were selected by a process of trial and error to identify the most sensitive setting for each membrane.

4.4.3 Experimental Arrangement

In order to minimise the tendency of environmental variations in air to influence results, all experiments were conducted in a controlled environment, with temperature and humidity monitored and maintained constant at 20.5°C and 40% respectively. A precision three axis manipulator was used within this environment for the positioning of the transmission and reception devices. This included a facility for angular manipulation in order to ensure normal incidence between transmitting and receiving devices. A schematic diagram of the experimental set-up, including details of wideband and narrowband testing of both composites and electrostatics, is shown in Figure 4.4. Wideband excitation was achieved using a Panametrics pulser unit which generated a differentiated step function of 200-V with a rise time of 10ns, while narrowband tests were performed using a LeCroy arbitrary function generator to supply a tone burst at the centre frequency of the transmitter, with a desired peak to peak voltage between 50mV and 10-V. A Brandenburg variable voltage supply was used to supply the bias voltage when electrostatic transducers were being tested and the decoupling circuit of Figure 4.3(b) was also included.

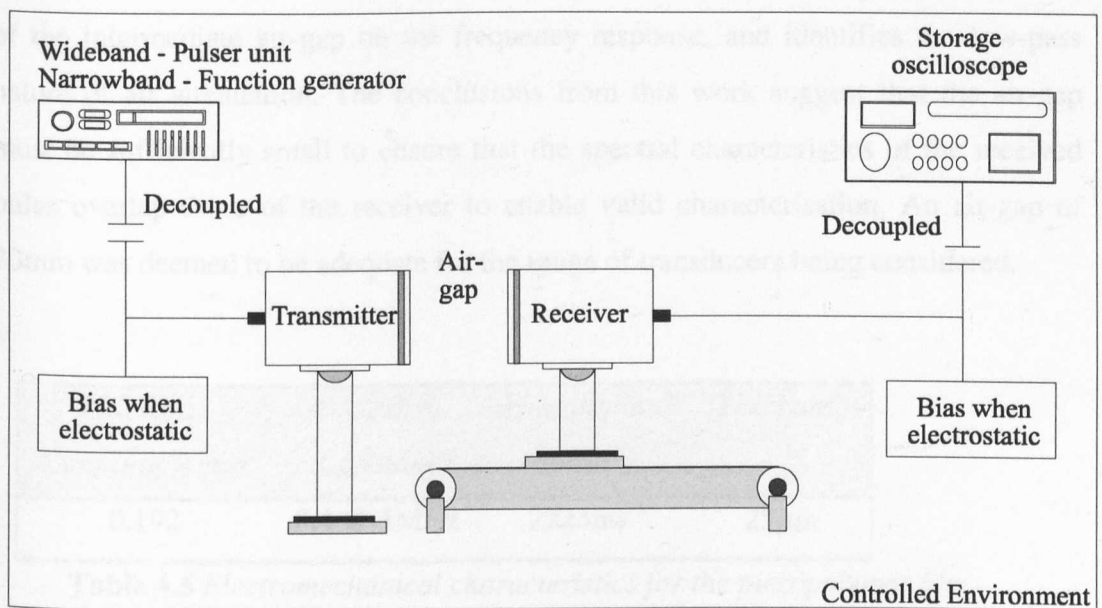


Figure 4.4 *Experimental arrangement for electrostatic and composite, wideband and narrowband comparison experiments.*

Wideband PVDF transducers were utilised to make calibrated transmission and reception measurements. Suitable characteristics of PVDF for this purpose include low specific acoustic impedance and potentially wide bandwidth. It has also been shown [67] that PVDF probes can be manufactured that approximate well to an ultrasonic plane wave source. This is an important consideration in characterisation applications where it is necessary to minimise response variations due to aperture diffraction. Although low dielectric constant and coupling factor result in poor drive performance in transmission, overall the benefits were thought to outweigh the disadvantages.

The wideband PVDF transmitter used was designed and manufactured by Anthony Gachagan and Walter Galbraith within the ultrasonics group at the University of Strathclyde. Theoretical assessment was achieved using the linear systems modelling technique mentioned in Section 4.2, and detailed results are provided in [68]. The device used had a circular active area of 20mm diameter and was manufactured using PVDF film, details of which are given in Table 4.5. The film was bonded to a perspex block, which provided close to 100% backing, and enabled a potential

bandwidth of 20MHz. Theoretical analysis in [68], however, considers the influence of the intermediate air-gap on the frequency response, and identifies the low-pass nature of air attenuation. The conclusions from this work suggest that the air-gap must be sufficiently small to ensure that the spectral characteristics of the received pulse overlap those of the receiver to enable valid characterisation. An air-gap of 20mm was deemed to be adequate for the range of transducers being considered.

<i>Thickness</i>	<i>Dielectric</i>	<i>Longitudinal</i>	<i>Thickness</i>
<i>Coupling factor</i>	<i>Constant</i>	<i>velocity</i>	
0.192	8.4 @ 1MHz	2225ms ⁻¹	25µm

Table 4.5 *Electromechanical characteristics for the piezopolymer film.*

The linear systems model was also used to show that a membrane hydrophone, calibrated for use in water, could also be used to make absolute pressure measurements in air, providing the electrical loading is kept within certain limits. This is due to the fact that the cable capacitance dominates the hydrophone response, producing near identical spectral profiles for air and water between 50kHz and 5MHz. It is recommended that, in order to make this assumption, the parallel load resistance should be greater than 50kΩ and the end of cable capacitance, including any connectors or cable, should be greater than 50pF. The hydrophone used to make the absolute pressure measurements in air was made from bilaminar PVDF [69], and had a film thickness of 28µm and an active area of 0.2 mm². This small active area was necessary to avoid interference with the acoustic field profile because of the short wavelengths of ultrasound in air (0.3mm @ 1MHz). The calibration data for this device are shown in Table 4.6 and was used to calibrate the PVDF transmitter using the substitution method described in [70].

Frequency (MHz)	2	3	4	5	10
Sensitivity (nV/Pa)	53	53	53	54	59

Table 4.6 Calibration data for membrane hydrophone.

4.5.4 Wideband Characterisation

Conventional immersed transducer characterisation would normally be performed at or around the “near field-far field” boundary, corresponding to the last axial maximum of the spatial response. This minimises the risk of large signal variations with small differences in transducer positioning. For continuous wave operation in air, however, the reduced velocity and high attenuation mean that this would occur at around 350mm, with a magnitude considerably below the level of the maximum spatial response. The concept is therefore not strictly valid in air, and since the spectral characteristics are so severely influenced by attenuation, testing in the near field region was required. It was therefore necessary to determine field characteristics experimentally, in order to identify the position of peak transducer performance for each individual case. For wideband testing, this resulted in air-gap separations of between 17.5 and 23mm. The transmit, receive and pulse-echo characterisation results of sensitivity and bandwidth under wideband conditions are summarised in Table 4.7, with the most significant results represented in bold typeface.

	<i>Transmit Voltage Response</i>		<i>Open Circuit Voltage Response</i>		<i>Pulse-echo Impulse Response</i>	
	(dB re 1μPa/V)	-3dB B/W (kHz)	(dB re 1V/μPa)	-3dB B/W (kHz)	IL (dB)	-6dB B/W (kHz)
Composite						
PZT5H	116.8	19	-210.2	13		
C20	115	22	-200.9	19		
C30ML	122.3	71	-186.1	58	-113.3	5% @ 600
C40	116.8	54	-199.7	77		
C40MLB	118.8	148	-194.2	132	-101.5	25% @ 394
C60	117.9	22	-202.2	14		
C70ML	134.6	62	-188.8	41	-92.3	5% @ 601
C70	120.5	24	-204.5	15		
Electrostatic						
PS-2.5	120.1	806	-193.2	677	-97.3	90% @ 1403
LA-2.5	121.7	594	-196.9	632	-79.3	168% @ 672
7RB-2.5	122.4	458	-189.4	525	-77.1	126% @ 597
PS-3.5	118.6	587	-199.1	590	-99.5	92% @ 1220
LA-3.5	119.3	486	-204.1	556	-89.3	142% @ 645
RB-3.5	121.1	329	-193.7	483	-85.0	73% @ 551
PS-5	117.5	311	-201.8	375	-101.5	138% @ 470
LA-5	118.0	293	-206.6	348	-89.9	124% @ 457
RB-5	119.4	242	-196.3	322	-87.0	109% @ 403

Table 4.7 Results of the wideband characterisation experiments measured at close to 21mm separation where the peak transducer performance was identified.

a) Transmission Response Using PVDF Membrane Hydrophone

For evaluation of transmission voltage response, the voltage received by the PVDF membrane hydrophone was used to calculate the absolute pressure level at the source, resulting from an impulsive excitation by the pulser unit. Examination of these results reveals that the composite transducer C70ML provides the best transmission response in terms of sensitivity. This was expected to be the most sensitive

composite in transmission due to its theoretically desirable volume fraction of 70%, and the fact that it incorporates an efficient front face matching layer to further improve the acoustic impedance match with air. Air backing has also maximised sensitivity, although the bandwidth of only 62kHz is an indication of the narrowband nature of the technology. The most sensitive electrostatic (RB2.5) represents a reduction in sensitivity of 12.2 dB compared to the value for C70ML. Again, theory could have predicted that this would be the most sensitive electrostatic device, due to the fact that it had the largest average air-gap (providing the least degree of damping) and the thinnest membrane (providing the best acoustic impedance match to air). It should be noted, however, that in all cases the bandwidth of the electrostatics is significantly higher than the most wideband composite (C40MLB), which has achieved slight bandwidth enhancement at the expense of sensitivity, with the attachment of an 8MRayl tungsten loaded epoxy backing block. Note that the inclusion of the matching layer on C70ML has resulted in a 14.1dB improvement in sensitivity over the otherwise similar C70. Indeed, the only other major difference is that C70 is manufactured from PZT5H, which possesses superior transmitter characteristics to the PZT5A used for C70ML.

b) Reception Response Using PVDF Transmitter

Reception calibration data was acquired by using the PVDF transmitter to produce a known impulsive pressure at the surface of the receiving device under test and measuring the open circuit voltage response. In practice, this was achieved by measuring the voltage input directly to an oscilloscope channel with $1M\Omega$ input resistance. In accordance with the theory, the matched 30% composite (C30ML) provides the best reception sensitivity of the composites tested, at -186.1dB relative to $1V/\mu Pa$. Predictably, RB-2.5 is again the most sensitive electrostatic, however the response falls 3.3 dB short of matching that of the composite. Also, the bandwidths of the electrostatics are once again significantly superior to the composites across the range. Note that the bandwidth variation of the electrostatic devices closely follows the trends that are suggested by theory, that bandwidth increases with decreasing membrane thickness and decreasing average roughness.

c) **Pulse-Echo Response from a Flat Reflector**

A polished glass block was used as a normal reflector at a distance of approximately 10mm from the face of the transducer, to enable wideband pulse-echo tests to be made. Again, the received voltage was taken from an oscilloscope of input resistance $1M\Omega$. The temporal and spectral responses of the most sensitive electrostatic (RB-2.5) and the most sensitive composite (C70ML) are shown in Figures 4.5 and 4.6 respectively. From the results in Table 4.7, it is clear that the pulse-echo performance of the composite transducers tested is extremely poor, and that the electrostatics are superior in almost every case. Indeed, on the occasions where no value is displayed, there was insufficient signal to permit accurate measurement. This could have been anticipated from the theory discussed in Section 4.2 and serves to illustrate some of the important composite transducer design parameters. The fact that transmission and reception responses are optimised for quite different frequencies is compounded by the narrowband nature of the technology and volume fraction dependent performance, and severely inhibits design for reciprocal performance. The frequency response displayed in Figure 4.6b illustrates well the resonant frequencies associated with transmission and reception. The splitting of the upper two and the lower two peaks are due to the electrical and mechanical resonances of the transducer. The separation of the lower two peaks from the upper two peaks is due to a cavity resonance phenomenon, where the transducer and the matching layer react as a single layer due to energy entrapment. This will be discussed in detail in Chapter 5.

It is also interesting to note that the value of the frequency for peak spectral response for composite C40MLB is lower than expected at 349kHz. This is due to the sub-optimal matching and can also be attributed to the cavity resonance theory. The results indicate that the electrostatic transducers are well adapted to pulse echo performance. It is also important to note that the peak spectral response of the most efficient electrostatic device (RB-2.5) is very close to 600kHz. This was the operational frequency of the most efficient composites (C30ML and C70ML), thus further emphasising the validity of the comparison.

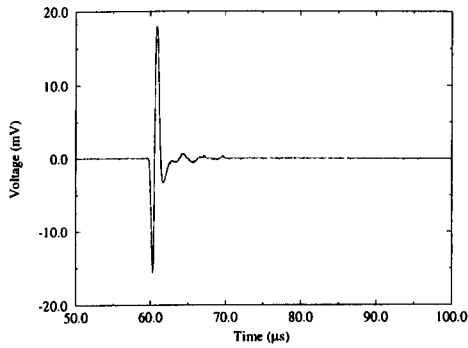


Figure 4.5 a) *Pulse-echo temporal response of RB-2.5 after wideband excitation.*

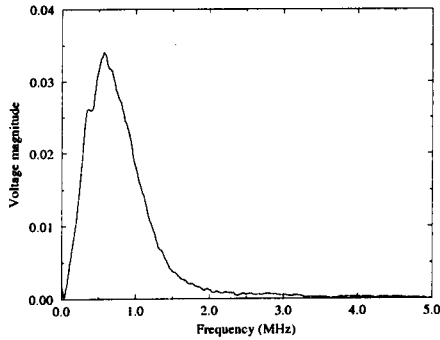


Figure 4.5 b) *Pulse-echo spectral response of RB-2.5 after wideband excitation.*

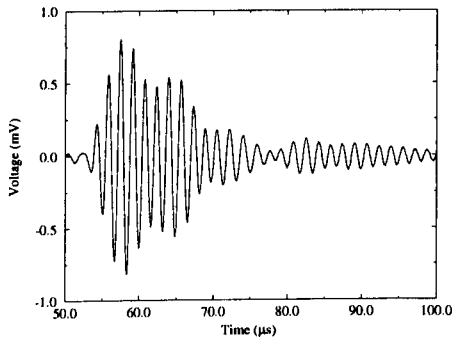


Figure 4.6 a) *Pulse-echo temporal response of C70ML after wideband excitation.*

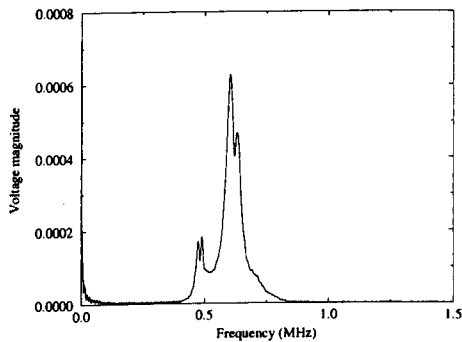


Figure 4.6 b) *Pulse-echo spectral response of C70ML after wideband excitation.*

4.5.5 *Narrowband Characterisation*

Narrowband comparison experiments were then conducted on those transducers identified as being the most sensitive. The LeCroy arbitrary function generator was used, in conjunction with a 50dB power amplifier, to produce a 75V peak to peak excitation signal of 20 cycle duration, at a frequency of 600kHz. This was used to facilitate narrowband transmit voltage response comparison of RB-2.5 and C70ML. Again, the membrane hydrophone was used as the reception device, and in both cases the air-gap was maintained at 20mm. The measured values of transmit sensitivities were 138.2 dB (relative to 1 μ Pa/V) and 126.8 dB (relative to 1 μ Pa/V) for the composite and electrostatic devices respectively. The expected improvement in the sensitivity response of the composite device is evident.

4.5.6 *Pitch-Catch Insertion Loss*

There have been several attempts at using the concept of insertion loss for the comparison of the sensitivity performance of different transducers in air [39,52,71,72]. Both one way and two way insertion loss results have been presented, although precise experimental details, enabling repetition and comparison of results, have often been omitted, and there has lacked until recently a definitive approach. For the present work, two way insertion loss is defined using the following expression:

$$IL = 20 \log_{10} \left(\frac{V_R}{V_I} \right) \quad \text{Equation 4.2}$$

V_R , in this case, is the voltage measured across a receiver operating into an open circuit, and V_I is the open circuit voltage supplied by the electrical excitation circuitry. In both cases, these measurements were performed in practice using an oscilloscope with an input impedance of 1M Ω in parallel with 20pF. For the

transducers considered, this is known to represent a close approximation to an open circuit [39]. This approach minimises the influence of loading effects, which may be caused with the use of amplifiers, and has the advantage that maximum voltage reception sensitivity is often achieved under conditions of open circuit loading.

Throughout the insertion loss measurements, the air-gap between the transducers was maintained at 20mm. Two pairs of transducers, representing the most efficient combinations, were tested. A transducer pair consisting of C70ML as transmitter and C30ML as receiver was the obvious choice to represent the most sensitive composite combination, and good reciprocal performance meant that a pair of RB-2.5 transducers would provide the best electrostatics results. Note also that these composites had been manufactured as a pair and as such were matched with respect to resonant frequencies of transmission and reception at 600kHz. The pulse-echo result in Table 4.7 indicates that RB-2.5 also produces a peak spectral response very close to 600kHz.

Wideband excitation was achieved using the pulser unit, and the resulting insertion loss values were 61.3dB and 74.4dB for composite and electrostatic pairs respectively. The experimentally acquired signals in both cases are shown in Figures 4.7 and 4.8. The superior sensitivity of the composite pair is apparent from this testing, although the resonant activity has again hindered wideband performance.

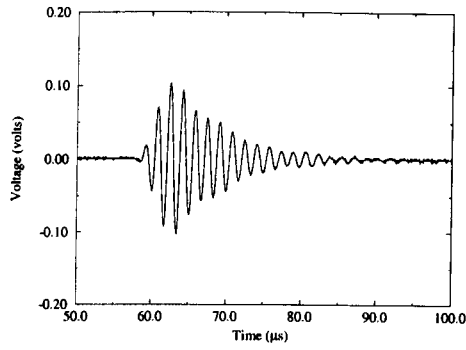


Figure 4.7 *Wideband excitation of C70ML and reception with C30ML.*

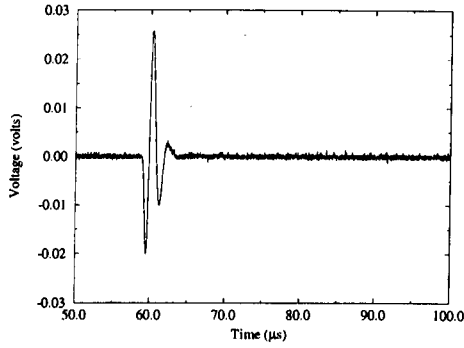


Figure 4.8 *Wideband excitation between a pair of RB-2.5 transducers.*

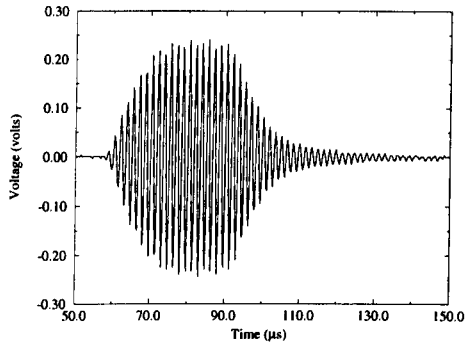


Figure 4.9 *Toneburst excitation of C70ML and reception with C30ML.*

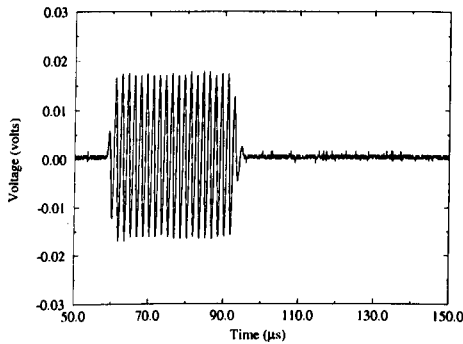


Figure 4.10 *Toneburst excitation between a pair of RB-2.5 transducers.*

A 20 cycle 10 volt peak to peak tone burst from the LeCroy function generator was used as the excitation signal to perform narrowband insertion loss testing. In each case, the centre frequency of the transducer pair was confirmed at 600kHz prior to signal acquisition. The received signals are displayed in Figures 4.9 and 4.10, and the calculated insertion loss figures for the composite and electrostatic pairs were 28.4dB and 50.8dB. The difference in performance in favour of the composites is considerably greater in this case, further emphasising the suitability of the technology for narrowband applications. The lack of reverberation in the received tone burst of the electrostatic pair is a clear indication of the high degree of damping provided by the bias, which contributes to the invariably wideband performance with the randomly rough approach.

A further comparison experiment was conducted in order to determine the sensitivity of a combination of composite and electrostatic transducers. Under the same conditions as the narrowband testing above, the C30ML composite was used to receive a signal transmitted from the RB-2.5 electrostatic, and C70ML was used to transmit a signal that was received by RB-2.5. The calculated insertion losses indicated a 13.6dB and 11.4dB improvement over the RB-2.5 electrostatic pair for composite reception and transmission respectively.

4.5.7 Robustness and Environmental Considerations

It is important to point out that, although electrostatic performance was generally optimised for the 2.5 μ m thick Mylar membrane, the necessity for adequate system robustness cannot be overlooked, particularly when prolonged operation in the relatively harsh environment of an aerospace manufacturing workshop is considered. In the experience of the author, the use of the 5 μ m Mylar would be the minimum thickness requirement to ensure any degree of confidence and this is in agreement with the findings of Carr and Wykes [48]. This, however, further limits the sensitivity capability of the technology, as can be seen from the results in Table 4.7. Insertion loss experiments were conducted for a RB-5 electrostatic pair, under the same conditions as previously, resulting in 6.4dB and 7.4dB reduction in

performance, relative to the RB-2.5 pair, under narrowband and wideband conditions respectively. Even with the use of a 5 μ m thick membrane, however, it is clear that some other form of protection would be required. This has been recognised in commercial probes for relatively low frequency (\sim 50kHz) range finding applications, where the solution has been to provide a protective “guard cage” over the surface of the fragile membrane. This is not a practical solution for the frequencies under consideration ($>$ 500kHz), which would necessitate a similarly fragile “cage” to avoid interference with the acoustic field. From the wideband characterisation presented earlier it is also clear that there would be added difficulty in producing an electrostatic with frequency response extending to the desired operational frequency when using a 5 μ m thick membrane.

4.5.8 Focusing Performance

As indicated in the previous Chapter, the ability to achieve focusing is essential in order to meet the resolution requirements. Two methods of producing a focused composite transducer were considered. Initially, attempts were made to manufacture a 600kHz 70% volume fraction device of 30mm square active area using PZT5H and soft setting epoxy, with the intention to achieve focusing by ‘bending’ the transducer. Excess epoxy (5mm) was left round the perimeter of the device to facilitate bonding to a square concave holder with the desired radius of curvature, and a square aperture to ensure air backing to the active area. This, however, proved unsuccessful for radii of 30mm, 40mm and 50mm, due to the inability of the epoxy to withstand the resulting expansion and contraction at the inner and outer extremities of the 2.9 mm thick device, and the bond to the pillars was invariably broken under the applied stress.

A composite with the same characteristics was then manufactured using hard setting epoxy, and a Perspex lens, with concave line focus of 40mm radius of curvature, was attached using a thin layer of hard setting epoxy. Perspex is a hard plastic material and was chosen due to its low attenuation and the ease with which it could be cut to shape. A radius of 40mm was selected as a first attempt as a compromise between

achieving the desired tightness of focus while still avoiding the possibility of collision. A matching layer of the type discussed in Chapter 5 was then attached to the front face of the Perspex lens and bonded with hard setting epoxy. It was found to be necessary to manufacture the matching layer with vertical and horizontal dimensions approximately 5mm larger than the lens. The matching layer then overlapped the edges of the lens. This was to reduce the edge waves from the sharp lens edges that were noted to interfere with the beam profile, producing fringe patterns when the matching layer was not in place. The manipulator arrangement in Figure 4.4 was then used to make measurements of the transmitted beam profile. Reception was achieved using a piezoelectric “pinducer” with 1mm active diameter, and this was scanned under computer control in the field perpendicular to that of the line focus in 0.5mm steps. Peak to peak voltage values after amplification were automatically acquired at each point using a Sonotek data acquisition card. The transducer excitation signal was a 20 cycle tone burst from the function generator at 600kHz centre frequency. Figures 4.11, 4.12 and 4.13 highlight the most important results. These are the two dimensional beam profile, the axial beam profile and the lateral beam profile at the focal region respectively. The dark region near the centre of Figure 4.11 represents the focal region of the transmitted pressure. The excellent symmetry of this beam profile is apparent. Note from Figure 4.12 that there is a three fold increase in the on axis signal strength at the focal region. More importantly, however, it can be seen from Figure 4.13 that the focal region is approximately 2mm in width, with a reduction in signal level of about 10dB at 1mm either side of the focal centre, indicating that the device possesses adequate resolution.

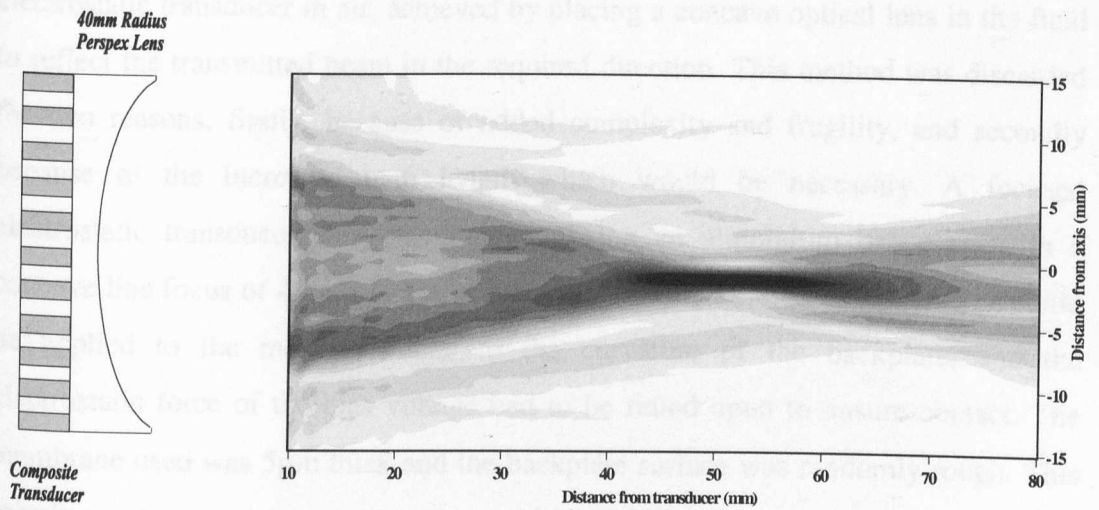


Figure 4.11 Two-dimensional beam profile of a focused composite transmitter.

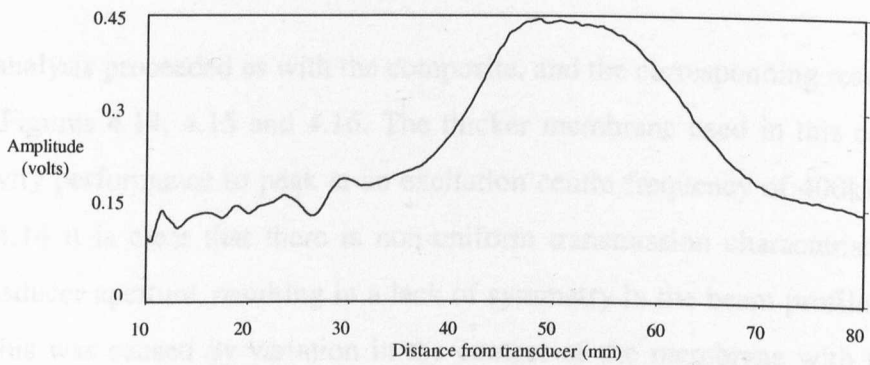


Figure 4.12 Axial beam profile of a focused composite transmitter.

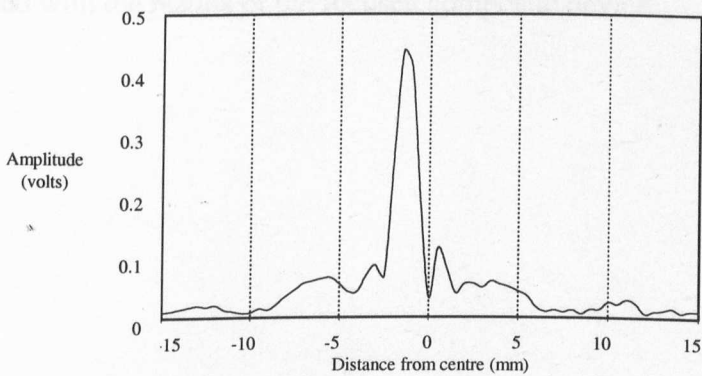


Figure 4.13 Lateral beam profile of a focused composite transmitter.

Schindel and Hutchins [57] have shown surface profiling results of a focused electrostatic transducer in air, achieved by placing a concave optical lens in the field to reflect the transmitted beam in the required direction. This method was discarded for two reasons, firstly, because of added complexity and fragility, and secondly because of the increased path length which would be necessary. A focused electrostatic transducer was manufactured using an aluminium backplate with a concave line focus of 40mm radius of curvature. In this case, no direct tension could be applied to the membrane due to the curvature of the backplate, and the electrostatic force of the bias voltage had to be relied upon to ensure contact. The membrane used was 5 μ m thick and the backplate surface was randomly rough. This membrane was used in an attempt to avoid wrinkling, however it should be noted that in the absence of direct pressure, smooth contact across the backplate was difficult to attain.

Beam profile analysis proceeded as with the composite, and the corresponding results are shown in Figures 4.14, 4.15 and 4.16. The thicker membrane used in this case caused sensitivity performance to peak at an excitation centre frequency of 400kHz. From Figure 4.14 it is clear that there is non-uniform transmission characteristics across the transducer aperture, resulting in a lack of symmetry in the beam profile. It is likely that this was caused by variation in the contact of the membrane with the backplate. This will have contributed to the less well defined signal increase at the focal region in Figure 4.15, and the poorer lateral resolution apparent in Figure 4.16, when compared with the results of the focused composite device.

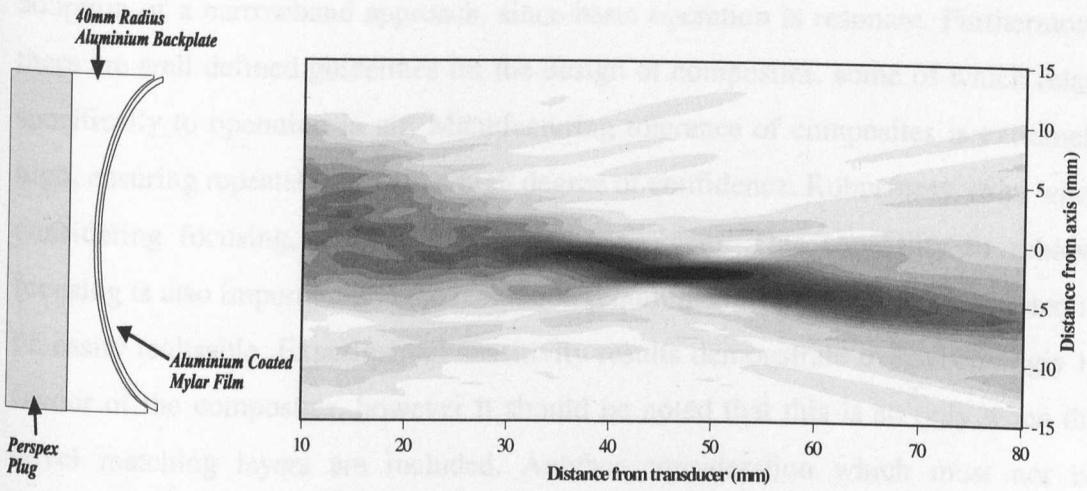


Figure 4.14 Two-dimensional beam profile of a focused electrostatic transmitter.

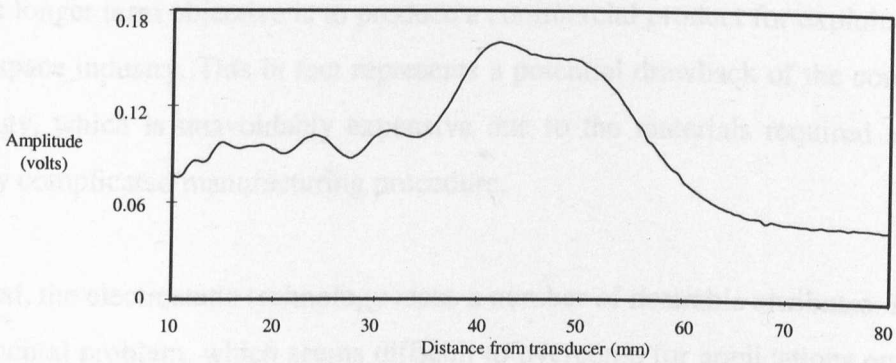


Figure 4.15 Axial beam profile of a focused electrostatic transmitter.

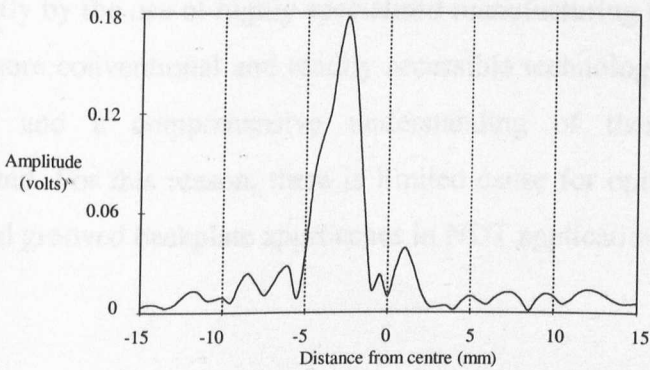


Figure 4.16 Lateral beam profile of a focused electrostatic transmitter.

4.5 Conclusions

Composite transducers have been found to possess clear advantages in almost every important aspect of the required application. The technology is well suited to the adoption of a narrowband approach, since basic operation is resonant. Furthermore, there are well defined guidelines for the design of composites, some of which relate specifically to operation in air. Manufacturing tolerance of composites is extremely high, ensuring repeatability with a high degree of confidence. Robustness, even when considering focusing, does not constitute a problem. This capability to achieve focusing is also important and the resolution requirements have been demonstrated to be easily realisable. Experimental sensitivity results demonstrate overwhelmingly in favour of the composites, however it should be noted that this is so only when the novel matching layers are included. Another consideration which must not be overlooked is that a comprehensive composite manufacturing facility already exists at Strathclyde. It would have been foolish to proceed on this basis alone, however, since the longer term objective is to produce a commercial product for exploitation in the aerospace industry. This in fact represents a potential drawback of the composite technology, which is unavoidably expensive due to the materials required and the relatively complicated manufacturing procedure.

In contrast, the electrostatic technology lacks a number of desirable attributes. Firstly, a fundamental problem, which seems difficult to overcome for applications outside a controlled environment, is the lack of robustness. Secondly, successful and repeatable designs in the frequency range under consideration, have been achieved only recently by the use of highly specialised manufacturing technology. Approaches utilising more conventional and readily accessible technology lack definitive design guidelines and a comprehensive understanding of them has not yet been demonstrated. For this reason, there is limited cause for optimism for the future of random and grooved backplate approaches in NDT applications.

Even if these problems could be overcome, however, there remains a gulf between the two technologies in terms of narrowband transmit and receive sensitivity. Electrostatics may find application in controlled environments, and possibly as device standards in laboratory calibration. In the light of this experimental and theoretical evidence, therefore, the composite technology is the obvious choice for creation of a practical through air, array scanning facility.

CHAPTER 5

DEVELOPMENT OF A NOVEL AIR-COUPLED MATCHING LAYER

Abstract

Background information into the problem of acoustic matching in air is discussed. A novel acoustic matching layer is then presented and the results of a theoretical and experimental program of work are given. These matching layers were first analysed experimentally and the results were incorporated into in a linear mathematical model. This then enabled theoretical investigation of the matching layers and their influence on transducer performance in air. Close correlation between experimental and theoretical results is demonstrated. The matching layers were used with piezoelectric transducers (1-3 connectivity composites) operating in pitch/catch mode. A novel concept for the design and operation of matched transducers operating in air is proposed and explained with experimental examples. This is supported with the results of the linear mathematical model. The work has resulted in the definitive design for these matching layers being proposed for the current application and the necessary understanding for design of matching layers in other air coupled systems being achieved. The most efficient design has been implemented in a pitch/catch air-coupled system and an improvement in received signal amplitude of 30dB was measured when both transmitter and receiver were matched.

5.1 Introduction

The requirement for efficient acoustic matching in order to develop a successful air-coupled NDT system is recognised, however the difficulty in achieving solutions to the problems involved cannot be underestimated. It has been noted [19] that the removal of the water, in a water-coupled system, will increase the system insertion loss by around 140dB. The main reason for this is the massive increase in the acoustic impedance mismatches at the media boundaries through the propagation channel. To some extent this has been recovered by adopting a narrowband approach with high gain, low noise amplification in reception and the use of alternative transducer technology that is specifically designed for use in an air-coupled through transmission system. The transducer technology selected in Chapter 4 was 1-3 connectivity piezocomposite, and although much more efficient and better matched to air than conventional water-coupled transducers, the mismatch between the transducers and air is still considerable. The best way of overcoming this mismatch further, and so increase system efficiency and flexibility, is the use of acoustic matching layers.

A novel matching layer has been developed for this purpose with successful results. The structure of the matching layer comprises two sub-layers, integrated in such a way that the final material exhibits varying specific acoustic impedance along its thickness, changing from 1 MRayl to 0.12MRayl. In order to achieve the best possible matching layer design, and appreciate the complexity of the problem of efficient coupling in air, a programme of experimental and theoretical work has been undertaken. Firstly, the intensity transmission coefficients in a lossless through transmission system were studied theoretically in order to gain a clear insight into the problem. Experimental analysis of the matching layers was conducted using optical and scanning electron microscopes to determine the microscopic structure. The acoustic properties of the constituent materials and the matching layers as a whole were then determine using an acoustic resonance technique in air. This enabled a linear mathematical model of the matching layers to be developed and incorporated into the linear systems model. This has provided a facility to theoretically investigate

the matching layers in an attempt to understand them more fully and to produce the most efficient designs for pitch catch operation in the air-coupled through transmission NDT system.

During the course of these investigations a new and important hypothesis emerged that contradicts previous thinking on the problem of acoustic matching in air and proves that, in the absence of suitable materials, conventional matching layer theory cannot be employed. The basis of this is that when a transducer operates in air, the mismatches at the boundaries are such that there is a tendency for energy to be trapped within the structure as a whole. The transducer and matching layer then operate as a single cavity with only minimal resonant activity being contained within the transducer or within the matching layer. Normal matching layer performance is therefore suppressed. Resonances within the cavity as a whole therefore determine the frequencies of operation. Strong destructive interference occurs at odd integer multiples of $\lambda/4$ cavity thickness and so leads to minima in the frequency spectra. Between these minima there is constructive interference to varying degrees resulting in maxima at or close to integer multiples of $\lambda/2$ cavity thickness. This new design concept will be discussed in detail within this Chapter and the definitive matching layer designs produced using the linear systems model, and supported with empirical investigations, will be presented.

5.2 Background

5.2.1 *Evaluation of Standard Matching Layer Theory*

This Section will briefly review the classic matching approach with reference to three key works [73,74,75]. Firstly, Jackson [73] describes the design procedure to increase the efficiency of the acoustic energy transfer between the transducer and the load medium by employing the attachment of matching layers with thicknesses equal to one quarter wavelength of the transmitted signal. An expression was derived for the acoustic impedances (Z_{iOPT}) of a number of quarter wavelength layers (n) attached to a transmitter to achieve optimum performance in terms of maximising the transmission coefficient. This is given in Equation 5.1, where Z_L and Z_T are the

acoustic impedances of the load and the transducer respectively. The figure (i) denotes the number of the quarter wavelength layer in question, and this varies from 1 to (n) in steps of 1.

$$Z_{iOPT} = (Z_T^{(n+1-i)} Z_L^i)^{1/(n+1)} \quad \text{Equation 5.1}$$

For a single layer the value for the matching layer impedance is equal to the geometric mean of the impedances of the transducer and the load medium. Jackson extended his analysis to consider the effectiveness of adding additional layers when the impedances are always chosen to be optimal according to Equation 5.1. He concluded that although addition of a single ideal quarter wavelength layer can provide significant improvement in efficiency, increasing the number of layers provides progressively less of an additional improvement. He also notes that the improvement factor, described as the total energy transmission factor, is in direct relation to the impedance ratio Z_L/Z_T . This would imply that the effectiveness of adding additional quarter wavelength layers when the load is air would provide a very limited improvement in transmission coefficient. All of the results are equally applicable to reception coefficient when considering receive transducers.

Kossoff [74] discusses matching and backing effects on performance in both transmission and reception of PZT transducers when operating into a water load. He states that the addition of quarter wavelength matching layers can produce wide bandwidth transducers with improved efficiency by acting as a mechanical transformer. Acoustic backing however generally reduces efficiency since a large portion of available energy is transmitted into the backing, although bandwidth increases as a result. The point is made that when the backing is air, the transmitter produces the maximum output, while bandwidth is small due to the acoustic impedance mismatch and the internal reverberation of energy. This is in agreement with the design decisions made for the current air-coupled system. Kossoff also makes the point that efficient transducers with very wide bandwidth may be obtained by using quarter wavelength matching to both the load and the backing. This, however this is not applicable to the current system since operation has been chosen to be narrowband.

The different effects of matching and backing of transducers were analysed using a matrix technique presented by Lewis [75] and the results were discussed. The matrix model that was developed simplifies the frequency analysis of multiple layer front matched and backed piezoelectric ceramics by considering the force and particle displacement in each layer and setting up appropriate boundary conditions. Inverse fast Fourier Transforms were utilised to find the time domain pressure responses. As an example of the use of the model a goal was set to maximise the gain-bandwidth product by transmitting the maximum energy in the shortest time into body tissue. It was shown that the use of an exponentially graded impedance plate transmits a pressure impulse as a single impulse containing all the energy of the initial pulse and so, in theory, could maximise the gain-bandwidth product. The matrix inversion modelling technique was then used to show that an exponential taper could be approximated using ten quarter wavelength matching layers.

5.2.2 *Review of Air-Coupled Matching Techniques*

Several workers using a number of different approaches [71, 72, 76, 77, 78] have considered the problems of achieving efficient mechanical matching to air. The basic problem affecting all of this work is that no suitable homogeneous material exists with suitable characteristics in terms of specific acoustic impedance as suggested by Equation 5.1 and attenuation. When it is considered that the impedance of air is 0.0004MRayl, and the impedance of a typical composite transmitter is 20MRayl, the extent of the mismatch may be appreciated. The ideal single matching layer would have impedance of 0.089MRayl. Silicone rubber is one material that has been attempted in the past as a matching material to air. This however has acoustic impedance of 1MRayl, a factor of more than 10 larger than the ideal value. One method of reducing this further is the inclusion of low density, air filled microspheres [71], but this has the disadvantage of increasing the attenuation and scattering within the material. Other attempted materials include silicone aerogels [76,77], cork, balsa wood [77] and microporous membrane filters [71], which possess varying degrees of porosity and attenuation, and have had varying levels of success. The works presented in [72] and [78] describe different attempts at

developing manufacturing methods to introduce pockets of air into the matching layer structure. In both cases, however, manufacturing complexity was a limiting factor to the success of the technique. No ideal material has yet been found and acoustic matching to air remains a problem.

As a consequence of the lack of suitable materials, conventional matching layer designs are difficult to implement in air and a new approach for operation in air must be developed. Investigations within this work have concluded that the mismatches at the transducer/air boundaries (assuming air backing) result in energy entrapment within the transducer structure and the transducer/matching layer operating as a single cavity. This will be explained fully with theory and experiment in Section 5.3.2, where the effect of the mismatch in air compared to that in water will also be demonstrated by considering the intensity transmission coefficient.

5.3 Introduction to the Proposed New Matching Layer

5.3.1 Basic Novel Matching Layer Concept

The philosophy behind the design was to produce an integrated acoustic impedance that reduced in impedance from the transducer side to the outside in contact with the air load. The constituent materials are silicone rubber and micro-porous membrane filters. The use of both of these materials has been attempted in the development of air-coupled matching layers before, but with limited success. Silicone rubber alone does not possess a low enough acoustic impedance. The filters [71], which contain pores with controlled dimensions in the sub-micron range, were attached to the transducer directly using a hard setting adhesive which contaminated the pores and adversely influenced performance.

In the new concept, the silicone rubber is set to a desired thickness between the filter and the transducer. During the curing process, the silicone rubber partially impregnates the filter producing some gradation in acoustic impedance, with pure silicone rubber in contact with the transducer and unsaturated, porous filter at the outside, in contact with the air load. The porous filters are a useful material when

coupling to air since it is known that the large quantity of air present within the structure means that the acoustic impedance is potentially very low and so they provide a good match to air. The material properties for the filters used here are calculated within this Thesis and are presented in Section 5.5.2. These are found to be close to ideal quarter wavelength matching for solid ceramic at 715kHz if direct attachment without pore contamination could be achieved. However, this is no longer the case when attachment using the silicone rubber is performed. Also, this quarter wavelength resonance was modelled to be very narrowband and so would make frequency matching between the transmitter and receiver very difficult.

Porous materials have a very complex structure and the investigation of acoustic propagation is not a trivial problem. During the last 30 years Biot's theory [79,80] has been extensively used to study the propagation of sound in many different kinds of porous materials. It is one such porous material that forms the basis of the new matching layer and Biot's theory is used for the investigation of part of the structure. This is discussed in Section 5.5.1(c), and the materials used and the matching layer manufacturing process will be presented in Appendix A.

5.3.2 Cavity Resonance Hypothesis

In order to appreciate the effects of the resonant behaviour in a cavity suspended in air, the intensity transmission coefficient was analysed using the fundamental relationship given in Equation 5.2 [81]. This assumes a lossless environment with zero attenuation through the propagation channel.

$$T_1 = \frac{4}{\left[2 + \left(\frac{Z_1}{Z_3} + \frac{Z_3}{Z_1} \right) \cos^2(k_2 L) + \left(\frac{Z_2^2}{Z_1 Z_3} + \frac{Z_1 Z_3}{Z_2^2} \right) \sin^2(k_2 L) \right]} \quad \text{Equation 5.2}$$

Equation 5.2 was used to investigate the coefficient of intensity transmission (T_1) through a layer (Layer 2) with the arrangement shown in Figure 5.1 as a function of

frequency. With reference to this Figure, Z_1 , Z_2 and Z_3 are the specific acoustic impedances of Layer 1, 2 and 3 respectively. L is the thickness and k_2 is the wave number of the material in Layer 2. Load media of both air and water were considered in order to appreciate the effect that the removal of water has on signal intensity transfer in an NDT system. The coefficient was calculated for a signal transmitted from Layer 1 that is incident normally on Layer 2 before passing into Layer 3. The layer through which the signal passes in this investigation (Layer 2) has properties approximating those of silicone rubber. These are given in Table 5.1 and the thickness of the layer (L) is assumed to be 0.5mm. This thickness was chosen as it is representative of the matching layer thicknesses used and also because it simplifies the results, as will be seen. Table 5.1 also provides the relevant parameters of air and water.

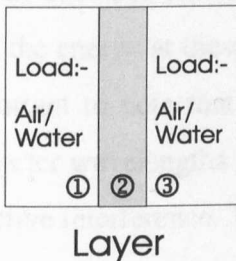


Figure 5.1 Layer arrangement considered in the intensity transmission coefficient investigation.

	Impedance (MRayl)	Thickness (mm)	Density (kgm^{-3})	Longitudinal Velocity (ms^{-1})
Layer 2	1	0.5	1000	1000
Air	0.0004	Load	1.24	343
Water	1.48	Load	1000	1483

Table 5.1 Parameters for the layer transmitted through and the two loads used in the calculations.

The result of the transmission coefficient variation with frequency for air loading are given in Figure 5.2. There is an extremely sharp transition from close to zero transmission coefficient to perfect (unity) transmission coefficient. The sharpness of this peak is a consequence of the massive acoustic impedance mismatch between the layer and air. The frequency of this peak is at 1MHz and this represents the half wavelength frequency for the layer calculated with Equation 5.3 and using the parameters given. Perfect through transmission occurs at this frequency due to the perfect constructive interference that occurs, since the layer is $\lambda/2$ thick for this frequency. Analysis of Equation 5.2 reveals that perfect through transmission occurs for all those frequencies that represent an integer multiple of half wavelengths within the layer. Again, this is due to the perfect constructive interference that occurs within the layer at those frequencies. Without this constructive interference the transmission coefficient in air becomes extremely low to the point where through transmission is negligible and the energy at these frequencies is reflected or trapped within the layer. It is also important to note that all those frequencies that represent an odd integer multiple of quarter wavelengths within the layer (e.g. 500kHz and 1.5MHz) produce perfect destructive interference. The effects of this are discussed in the next Section.

$$\lambda = \frac{V_L}{f}$$

Equation 5.3

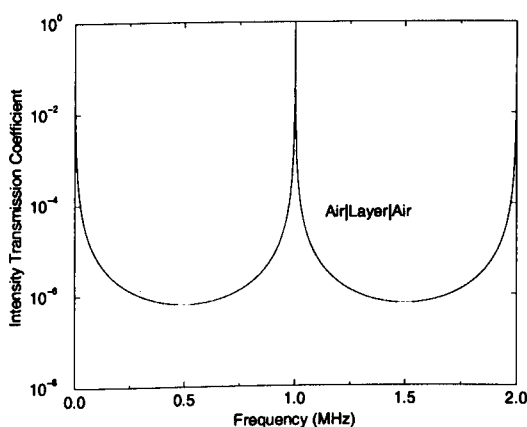


Figure 5.2 Intensity transmission coefficient as the frequency of a normally incident signal is varied with air load.

When water loading is considered the mismatch is very much reduced and the change from constructive to destructive interference as the frequency changes is much less well defined, as shown in Figure 5.3. In this case, transfer of energy through the layer can occur for all frequencies much more readily and so the effects of destructive interference of internally reverberating energy are greatly reduced, since there is not the same degree of energy entrapment within the layer. Note however that the influence of the interference within the layer as the frequency changes is still apparent. Again, the maxima correspond to those frequencies representing an integer multiple of half wavelengths within the layer. It is also simpler to appreciate from the Figure 5.3 that minima occur at those frequencies that represent odd integer multiples of quarter wavelengths, where destructive interference occurs.

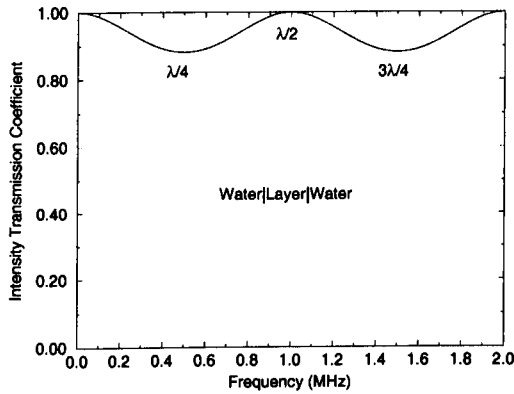


Figure 5.3 Intensity transmission coefficient as the frequency of a normally incident signal is varied with *water* load.

The effects of energy entrapment and the resulting interference within a structure suspended in air are particularly significant when considering the problem of acoustic matching of an air-coupled transducer. It is concluded here, both theoretically and experimentally, that the conventional matching layer designs are not applicable due to a lack of suitable materials. Successful quarter wavelength matching requires two conditions to be satisfied. Firstly, the acoustic impedance must satisfy Equation 5.1 depending on the impedances of the transducer and the load. Secondly, the thickness must be correct to promote quarter wavelength resonance at the operational frequency of the transducer. The first of these requirements is difficult to satisfy in air

since materials with the very low impedance required ($\sim 0.1 \text{ MRayl}$) are difficult to produce accurately and are invariably highly attenuative. The second is difficult to satisfy in air due to the fact that resonance in a solid in air is peculiarly sensitive to the precise thickness (Figure 5.2). When these conditions are met then reverberation of energy within the matching layer is in phase with reverberation of energy within the transducer and increased output at the operational frequency of the transducer is achieved.

When operating in air, the difficulty of meeting the requirements and the resulting energy entrapment within the matched transducer can cause a situation where a significant proportion of the acoustic energy reverberates within the transducer and matching layer as a whole cavity and very limited energy is contained within the matching layer or the transducer alone. This means that the constructive interference of energy reverberating within a quarter wavelength matching layer with energy reverberating within the transducer is suppressed. The cavity resonance is then at three quarters of a wavelength and causes destructive interference at the operational frequency of the transducer.

The linear systems model is now employed to demonstrate theoretically the effects of transducer matching in air for both ideal and non ideal matching and the results are given in Figure 5.4 (a) to (d). Ideal matching properties were based on the properties of the membrane filter material that is used to produce the new matching layer as discussed in Section 5.5. This has exactly the correct impedance for matching a solid PZT5A transducer and so a transducer of this type is also assumed in this theoretical investigation. Perspex is assumed with the modelling for non ideal matching and this is appropriate due to the required attachment of Perspex lenses to the front faces of each transducer in the present application

Figure 5.4(a) shows the variation in performance at the transducer operational frequency as thickness of an ideal matching layer is increased. In this case, peak performance occurs at the operational frequency of the transducer at quarter

wavelength matching layer thickness. The layer therefore operates as a conventional quarter wavelength matching at the relevant thickness. The phase relationship of energy in the transducer and in the matching layer at quarter wavelength thickness results in constructive interference. At thicknesses of three and five quarter wavelengths, the phase relationships again support constructive interference and increases the output at the transducer operational frequency. Consecutive maxima have lower magnitude due to the high attenuation in the filter material (120dB/cm) and the increased influence of this as the layer becomes thicker. A minimum in magnitude is produced each time the thickness is an even multiple of quarter wavelengths due to the resulting destructive interference.

Frequency responses at half and quarter wavelength matching layer thicknesses are provided in Figure 5.4(c). This shows that performance does indeed produce a maximum at 600kHz, with a significant improvement over the case with no matching. Use of this filter as a matching layer in practice, however, is not considered to be an option due to difficulty of attachment. The response with half wavelength thickness is interesting since it demonstrates cavity resonance performance, even although the impedance is ideal, showing that both thickness and impedance must be correct for quarter wavelength matching. The small peak at 300kHz is the half wavelength cavity resonance and the peak at 600kHz (that is coincident with the response with no matching) is the cavity one wavelength resonance.

Figure 5.4(b) demonstrates the variation in performance as the thickness of a non ideal matching layer is increased. In this case, the opposite performance is in evidence as odd multiples of quarter wavelengths produce minima in performance. As explained earlier, this is due to the non ideal arrangement and the destructive interference of the cavity resonance of the trapped energy. Constructive cavity resonance, when the thickness is even multiples of quarter wavelengths, is also evident. Figure 5.4(d) is provided to show the frequency responses at two different Perspex thicknesses. The maximum and minimum at 600kHz for half and quarter

wavelength layer thickness respectively are further evidence of the cavity resonance response with this non ideal matching.

The two situations modelled here are obviously extreme cases. It is supposed here that in practice there would be a gradual and complex change from one condition to the other as the parameters for thickness and/or acoustic impedances are altered. It is important, in this case, to know the performance at the transducer operational frequency. Peak performance at this frequency would, in theory, change between matching layer thicknesses of odd and even multiples of one quarter wavelength.

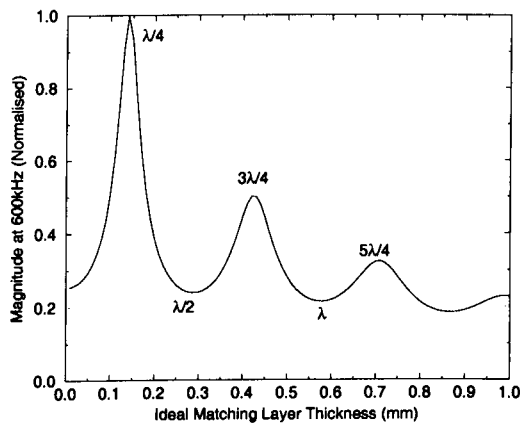


Figure 5.4(a) Peaks in frequency response at 600kHz as the thickness of an ideal impedance matching layer is increased.

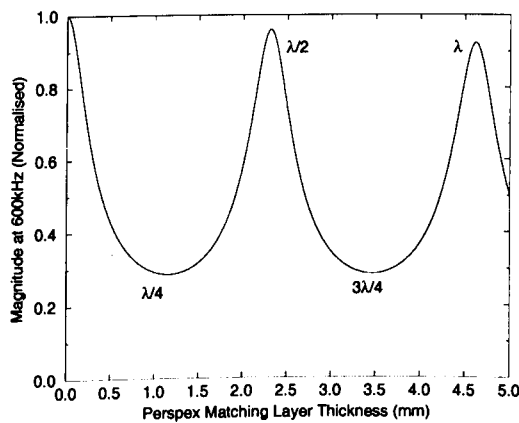


Figure 5.4(b) Peaks in frequency response at 600kHz as the thickness of a Perspex matching layer is increased.

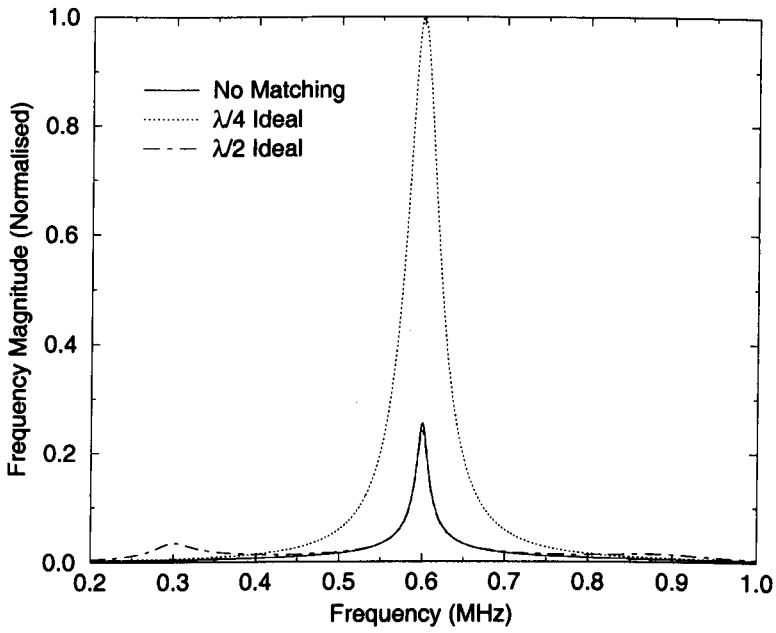


Figure 5.4(c) *Frequency response of a transmitter output with ideal impedance matching at half and quarter wavelength thickness.*

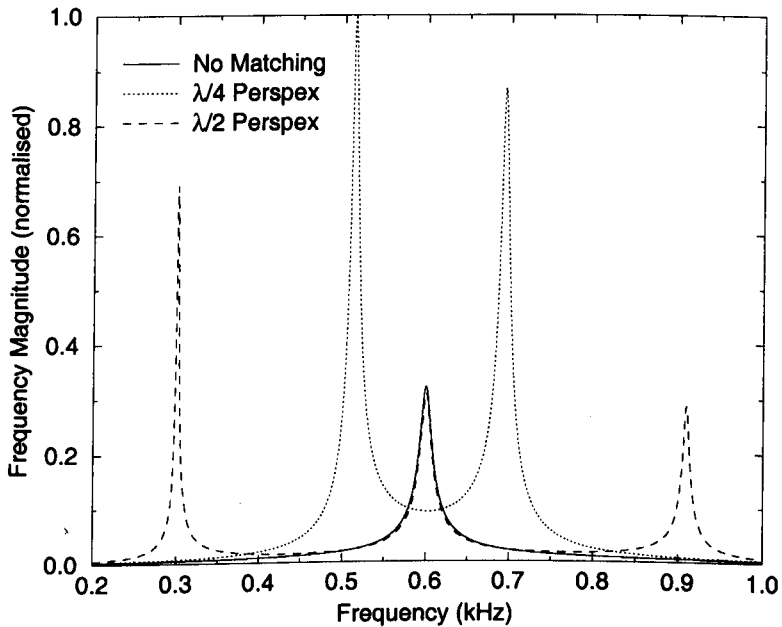


Figure 5.4(d) *Frequency response of a transmitter output with Perspex matching at half and quarter wavelength thickness.*

This cavity resonance concept was investigated experimentally using three 600kHz piezo-composite transmitters with 70% volume fraction. One of these was unmatched, one had a $\lambda/4$ Perspex plate attached and one had a $\lambda/2$ Perspex plate attached. The experimental responses were received using a wideband electrostatic transducer with spectral responses as shown in Figure 5.5. Excitation of the transmitter was achieved using a Panametrics Pulser. The linear systems model has been used to support the findings and the experimental/theoretical results are shown in Figure 5.6. The purpose of these investigations was to demonstrate experimentally the influence of the energy entrapment within the transducer and matching layer, and show the resulting cavity resonance maxima and minima.

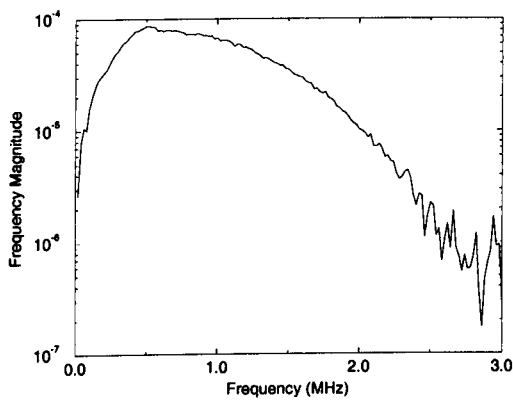


Figure 5.5 Spectral wideband response of the electrostatic transducer used in reception.

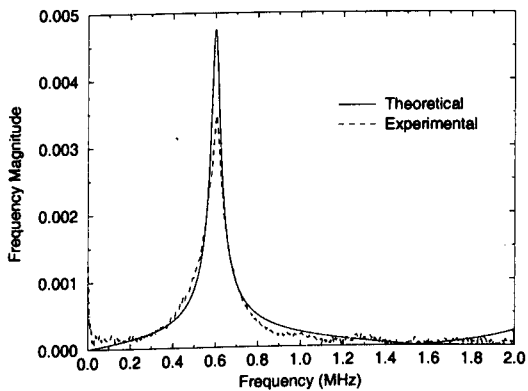


Figure 5.6(a) Theoretical and experimental results of transmitter frequency responses without perspex matching layers attached.

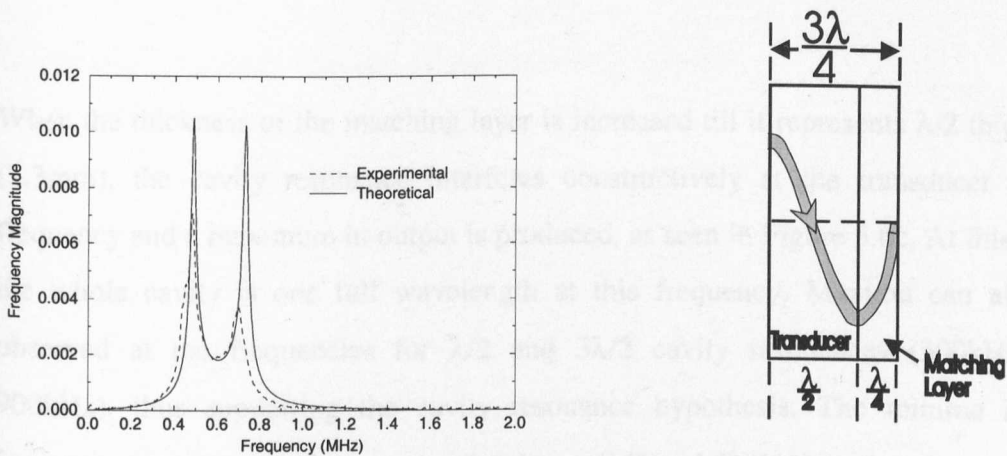


Figure 5.6(b) Theoretical and experimental results of transmitter frequency responses with a $\lambda/4$ Perspex matching layer attached, plus schematic diagram.

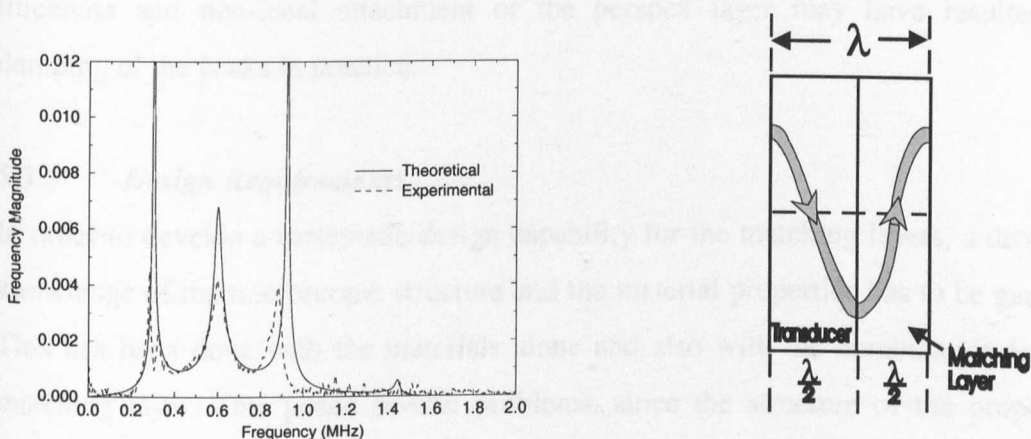


Figure 5.6(c) Theoretical and experimental results of transmitter frequency responses with a $\lambda/2$ Perspex matching layer attached, plus schematic diagram.

Firstly, Figure 5.6a shows the frequency response of the 600kHz transmitter without matching layer. Figure 5.6b shows the result of attaching a quarter wavelength matching layer of perspex (1.15mm with $V_L=2770\text{ms}^{-1}$), where a minimum appears at the centre frequency of the transducer (Electrical resonance at 600kHz). This is due to $3\lambda/4$ cavity destructive interference at this frequency. The two resulting maxima on either side of this minimum are controlled by the 'strength' of the minimum. This in turn is controlled by the degree of mismatch between the cavity and the air load, or the degree of energy entrapment within the cavity. These peaks are not at $\lambda/2$ and λ frequencies although they do tend towards them as the thickness of the matching layer is increased.

When the thickness of the matching layer is increased till it represents $\lambda/2$ thickness (2.3mm), the cavity resonance interferes constructively at the transducer centre frequency and a maximum in output is produced, as seen in Figure 5.6c. At this point the whole cavity is one full wavelength at this frequency. Maxima can also be observed at the frequencies for $\lambda/2$ and $3\lambda/2$ cavity resonances (300kHz and 900kHz), thus supporting the cavity resonance hypothesis. The minima in the frequency response are also measured to be at $3\lambda/4$ and $5\lambda/4$. Note that the modelled peaks at 300kHz and 600kHz overestimate the peaks observed in practice. These peaks are very narrowband, however, and it is thought that slight variation in the thickness and non-ideal attachment of the perspex layer may have resulted in damping of the peaks in practice.

5.3.3 *Design Requirements*

In order to develop a systematic design capability for the matching layers, a detailed knowledge of the microscopic structure and the material properties has to be gained. This has been done with the materials alone and also with the combination in the matching layer. This posed several problems, since the structure of the proposed porous filter is very complicated and contact with water could not be tolerated in the characterisation due to water ingress and modification of the characteristics. Air-coupled characterisation had to be used and this process is described in the next Section. The main aim here was to gain sufficient understanding of the matching layer microstructure, and subsequently of the acoustic properties (in Section 5.5), to develop a linear structural approximation, which could be incorporated into the linear systems model used in Chapter 3. The overall objective was to establish a comprehensive set of rules for matching layer design.

Microscopic Characterisation of the Matching Layers

5.3.4 Introduction

The microstructure was investigated using a combination of scanning electron and optical microscopes to look at a cross section in the thickness direction.

This work focused on the determination of:

- a) Porosity and pore size of the filter.
- b) Degree of silicone rubber penetration into the filter.
- c) Effect of the presence of the porous filter on the curing of the silicone rubber.

5.3.5 Scanning Electron Microscope (SEM) Analysis

SEM micrographs were used to determine values for (a) and (b) and one such figure is presented in Figure 5.7. The captured images were digitised and transferred to a computer to obtain an estimation of the surface porosity. The dark area on the right-hand side corresponds to the silicone rubber and the thickness of this phase is not shown fully. It can be appreciated that the porosity and pore size of the porous filter (on the left-hand side) varies along the thickness, resulting in an asymmetric structure. The filter used in the matching layer manufacture was 120 μm thick. This surface was divided into four regions (30 μm each) and the porosity was calculated for each one. Percentage porosity is defined as the ratio of air to solid filter and/or silicone rubber in a particular region, i.e. 0% would equate to totally solid and therefore completely saturated, and 100% to totally air. The average porosity was measured to be 75% and this agrees well with the value provided by the manufacturer at 70%. The highest porosity was measured at 85% and this corresponds to the area in contact with the silicone rubber, while the porosity of the outer face is the lowest and was measured at 40%. The average pore size at the area in contact with the silicone rubber is measured to be 0.6 μm .

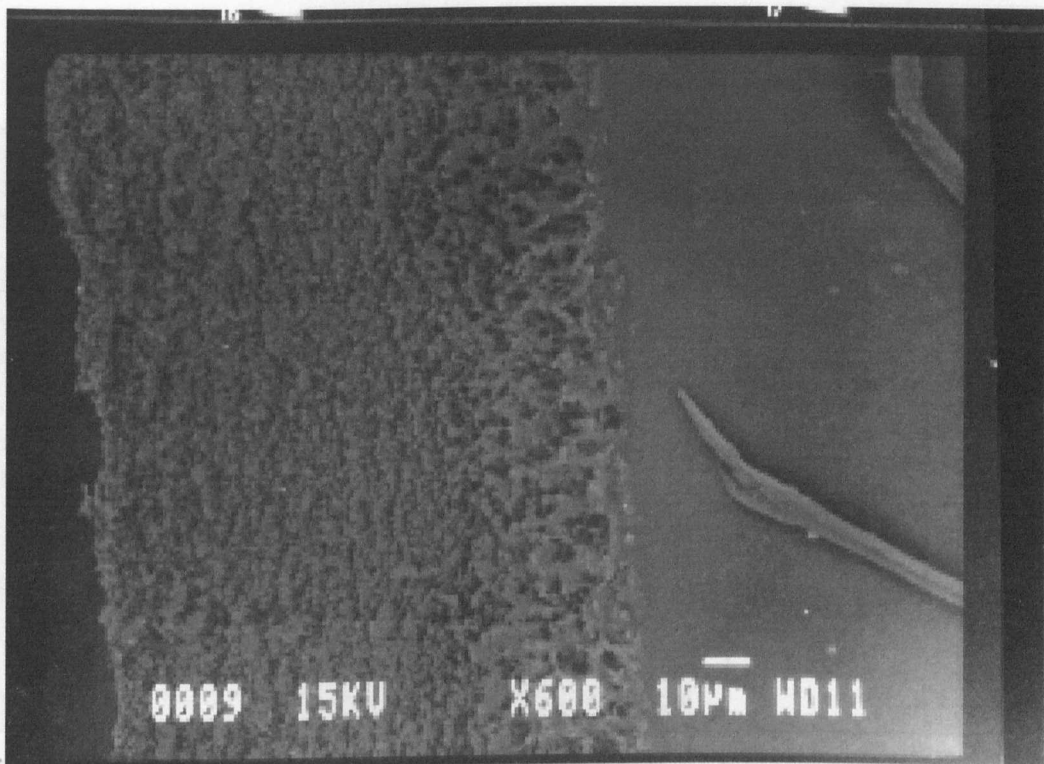


Figure 5.7 SEM image of the cross section of the matching layer. From left to right: free porous filter, porous filter impregnated with silicone rubber and silicone rubber. (Fine segments of the filter, remaining from the slicing of this section, are also apparent at the middle and top of the right hand side)

The penetration of the silicone rubber into the pores is observed to extend up to $10\mu\text{m}$ into the porous filter by measuring the distance from the visible edge of the filter. This results in a section of filter that is partially saturated with silicone rubber and this phase is characterised using Biot's theory, as explained in Section 5.5. The values for pore size and porosity at this section of the matching layer that were measured at $0.6\mu\text{m}$ and 85% from Figure 5.7, are used in this characterisation.

5.3.6 Optical Microscopy Analysis

Optical microscopy of the matching layers was then performed. Firstly, this was done to check the SEM results concerning the penetration of the silicone rubber into the porous filter, and secondly to analyse the effect of the porous surface of the filter in contact with the silicone rubber on the properties of the silicone rubber.

5.3.7 Summary of Results

As a result of this study, it was considered reasonable to divide the matching layer into four distinct sub-layers for modeling purposes. Each layer has different

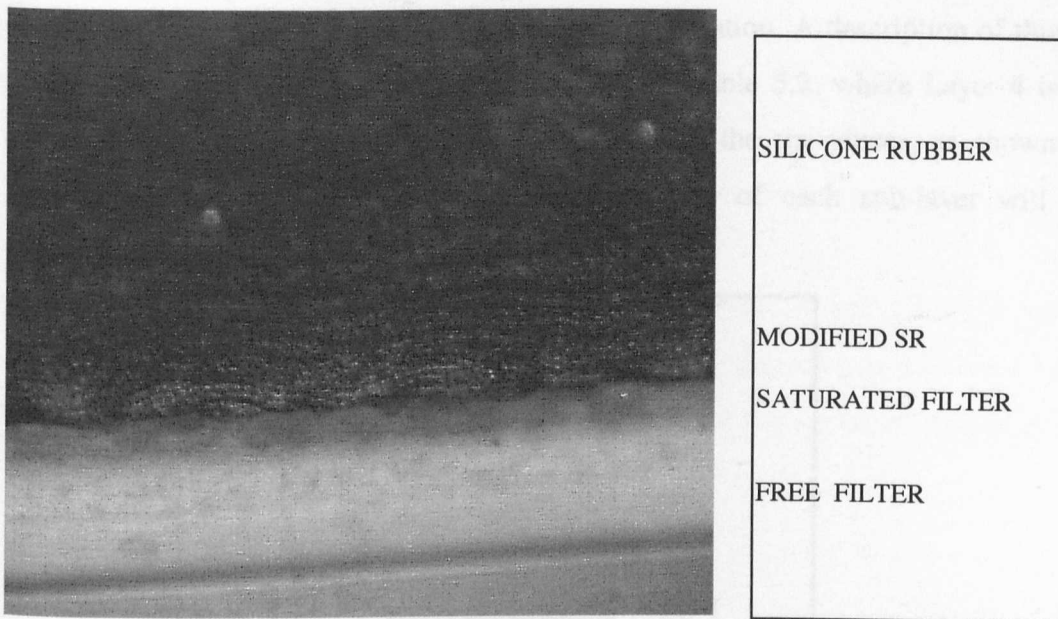


Figure 5.8 *Optical micrograph of the cross section of the matching layer.*

Figure 5.8 shows the optical micrograph of the edge of the matching layer. The penetration of the silicone rubber inside the filter is in agreement with the SEM results. In addition, a band-pattern in the silicone rubber is clearly observed at the area near the filter. This area extends up to $80\mu\text{m}$ away from the filter. This is an important observation and corresponds to a modification of the silicone rubber. This was believed to be due to the presence of the porous filter in contact with it during the curing process. It will be referred to as the “modified silicone rubber layer” or MSR. It has been determined in this work that this modification of the silicone rubber has an effect on its elastic properties. In particular, the velocity of sound propagation in this area is noted to be lower when compared to that of unmodified silicone rubber.

Table 5.2 Description of the four sub-layers found with numerical values for the micrographs.

5.3.7 Summary of Results

As a result of this study, it was considered reasonable to divide the matching layer into four different sub-layers for modelling purposes. Each layer has different characteristics for density, acoustic velocity and attenuation. A description of this 4-sub-layer model for the matching layer is given in Table 5.2, where Layer 4 is in contact with the air and Layer 1 is in contact with the transducer, as shown in Figure 5.9. Determination of the acoustic properties of each sub-layer will be obtained in the next Section.

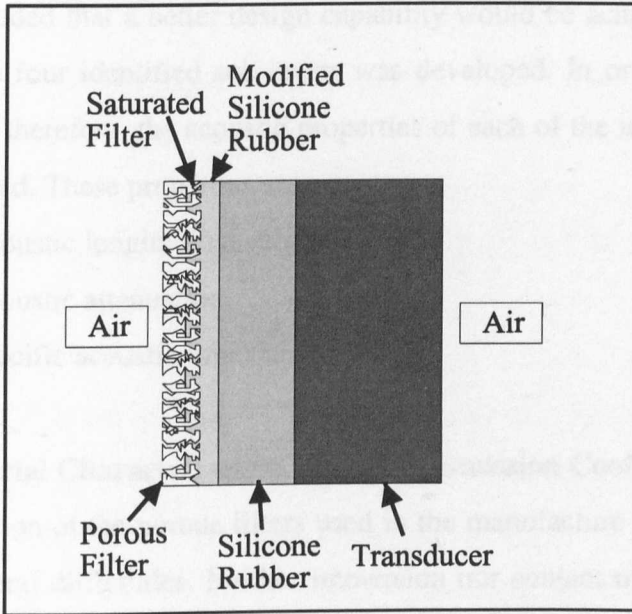


Figure 5.9 Schematic representation of the matching layer.

Layer	Description	Thickness (μm)
1 SR	Silicone Rubber	380
2 MSR	Modified Silicone Rubber	80
3 SF	Porous Filter Saturated with SR	10
4 PF	Porous Filter	110

Table 5.2 Description of the four sublayers from data measured using the micrographs.

5.4 Acoustic Characterisation of the Matching Layers

5.4.1 The Characterisation Approach

a) Introduction

To characterise these matching layers fully it is necessary to characterise not only the two basic components (porous filter and silicone rubber) but also the whole matching layer. This is because the materials are modified to some extent when the matching layer is made, as the microscopic study of the previous section demonstrated.

It was concluded that a better design capability would be achieved if a linear model based on the four identified sub-layers was developed. In order to develop a valid linear model therefore, the acoustic properties of each of the identified sublayers had to be estimated. These properties are :

1. Acoustic longitudinal velocity.
2. Acoustic attenuation.
3. Specific acoustic impedance.

b) Material Characterisation Using Transmission Coefficient Calculations

Characterisation of the porous filters used in the manufacture of the matching layers presents several difficulties. Neither immersion nor contact transmission techniques are suitable. The use of water as the coupling fluid can change the properties of the porous filter due to water percolation into the porous structure, and so the integrity of any measurements taken will be affected. Dry contact techniques [82] can be used, but these procedures are cumbersome and the experimental error when very thin layers are involved is potentially very high since the contact can influence the thickness of the sample and so change the results for attenuation and sample transit time. This means that dry contact techniques are not suitable in the present case due to the 120 μ m filter thickness.

Air-coupled ultrasound is used as an alternative, but in this case, the acoustic velocity cannot be measured by a conventional through transmission or pulse-echo technique. The problem is that the small thickness of the sample, and the similarity of the

acoustic velocity to that of air, makes it impossible to measure accurately any change in the arrival time of the signal. High attenuation, strong dispersion, and the interference caused by multiple reverberations within the sample are other causes of measurement error.

To avoid these problems a technique based on the generation of normal modes in the samples was used. Thickness resonances were excited in plate shaped samples and they were generated and measured using wideband air-coupled ultrasound. These resonances occur due to the constructive interference of the multiple reverberations of the wave inside the sample as explained in Section 5.3.2. They were investigated in the filter alone, and also in samples of SR alone and in samples of completed matching layers, by measuring the coefficient of sound transmission through the samples. These transmission coefficient measurements formed the basis of the matching layer characterisation approach.

The experimental measurement of the transmission coefficient through samples under investigation over a wide frequency range was achieved as follows: Firstly, electrostatic transducers were designed to have a frequency bandwidth that comprised at least one of the anticipated frequency thickness resonances of the samples. Wideband air-coupled ultrasonic signals were then used in a through transmission experiment. First of all, a reference signal was obtained with the wideband signal transmitted between the two electrostatic transducers with no sample in place. Then a signal was received through the sample when it is located in between the transducers at normal incidence (*sample signal*). These two signals were acquired, digitised and stored in a computer. The FFT of both signals was calculated and the coefficient of sound transmission (T) is found from the relation:

$$T = \left(\frac{|FFT(\text{sample signal})|}{|FFT(\text{reference signal})|} \right)^2 \quad \text{Equation 5.4}$$

Figure 5.5 (on page 133) shows the reference signal in the frequency domain and the frequency band of the emitting-receiver system can be appreciated.

Acoustic characterisation of the sample may be achieved through investigation of the properties of the resulting transmission coefficient resonances. One simple method of achieving this involves measuring the frequency location and the width (Q) of the resonance peaks observed. From these data it is possible to obtain the longitudinal velocity (Equation 5.5) and attenuation (Equations 5.6 and 5.7) of sound at the frequency of resonance if the density of the sample and the impedance of the surrounding media are known.

$$V_L = 2t \frac{f_n}{n} \quad n = 1, 2, \dots \quad \text{Equation 5.5}$$

where t is the thickness of the plate, f_n is the frequency of the resonance and n is the order of the resonance.

From [83], the total losses inside the plate ($\tilde{\alpha}$) are given by:

$$\tilde{\alpha} = \frac{k}{2Q} \quad \text{for } k\alpha > 10 \quad \text{Equation 5.6}$$

Where Q is defined as $f_n/\Delta f_n$, and Δf_n is the width of the resonance peak measured at half-maximum amplitude value and k is the wave number $2\pi/\lambda$.

To obtain the attenuation in the sample (α), it is necessary to consider the losses due to sound radiation from the plate to the surrounding media:

$$\alpha = \tilde{\alpha} - \frac{\log R^2}{2t} \quad \text{Npm}^{-1} \quad \text{Equation 5.7}$$

where $R = (Z_L - Z_M)/(Z_L + Z_M)$ (Reflection Coefficient) and Z_L and Z_M are the acoustic impedances of the surrounding medium and the plate respectively.

The acoustic impedance of the plate is first calculated here (Acoustic Impedance = Density * Longitudinal Velocity) by determining the density from mass and volume measurements (Density = Mass/Volume) and using the velocity calculated with

Equation 5.5. The absolute accuracy of this method alone is in doubt however, due to the inaccuracy of the mass and volume measurements.

There is another method of investigating the resonances that may be used, which complements the first method and overcomes the requirement for accurate knowledge of the sample density prior to testing. This involves calculating the value of the coefficient of sound transmission through the plate as a function of the frequency of the wave. Plane monochromatic waves with normal incidence to the plate are assumed in order to obtain the coefficient of sound transmission by solving the problem defined by the boundary conditions at both interfaces of the sample and the acoustic fields, both within and outside the plate [75]. For this method, the coefficient of transmission through the plate is calculated using the relationship given in Equation 5.2. The values of the velocity, density and attenuation of sound in the sample are obtained by fitting theoretical predictions to experimental measurements, not simply at the frequency of resonance but over a wide frequency range. Using this technique enables determination of the sample effective parameters by treating the material as a homogenous medium. This can be justified due to the fact that the wavelengths considered are much larger than any of the porous structure dimensions.

In this work, the first approach was adopted initially (using Equations 5.5, 5.6 and 5.7) to obtain estimates of the values of longitudinal velocity and the attenuation of sound inside the sample at the frequency of resonance. The theoretical predictions of the coefficient of sound transmission through the plate (using Equation 5.2) were then fitted to the experimental results (achieved with Equation 5.4) by making alterations to the values for velocity, attenuation and density. In this case, the velocity controls the frequency position of the resonant peak. The material density controls the width of the peak, which is related to the ratio of the load density to the test material density. When the material is much denser than the load, therefore, the resonant peak is very narrowband, as demonstrated in Figure 5.2. Also, the magnitude of the peak at the resonant frequency is influenced by the attenuation in the material at that frequency although this magnitude is also controlled by the

impedance mismatch and the resulting degree of energy entrapment. The values for velocity, attenuation of sound and density of the sample were adjusted slightly to obtain the best correlation between theoretical predictions and experimental results. The main source of error with this technique is believed to be due to the measurement of the thickness of the sample.

c) **Biot's Theory**

This theory deals with the propagation of stress waves in a porous elastic solid such as the membrane filter used for the matching layer. It is well known from Biot's theory that two longitudinal waves (fast and slow) may propagate in porous materials. In some instances, the velocity of the slow mode is lower than the velocity of sound in the fluid saturating the pores, leading to extremely low impedance values. In the case of air saturation, velocities of propagation of 150ms^{-1} in paper materials have been reported [82]. However, this mode can be strongly attenuated ($200\text{-}300\text{dBcm}^{-1}$), is not easily generated in porous materials and normally overlaps the fast longitudinal mode. Alternatively, if very soft porous materials are used then very low acoustic impedances can be achieved by generation of the fast longitudinal wave. In this case, the acoustic velocity is only slightly higher than the velocity of sound in the fluid inside the pores, but the attenuation is much lower. It is this fast mode that is believed to be generated within the filter phase of the new matching layers. The filter used in production is a very soft, highly porous material that provides low density and low acoustic velocity. The acoustic impedance is consequently very low.

Biot's theory of sound propagation in porous media can be used to predict the velocity and attenuation of sound from material parameters such as porosity, density and elastic modulus of the solid, and viscosity, density and elastic modulus of the material in the pores. It is shown in Section 5.5.2, however, that the transmission coefficient methods described in the previous Section are sufficient for characterisation of the porous filter (PF) and the silicone rubber (SR) phases of the matching layer. Nevertheless, the $10\mu\text{m}$ section of the filter that is partially saturated

with silicone rubber (SF), when the matching layer is manufactured, cannot be characterised in this way and Biot's theory must be employed to provide an estimate of the material parameters. A simple geometrical model to describe the porous structure based on the stacking of fibres [84] was used to predict the elastic constant of the porous filter. The results of this model and some other data required by Biot's theory found in [85,86], and from the microscopic characterisation, are shown in Table 5.3. A computer model that implements Biot's theory was coded using Mat Lab by Gomez [87] within the group at Strathclyde. This code was used in conjunction with the parameters in Table 5.3 to characterise the SF phase of the filter, as will be discussed in Section 5.5.2(c).

Pore Size (μm)	0.6
Porosity (%)	85
Young's modulus of the porous skeleton (MPa)	13.12
Young's modulus of the solid fibres (GPa)	8.3
Poisson ratio of the porous skeleton	0.12
Poisson ratio of the solid fibres	0.3
Density of the solid (kgm^{-3})	1200

Table 5.3 *Parameters of the filter used for the Biot's theory calculations.*

5.4.2 Acoustic Characterisation

a) Silicone Rubber

The procedure described in Section 5.5.1 (b) was employed to characterise the silicone rubber used to manufacture the matching layers. Two silicone rubber plates were made with different thickness: 0.31mm and 0.44mm. These thicknesses were selected from a first estimation of the velocity of sound propagation in the silicone rubber so that the first thickness resonance appears within the frequency band of the transmitter/receiver used to perform the test (Figure 5.5). Figure 5.10 shows the measured and calculated coefficients of sound transmission through the 0.44mm plate. The measured properties of the silicone rubber in both plates are summarised in Table 5.3.

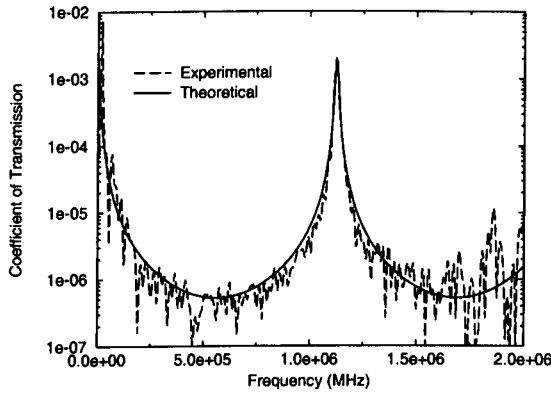


Figure 5.10 *Theoretical and experimental transmission coefficients through a 0.44mm thick silicone rubber plate.*

Thickness (mm)	Frequency of Resonance (MHz)	Velocity @ Resonance (ms^{-1})	Attenuation @ Resonance (dBcm^{-1})	Density (kgm^{-3})
0.31	1.59	985	3.17	960
0.44	1.17	995	3.40	951

Table 5.3 *Measured parameters of the two SR plates.*

As an example, the calculations for the initially estimated values using the equations given in Section 5.5.1(b) are now given for the 0.44mm thick SR sample. The initial value calculated for velocity, using Equation 5.5 was:

$$V_L = 2 \times 0.31e^{-3} \times 1.17e^3 = 1029 \text{ms}^{-1}$$

The sample was then cut to a 40mm square section and therefore had a volume of $7.04e^{-7} \text{m}^3$. The mass was measured at $6.96e^{-4} \text{kg}$. The initial estimate of the density of this sample was then:

$$\rho = \frac{\text{Mass}}{\text{Volume}} = \frac{0.49e^{-4}}{4.96e^{-7}} = 989 \text{kgm}^3$$

Next, the wavelength at resonance in the SR was calculated as:

$$\lambda = \frac{V_L}{f_n} = \frac{1029}{1.17e^6} = 0.88 \text{mm}$$

Then, $k = 2\pi/0.88e^{-3} = 7140$

Δf_n was measured to be 16kHz then

$$Q \text{ is } 1.17e^6/16e^3 = 73.1$$

The total losses inside the plate were calculated as:

$$\tilde{\alpha} = \frac{k}{2Q} = \frac{7140}{146.2} = 48.8 \text{ Npm}^{-1}$$

The specific acoustic impedance estimation for the SR is:

$$Z_1 = \rho V_L = 989 \times 986 = 0.975 \text{ MRayl}$$

Then the value of R is then calculated as 1.00 and so the actual value for the attenuation in the plate is just 48.8 Npm^{-1} , which is divided by 8.84 to find the value at 5.52 dBcm^{-1} .

b) Porous Filter

The coefficient of sound transmission through the porous filter and the corresponding theoretical calculations, are shown in Figure 5.11. The agreement between measurements and calculations is clearly very good and the noise level is very low. Therefore, the error in the calculation of velocity, density and attenuation of sound in the filter is also believed to be very low. A clear and highly damped peak in the transmission coefficient appears at 1.42MHz. At this point, velocity and attenuation of sound were calculated as previously described. These values agree well with those obtained from the calculation of the coefficient of sound transmission for the whole experimental frequency range and the fitting of the theoretical calculations to the experimental values. From this fitting, the density of the filter is also obtained. These results are shown in Table 5.4.

Velocity of sound (ms^{-1}) @ 1.42MHz	Attenuation of sound (dBcm^{-1}) @ 1.42MHz	Density (kgm^{-3})
343	120	360

Table 5.4 *Parameters of the Porous Filters.*

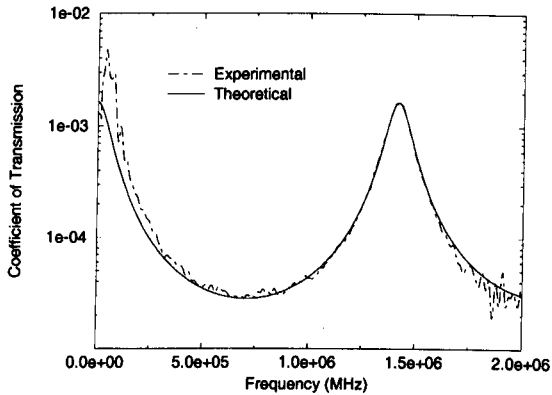


Figure 5.11 *Theoretical and experimental plots of transmission coefficient through a porous filter sample.*

c) Matching Layer

Next, the properties of the matching layers were measured. First cross-correlation techniques [88] were used to measure the time delays. This was done by receiving a narrowband and low frequency reference signal (600kHz) in air between two transducers and then receiving the signal when a sample matching layer is in place between the transducers. The signals were stored using a digital oscilloscope and the envelopes of the moduli of the two signals were taken. These two envelopes were then multiplied together, with the signal through the sample being shifted by one sample at a time. When a maximum in signal is found then the number of sample shifts at that point represents the increase in transit time through the matching layer when compared to air alone. Since the thickness of the matching layer can be measured, the average velocity within it can be calculated.

An estimate of the expected velocity of sound propagation in the matching layer can also be calculated from the thicknesses and the velocities of sound in the porous filter and the silicone rubber layers. The measured and calculated velocities obtained for two matching layers with different thickness are summarised in Table 5.5. It is noted that the calculated values are always higher than the experimental measurements. This can be explained by considering that the velocity of sound propagation in the

modified silicone rubber layer observed in the optical micrographs is slower than that in the unmodified silicone rubber. Considering the thickness of the modified silicone rubber to be 80 μm (as obtained from the optical microscopic images), a velocity of sound in the modified silicone rubber of 714 ms^{-1} (0.55mm sample) and 620 ms^{-1} (0.64mm sample) must be used to fit the theoretical values to the experimental measurements.

Matching Layer Thickness (mm)	Measured velocity of sound Using Cross Correlation (ms^{-1})	Calculated velocity of Sound Using 2 Layer model (ms^{-1})
0.55	656	702
0.64	686	732

Table 5.5 *Measured and calculated velocities in two matching layers.*

In addition, as noted in Section 5.1.1(c), there is a very thin (10 μm) portion of the porous filter partially saturated with silicone rubber (SF). This part of the matching layer cannot be isolated, making a direct measurement of its properties impossible. An exact calculation of its mechanical properties is well beyond the scope of this work, as the microstructure of the porous filter, and the uneven penetration of the silicone rubber in it, make investigation an extremely complex process. The velocity of sound in this layer can be estimated using the Biot's theory, with the data in Table 5.3, and the Mat Lab code produced by Gomez. This considered that the pores are saturated by a mixture of air and silicone rubber. The extremes of porosity in the saturated filter region were estimated to be between 20% and 40% air content. The result of this study was that the velocity in the SF phase of the matching layer varies between 950 ms^{-1} and 1030 ms^{-1} . When it is considered that this impregnation occurs over a layer of 10 μm thickness, then the estimated velocity of the modified silicone rubber phase must be altered to 520 ms^{-1} (0.64mm sample) and 620 ms^{-1} (0.55mm sample) to take account of this. For the purposes of modelling, a value of 570 ms^{-1} was selected for the MSR phase and a value of 980 ms^{-1} for the SF phase.

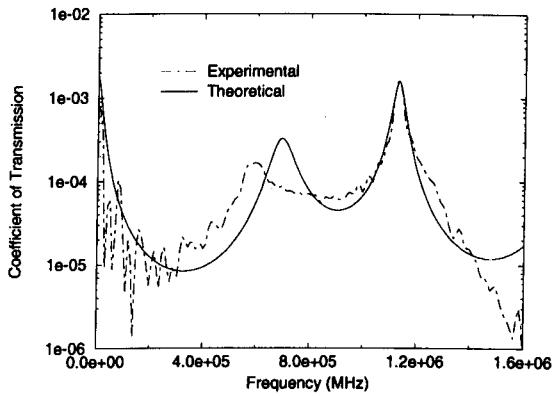


Figure 5.12 *Theoretical and experimental transmission coefficients through a matching layer.*

Figure 5.12 shows the transmission coefficient of the matching layer, measured as it was done in the previous cases. The total matching layer thickness for this experiment was 0.56mm. The final modelling parameters used for the four sublayer linear model are given in Table 5.6. These were the parameters used for the calculation of the theoretical transmission coefficient in Figure 5.12 For the remainder of this work, all linear systems modelling of the matching layers uses these parameters, and the only variable parameter is the thickness of the silicone rubber (SR) phase.

Layer	Density (kgm ⁻³)	Thickness (mm)	Attn @ 1MHz (dBcm ⁻¹)	Elastic Stiffness (Nm ⁻³)	V _L (ms ⁻¹)	Transit Time (μs)
1 SR	951	0.36	10	9.41e8	995	0.358
2 MSR	951	0.08	18	3.09e8	570	0.14
3 SF	697	0.01	100	6.97e8	980	0.010
4 PF	360	0.11	120	4.2e7	343	0.32

Table 5.6 *Characteristics of the four distinct sub-layers of the matching layers identified experimentally.*

Two resonance peaks appear in the coefficient of sound transmission shown in Figure 5.12. As explained previously, these peaks are due to the constructive and destructive interference of the signal trapped within the structure. The position of these can be confirmed if the transit time within the matching layer is considered. The total transit time would be 0.828μs corresponding to a $\lambda/2$ cavity resonance of 604kHz and a λ cavity resonance of 1.2MHz. These figures correlate reasonably well with the positions of the two peaks in Figure 5.12 and re-emphasise the importance of the cavity resonance with operation in air. The first resonant mode has been estimated less accurately than the second stronger mode. It is reasonable that this may be the case due to the extremely complex interactions and the absence of a perfect linear structure in practice, as is assumed by the model.

5.4.3 Conclusions

Microscopic and acoustic characterisation of the matching layers has been performed. As a result of this, a four sub-layer linear model has been developed to enable linear systems modelling to be performed and so provide a valuable tool for theoretically investigating the matching layers. It will now be possible to study theoretically the effects of varying key design parameters and so to produce the definitive designs for the most efficient operation at a given frequency for attachment to air-coupled transmitters and receivers.

5.6 Development of the Matching Layer Design Strategy

5.6.1 Introduction

The main objectives in this section are four fold:

- a) Use the model to investigate key matching layer/transducer design parameters.
- b) Verify the validity of the model experimentally.
- c) Produce comprehensive design guidelines for pitch-catch operation.
- d) Verify experimentally the chosen design for the current application.

It was proposed that the development of the matching layer design strategy would combine experimental investigations with a theoretical study of the influence of varying key design parameters using the new four layer linear model. The correlation between the theory and experiment is used as verification of the validity of the model. In order to achieve this, a range of transmitters, receivers and matching layers were manufactured with the intention of covering a broad range of possible consideration.

5.6.2 Transducer Considerations for Model Verification

a) Matching Layers Manufactured

In order to investigate the performance of the matching layers and the validity of the model experimentally, eleven matching layers were manufactured. The thicknesses of these are shown in Table 5.7. 'Modelled SR Thickness' is the thickness selected to model the thickness of the silicone rubber phase for each matching layer, given that the rest of the thickness (MSR plus SF and PF) remains unchanged at 0.2mm. 'Calculated Transit Time' is the calculated time for ultrasound to pass from one side of the matching layer to the other. The thicknesses varied over the range that has been manufactured successfully to date. Temporary attachment of the matching layers was achieved using coupling gel.

Matching Layer	Thickness (mm)	Modelled SR Thickness (mm)	Calculated Transit Time (μ s)
M1	0.21	0.01	0.47
M2	0.26	0.06	0.53
M3	0.35	0.15	0.62
M4	0.4	0.2	0.67
M5	0.44	0.24	0.71
M6	0.55	0.35	0.82
M7	0.66	0.46	0.93
M8	0.76	0.56	1.03
M9	0.85	0.65	1.12
M10	0.94	0.74	1.21
M11	1.06	0.86	1.33

Table 5.7 Matching layers used in experimental investigations.

b) Transducers Used in Testing

As well as the matching layers, eight transducers were manufactured for use in the experimental investigations. Descriptions of these are provided in Table 5.8 where the ‘Frequency’ column indicates the operational frequency for each transducer. The ‘Perspex Type and Thickness’ column indicates whether a perspex plate is attached to the front face and if so, what its thickness is in relation to the wavelength of operational frequency within it. This was calculated based on the assumption of a longitudinal acoustic velocity in Perspex of 2770ms^{-1} .

The acoustic transit times through each of the modelled layers are important as these will form the basis of the calculations of the transducer cavity resonances and the resulting frequency responses. The structure of the modelled layers and the transit times within these layers are shown in Figure 5.13. The silicone rubber thicknesses and transit times will be determined by the thickness of the matching layer under consideration.

Transducer Name	Type	Frequency (kHz)	Perspex Type and Thickness
TNP	Transmitter	Fe=600	None
TP4	Transmitter	Fe=600	$\lambda/4$ Plate – 1.15mm
TP2	Transmitter	Fe=600	$\lambda/2$ Plate – 2.3mm
TL4	Transmitter	Fe=600	$\lambda/4$ Lens – 1.15mm
TL2	Transmitter	Fe=600	$\lambda/2$ Lens – 2.3mm
RNP	Receiver	Fm=600	None
RP4	Receiver	Fm=600	$\lambda/4$ Plate – 1.15mm
RP2	Receiver	Fm=600	$\lambda/2$ Plate – 2.3mm

Table 5.8 Transducers used in experimental investigations.

Receiver 0.833 μ s	Perspex	Silicone Rubber	0.47 μ s		
	$\lambda/4$ 1.15mm 0.415 μ s		MSR	SF	PF
Transmitter 0.645 μ s	$\lambda/2$ 2.3mm 0.83 μ s	? μ s			

Figure 5.13 Cavity layer arrangement and modelled transit times.

c) Influence of Perspex on Design

As noted in Chapter 4, the current application includes the attachment of Perspex lenses to the transmitter and the receiver array to improve defect detection resolution. It was therefore imperative that the influence of the lenses on the design of the matching layers was determined. This was done by investigating the frequency responses of the two transmitters TL4 and TL2. These both had perspex lenses of 40mm radius of curvature attached. The only difference between the lenses was the thickness at the thinnest part as shown in Figure 5.14. This is the part of the lens that is 'parallel' to the active faces of the transducer and will be referred to as the

dimension 'a'. With the two test transducers, this dimension was chosen to be $\lambda/4$ (TL4) and $\lambda/2$ (TL2) thickness at the operational frequency of the transducer.

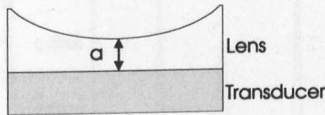


Figure 5.14 *Dimension of lens under investigation.*

Again, a wideband electrostatic transducer (Figure 5.5) was used to receive the wideband transmitted signals in air. The responses of the two transducers are shown in Figures 5.15 and 5.16. Also included in these Figures are the linear systems models, as presented in Figures 5.6b and 5.6c, that considered attachment of two plates with perspex of $\lambda/4$ and $\lambda/2$ thickness. It is clear from these results that dimension 'a' has a critical influence on performance and has a behaviour similar to that of a plate. Maxima and minima occur at the same frequencies shown in Figure 5.6 and it is therefore concluded that the transducer and the low, parallel part of the lens form a cavity within which the energy reverberates. This observation has had significant bearing on the remainder of this work. A plate of perspex will be assumed to simulate the behaviour of a lens when developing the optimum designs for the matching layers in this application. This simplifies the modelling and enables the linear systems model to be adopted.

Figure 5.15 *Measured response of TL2 with lens having a thickness of dimension 'a'*

Design of the Perspex Lens
In addition to the important lens dimension 'a' as discussed in the previous section, it was also required to determine the focal distance, that is, the point from a given lens radius of curvature. Basic design rules were employed to ensure a clear understanding of the perspex lens design. The design for an acoustic lens (29) is based on similar rules to those used for optical lens design, with the exception to calculate the focal length f_c is given in the following equation:

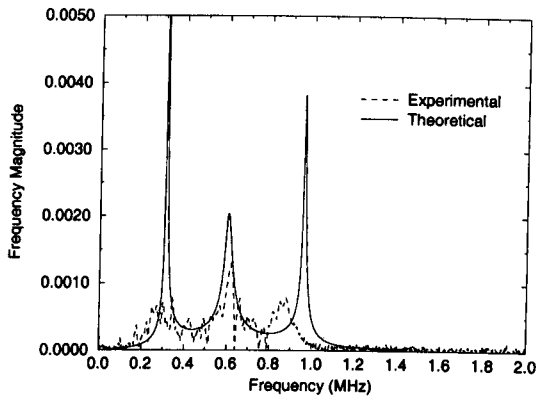


Figure 5.15 *Wideband response of TLA with lens having 'a' dimension of $\lambda/4$.*

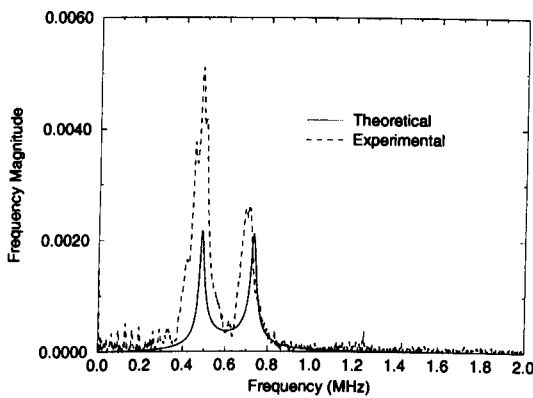


Figure 5.16 *Wideband response of TL2 with lens having 'a' dimension of $\lambda/2$.*

d) Design of the Perspex Lenses

In addition to the important lens dimension (a) as discussed in the previous Section, it was also required to determine the focal distance that is expected from a given lens radius of curvature. Basic design rules were employed to ensure a clear understanding of the perspex lens design. The design for an acoustic lens [89] is based on similar rules to those used for optical lens design, and the expression to calculate the focal length f_L is given in the following equation:

$$1/f_L = |(c_1 - c_L)/c_L| (1/r)$$

Equation 5.8

where r represents the concave radius of curvature of the lens outer surface, and c and c_L represent the speeds of sound in the surrounding medium and lens respectively. The radius of curvature (r) of the Perspex lens attached to the composite transducer scanned in the previous Chapter was approximately 40mm. The beam profile given in Figure 4.11 shows a focal length at around 45mm and this is in correlation with the calculation using Equation 5.8. This is based on velocities of sound in the Perspex lens and in the air load of 2770ms^{-1} and 343ms^{-1} respectively and results in a calculated f_L of 45.6mm.

5.6.3 Transmission Responses

a) Modelled Variation of the Thickness of the SR Layer

Next, the design of the matching layers for operation in transmission mode was considered. This was achieved theoretically using the linear systems model and the four sub-layer linear model that has been developed for the matching layers. As stated previously, the only matching layer design variable at present is the thickness of the silicone rubber sub-layer, so the effect on performance of varying this thickness was considered. The addition of perspex plates between the transducer and the matching layer (as shown in Figure 5.6b and 5.6c) was also included to simulate the inclusion of lenses. Both $\lambda/4$ and $\lambda/2$ Perspex thicknesses were considered and the results are given in Figures 5.17 and 5.18 respectively. In each case, variation of the pressure output as the silicone rubber thickness was varied from 0.02 to 2.0mm in 0.02mm steps was investigated. The peak pressure at each SR thickness is plotted (Frequency Magnitude) for both the frequency of the transducer (600kHz) and over the frequency band 0-1.5MHz.

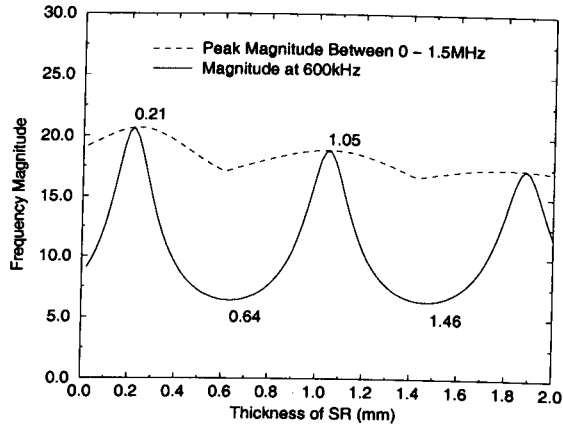


Figure 5.17 *Variation of SR thickness with $\lambda/4$ Perspex included in transmission.*

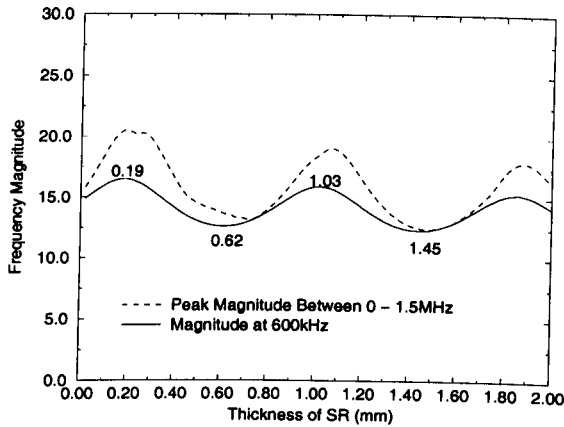


Figure 5.18 *Variation of SR thickness with $\lambda/2$ Perspex included in transmission.*

Although the variation over the full frequency band is included, it is of more interest to consider the variation at a certain frequency. This is important for pitch-catch operation since the transmitter and receiver must operate at the same frequency for optimum efficiency. First of all it is noted that, in both graphs, the distances between consecutive maxima and consecutive minima are $\lambda/2$ SR thickness. Also, the distance between each maximum and the next minimum is $\lambda/4$. This is consistent with the cavity resonance hypothesis. It is also important to note that the variation

between maximum and minimum response is much greater when $\lambda/4$ Perspex is included. Although there is not much difference between the maximum values, these results would still suggest that using $\lambda/2$ Perspex would be preferable, as it should result in more consistent performance.

b) Theoretical and Experimental Frequency Responses

Experimental wideband investigation of these results was performed and the results are given in Figures 5.19 to 5.21. Again, the electrostatic transducer with response as in Figure 5.5 was used as the reception device. These results include theoretical results using the linear systems model. The correlation between theoretical and experimental results serves as verification of the validity of the model. Figure 5.19 shows the response for matching layer M7, with SR thickness 0.46mm, and $\lambda/4$ Perspex thickness (TP4). Note that, in Figure 5.17, the response at 600kHz is close to a minimum for this SR thickness. It is now seen from Figure 5.19 that the response is very close to minimum at 600kHz for this matching condition.

Using the cavity theory with the transit times in the layers, the null at 620kHz in Figure 5.19 can be calculated to be very close to the $5\lambda/4$ destructive interference. That is:

$$\begin{aligned} \text{Transducer + Perspex + Matching Layer} &= (0.645+0.415+0.93)\mu\text{s} \\ &= 1.99\mu\text{s cavity transit time.} \end{aligned}$$

Corresponding to a $5\lambda/4$ cavity frequency of 628kHz

In the same way, the $3\lambda/4$ cavity frequency is calculated to be 377kHz, which is close to the first minimum in the spectrum.

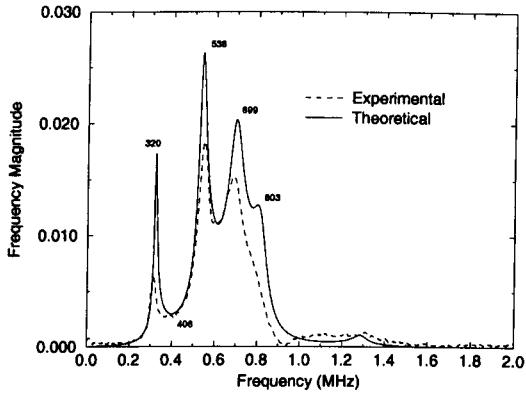


Figure 5.19 *Wideband response using TP4 and matching layer M7.*

Figures 5.20 and 5.21 show the responses with TP2 ($\lambda/2$ Perspex thickness) and matching layers M10 (SR thickness = 0.74mm) and M4 (SR thickness = 0.2mm) respectively. Both of these plots show a much greater concentration of energy around the centre frequency of the transducer. Again these results agree well with the cavity resonance theory if the transit times are calculated as above.

For example, with the transducer used for the Figure 5.20:

$$\begin{aligned} \text{Transducer + Perspex + Matching Layer} &= (0.645+0.83+1.33) \mu\text{s} \\ &= 2.8\mu\text{s cavity transit time.} \end{aligned}$$

Corresponding to $3\lambda/4$, $5\lambda/4$ and $7\lambda/4$ frequencies of 268, 446 and 625kHz ,
and $\lambda/2$ and λ frequencies of 178 and 357kHz.

These theoretical cavity frequencies agree very well with the maxima and minima of Figure 5.20 and therefore provide strong validation of the proposed cavity interference theory.

Note that the thickness of M4, used in Figure 5.21, is very close to the suggested optimum thickness at 600kHz in Figure 5.18. This is in keeping with the strong signal at 600kHz that is evident in Figure 5.21.

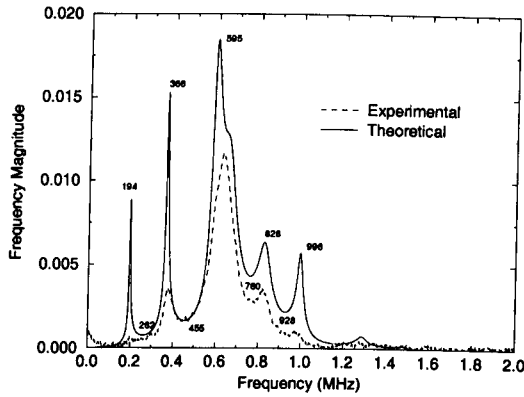


Figure 5.20 *Wideband response using TP2 and matching layer M10.*

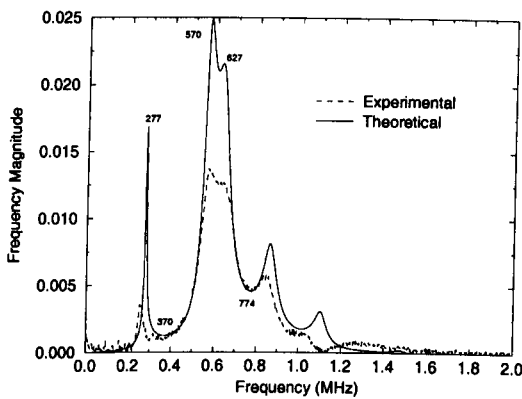


Figure 5.21 *Wideband response using TP2 and matching layer M4.*

c) Experimental Narrowband Behaviour

In order to verify the result of Figures 5.18 experimentally, transducer TP2 was tested in narrowband mode with the attachment of each of the matching layers in Table 5.7. The matching layers were attached using coupling fluid. Transducer TP2 was used to test the transmission performance with the wideband electrostatic transducer with a current amplifier used as receiver. Excitation was a 10 volt peak to peak 20 cycle, 600kHz tone burst and the device separation was 50mm. The received peak to peak signal was measured and plotted against the estimated silicone rubber thickness for each matching layer (as given in Table 5.7).

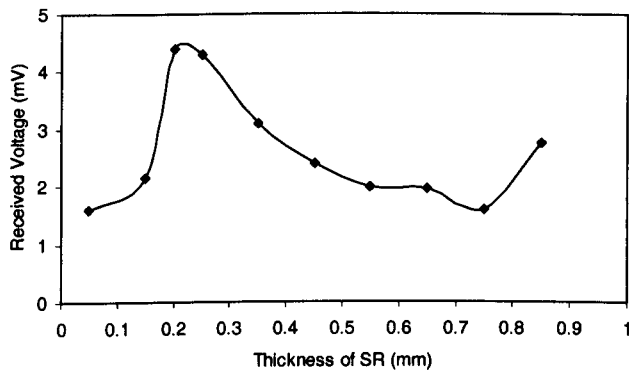


Figure 5.22 *Experimental narrowband transmission performances of TP2 with different matching layers attached.*

The results in Figure 5.22 are in reasonable agreement with the theoretical plot in Figure 5.18. Peak response occurs for matching layer M4 (matching layer thickness 0.4mm) which has presumed SR thickness of 0.2mm. The signal with no matching layer attached was also measured with the same arrangement. An improvement in transmitted amplitude of a factor of 8 was achieved with the attachment of matching layer M4. It should be recalled that the values for the SR thickness are based on measurement of the matching layer thickness and on the theoretical and experimental results presented in Section 5.5.2. Perfect matching layer and sub-layer thicknesses are assumed in the modelled results of Figure 5.18. Despite this, the peak value with matching layer M4 is in agreement with the peak at 0.2mm SR in Figure 5.18. The overall trends of the results of Figures 5.22 and 5.18 are also similar since the increase in response with M11 (SR thickness of 0.86mm) indicates an increase towards a second peak at $\lambda/2$ thicker than the first.

In relation to matching layer design, the results of Figure 5.22 are significant in that they demonstrate the practical accuracy of the theoretical results in Figure 5.18. A lack of absolute certainty of the properties of each individual matching layer will always mean that there will be an error factor that must be taken into consideration. However, it is believed that the best route to achieving the matching layer thickness for optimum performance is to use that predicted theoretically using the developed linear model.

5.6.4 Reception Responses

a) Modelled Variation of the Thickness of the SR Layer

Similar theoretical and experimental investigations to those in the previous Section were also carried out for the matching layer operation in reception. Figures 5.23 and 5.24 show the effect of varying the SR thickness on the reception at the centre frequency of the transducer and also over the band 0-1.5MHz. Again, the addition of perspex plates of $\lambda/4$ and $\lambda/2$ thickness was considered. The trends of these results agree with the cavity resonance hypothesis in a similar way to the results of Figures 5.17 and 5.18. Note, however, that the positions of the resonance maxima and minima are not the same. This could be due to the different volume fractions of the transmitter (70%) and the receiver (30%) used in the modelling.

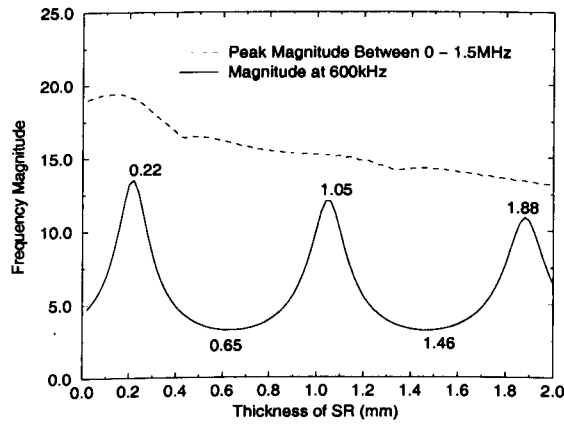


Figure 5.23 Variation of SR thickness with $\lambda/4$ Perspex included in reception.

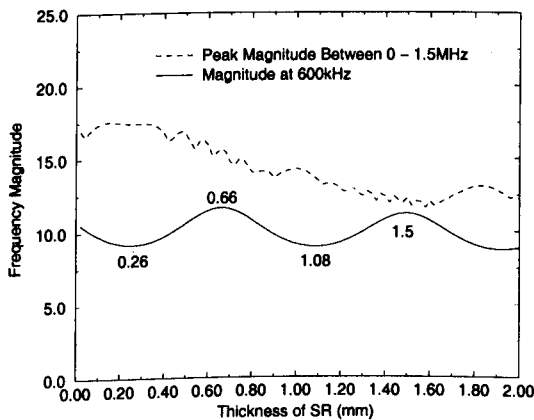


Figure 5.24 Variation of SR thickness with $\lambda/2$ Perspex included in reception.

b) Theoretical and Experimental Frequency Responses

These results have also been verified experimentally and the theoretical/experimental plots are shown in Figures 5.25 to 5.27. Note that the experiment and theory are again in close correlation. Figure 5.25 is included to show the response with no Perspex included. This demonstrates well that the cavity theory still stands without the perspex when it is considered that the calculated cavity transit time here is:

$$\text{Transducer + Matching Layer} = (0.833 + 0.93)\mu\text{s} = 1.763\mu\text{s}$$

Corresponding to a $3\lambda/4$ cavity frequency of 425kHz

Agreeing well with the minimum of Figure 5.25.

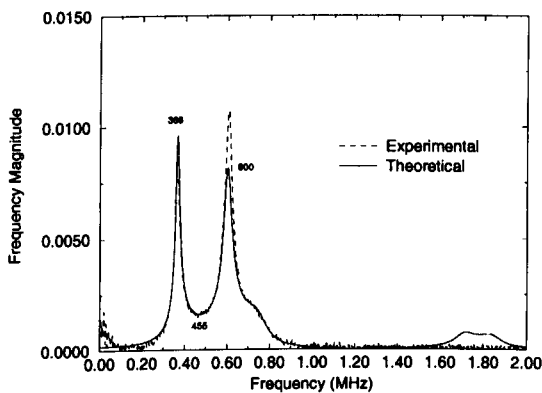


Figure 5.25 *Wideband response using RNP and matching layer M7.*

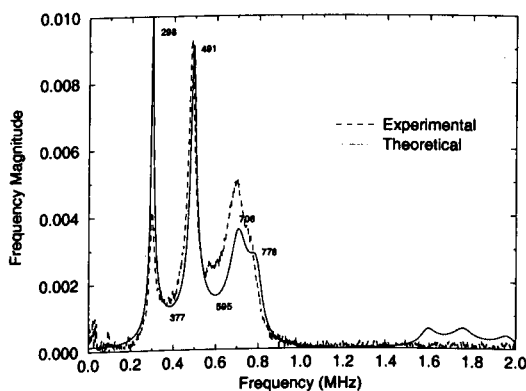


Figure 5.26 *Wideband response using RP4 and matching layer M7.*

Figure 5.26 shows a minimum and Figure 5.27 shows a maximum at 600kHz. This agrees with the values in the plots of Figures 5.23 and 5.24 for a silicone rubber thickness of 0.47mm. Calculation of the transit times also shows good agreement with the cavity resonance hypothesis. It is significant to note here that with the same matching layer (M7), the response at 600kHz changes from a maximum to a minimum between Figures 5.26 and 5.27 due only to the difference in Perspex thickness of $\lambda/4$.

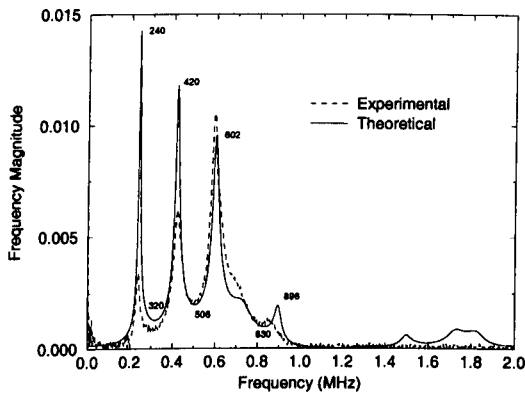


Figure 5.27 *Wideband response using RP2 and matching layer M7.*

c) Experimental Narrowband Behaviour

Transducer RP2 was used to test reception performance. This time, the electrostatic transducer was used as transmitter with the excitation signal and device separation remaining the same. Reception sensitivity with RP2, with the attachment of the same matching layers, was considered as described previously and the results are presented in Figure 5.28. These results demonstrate experimentally the theoretical results of Figure 5.24. Again, the general trends in performance as the matching layer thickness is increased have been predicted well by the model. The multi-layer linear model is therefore once more confirmed as an accurate and useful tool for the design of the matching layers. The optimum matching layer here was measured experimentally to be M7 (with SR thickness of 0.46mm) and this provided a factor of four improvement in reception sensitivity compared to the signal received with no matching layer attached.

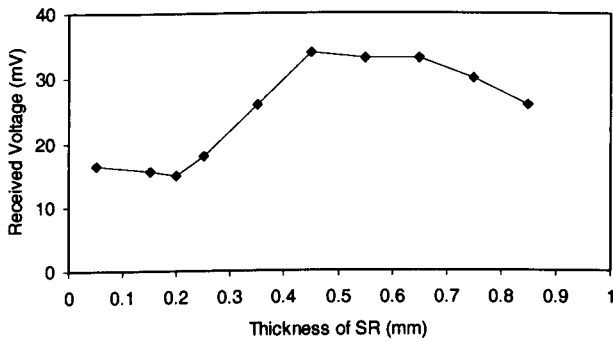


Figure 5.28 *Experimental narrowband reception performance of RP2 with different matching layers attached.*

5.6.5 *Electrical Impedance Responses*

The electrical impedances profiles of TP2 and RP2 with the matching layers that provided the best performance attached (M4 and M7 respectively) were measured and the results for both magnitude and phase are given in Figures 29 (a) and (b) and 30(a) and (b). The profiles predicted theoretically for the two cases were also calculated and these results are provided with the correlation again supporting the validity of the model. The frequency responses of both of these transducer/matching layer combinations have been measured previously and the results were in Figures 5.21 and 5.27. Note that the positions of the resonances have been predicted well. As mentioned previously, these resonances are in agreement with the cavity resonance theory. The magnitudes of some of the resonances have been overestimated, however. This may have been due to the non-ideal attachment of the matching layers using the coupling fluid. This should be overcome, at least in part, when the matching layers are permanently bonded onto the surfaces of the transducers.

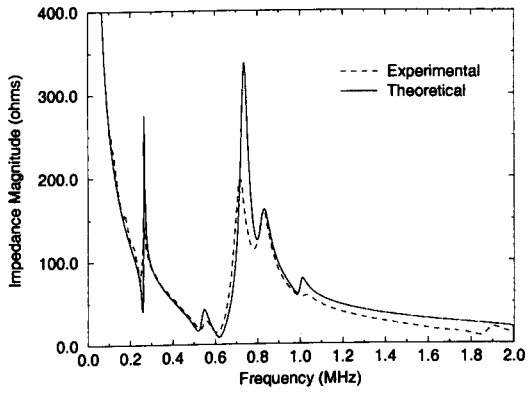


Figure 29(a) *Experimental and Theoretical electrical impedance magnitude of TP2 plus M4.*

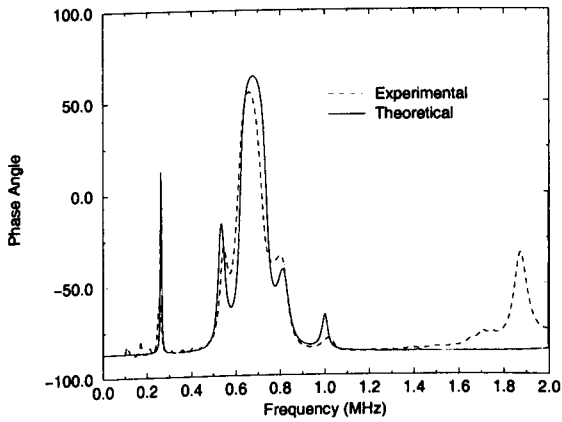


Figure 29(b) *Experimental and Theoretical electrical impedance phase of TP2 plus M4.*

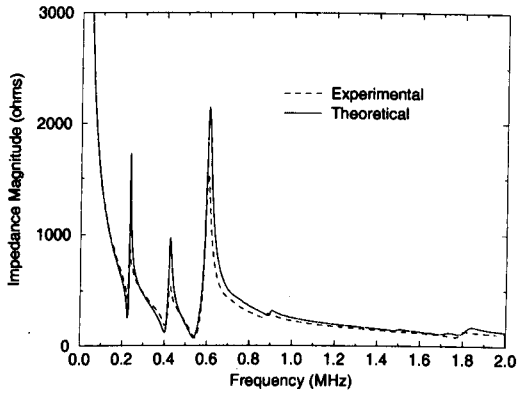


Figure 30(a) *Experimental and Theoretical electrical impedance magnitude of RP2 plus M7.*

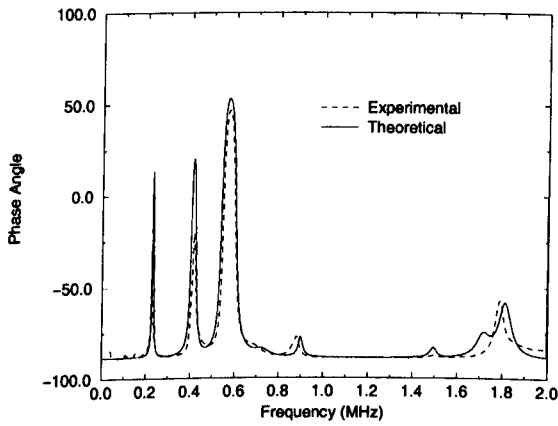


Figure 30(b) *Experimental and Theoretical electrical impedance phase of RP2 plus M7.*

5.6.6 Pitch-Catch Performance Investigation

The performance of the matching layers identified as being the best at 600kHz were tested in pitch-catch mode and the result is presented in Figure 5.31. Transducers TP2 and RP2 were used as transmitter and receiver respectively and excitation was a 10volt peak to peak tone burst of 20 cycles and 600kHz. No pre-amplifier was used and device separation was 100mm. The signals received with neither of the transducers, and only the transmitter matched are also included. The improvement in amplitude with attachment of both matching layers is measured to be 30dB.

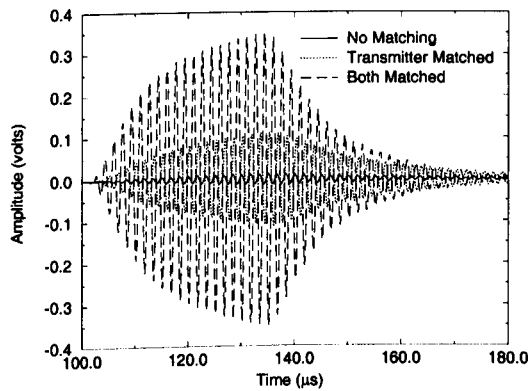


Figure 5.31 *Experimental narrowband pitch-catch responses with and without matching layers attached.*

5.6.7 Design Graphs and Guidelines

a) Introduction

As discussed in Section 5.3.2, in the absence of materials with suitable parameters in terms of acoustic impedance and attenuation, there is a tendency for the majority of acoustic energy to be trapped within the transducer structure when operating in air. This energy then reverberates within the transducer and matching layer as a single cavity. The interaction between the constructive and destructive interfering resonances within a matched transducer structure is extremely complex and is dependent on a number of system parameters. These include the thickness, attenuation, longitudinal acoustic velocity and acoustic impedances of each constituent part of the matching layer and the transducer.

It would be possible to make the relevant calculations for each individual case. However, the use of the linear model developed in previous Sections to produce design or 'lookup' graphs to assist in the design for specific applications and give a clear indication of the optimum arrangements would be significantly more efficient and would allow a broader picture to be attained. The main aim here will be to look at both the transmitter and the receiver performance in order to enable design for pitch-catch operation, as has been the case throughout this Thesis. Coupling in air will be the only consideration and for simplicity it will be assumed that air backing is selected in order to maximise the sensitivity and that operation is narrowband. Both with and without the inclusion of perspex will be considered and it will be assumed, as before, that $\lambda/2$ is the preferred thickness. Addition of the perspex is believed to be an adequate simulation of the effects of the cavity resonances when a lens is attached. For the most part, it will also be assumed that 70% PZT5H composite will be selected for transmitter and operational frequency is at electrical resonance and a 30% volume fraction PZT5A composite will be selected for receiver with operational frequency being at the mechanical resonance. The modelled results when the volume fraction is varied with a transducer possessing 600kHz operational frequency are also given for both transmission and reception. The overall aim in the matching layer design is to decide on the best operational frequency for a given application. The design decision that is then made, on the basis of the operational frequency chosen, is the thickness of the matching layer.

b) Transmitter Design Guidelines

First of all it should be noted that the performance in transmission with and without the $\lambda/2$ perspex included is almost identical as can be seen in Figure 5.32. The case with the perspex included is noted to be slightly less sensitive but the variation with SR thickness is the same. It is worth noting here again that although the variation of the magnitudes over the frequency band 0 to 1.5MHz are included, it is only the magnitude at the operational frequency that is of interest due to the unpredictable nature of other resonances.

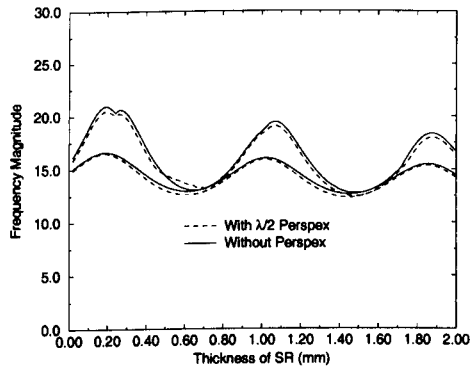


Figure 5.32 Theoretical variation of the SR thickness in transmission at 600kHz and over the band 0-1.5MHz, both with and without $\lambda/2$ Perspex.

Figure 5.33 shows the peak magnitudes for transducers with operational frequencies from 300kHz to 1MHz as the silicone rubber thickness was varied from 0.02 to 1mm in 0.02mm steps at each frequency. Figure 5.34 shows silicone rubber thicknesses that were used to achieve the peak frequency magnitudes plotted in Figure 5.33. It is re-emphasised here that the SR thickness represents the thickness of the whole matching layer minus 0.2mm. The suggested SR thickness in Figure 5.34 initially shows gradual decrease as the frequency considered increases. This is in keeping with the cavity resonance theory since as the frequency increases, the cavity wavelength decreases. Note that there is a rapid increase in the suggested SR thickness between 650kHz and 700kHz. This can be explained with reference to Figure 5.35, which shows a selection of the graphs modelled to produce the data of Figures 5.33 and 5.34. For 700kHz there are two maxima, at 0.02 and 0.72mm. These are two different cavity resonances separated by a SR thickness change of $\lambda/2$ at the operational frequency. The thickness selected for the 700kHz transducer is the thicker of the two peaks due to the difficulty in manufacturing accurately at the lower thickness. At 650kHz, the cavity wavelength was slightly larger than with 700kHz resulting in the slightly thicker SR thickness of 0.1mm at the lower peak being selected. Investigation of the results at the different frequencies in Figure 5.35 shows how the cavity resonances change with operational frequency. The values for maximum output magnitudes and the SR thicknesses used to achieve these at each frequency modelled are also given in Table 5.9.

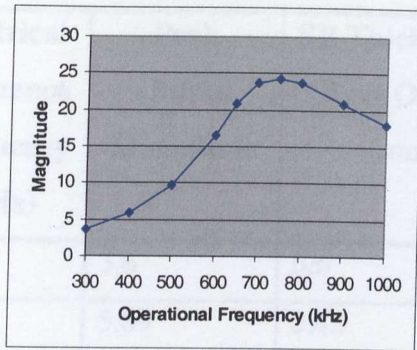


Figure 5.33 Theoretical peak transmitter output responses at different transducer operational frequencies as the SR thickness was varied.

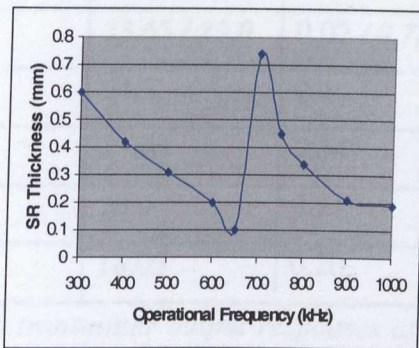


Figure 5.34 Theoretical silicone rubber thicknesses used to achieve the peak response magnitudes plotted in Figure 5.33.

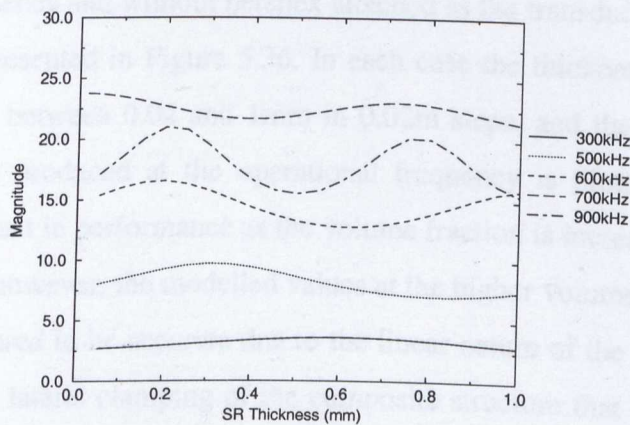


Figure 5.35 A selection of the theoretical SR thickness variation graphs that were modelled at different frequencies to produce the data plotted in Figures 5.33 and 5.34.

Electrical Resonance Frequency (kHz)	Peak Output Magnitude	SR Thickness at Peak Output (mm)	Transducer Thickness (mm)
300	3.6	0.6	5.12
400	5.89	0.42	3.84
500	9.7	0.31	3.07
600	16.5	0.2	2.56
650	20.9	0.1	2.36
700	23.65 / 23.0	0.02 / 0.72	2.20
750	24.3	0.45	2.05
800	23.65	0.34	1.92
900	20.9	0.21	1.70
1000	18.05	0.20	1.54

Table 5.9 Peak transmitter output responses at operational frequency and also the SR thicknesses at which they were achieved.

The variation of the peak performance of a composite transmitter with 600kHz operational frequency and without perspex attached as the transducer volume fraction is increased is presented in Figure 5.36. In each case the thickness of the matching layer was varied between 0.02 and 1mm in 0.02m steps, and the magnitude of the maximum signal produced at the operational frequency is plotted. This shows a steady improvement in performance as the volume fraction is increased. As discussed in Section 4.2.3, however, the modelled values at the higher volume fractions (>80%) cannot be considered to be accurate due to the linear nature of the model being used and the increased lateral clamping of the composite structure that is not considered. In light of this result, the transmitter volume fraction value of 70%, that has been assumed throughout this Thesis, is therefore also considered to be the recommended selection when the new matching layers are included.

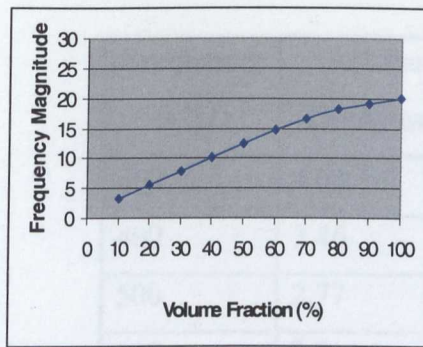


Figure 5.36 Theoretical transmitter performance variation as the volume fraction is increased.

c) Receiver Design Guidelines

It has been noted in reception that the performance with and without perspex does not demonstrate the same similarity as was seen in the transmission case. However, Figure 5.37 shows that the variation at the operational frequency of 600kHz (the lower two plots of the four) is again very similar. This was tested over the frequency range 300kHz to 1MHz with similar results at the operational frequencies in each case. Since this is the main consideration, it is believed that only the magnitude and SR thickness results without Perspex attached require to be given. For completeness, and for design simplicity, the Perspex thicknesses used for the modelling of $\lambda/2$ Perspex are given in Table 5.10 for a range of frequencies, based on a longitudinal velocity of 2770ms^{-1} .

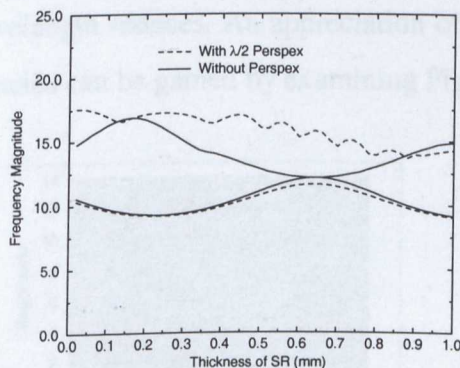


Figure 5.37 Theoretical variation of the SR thickness in reception at 600kHz and over the band 0-1.5MHz, both with and without $\lambda/2$ Perspex.

Frequency (kHz)	$\lambda/2$ Perspex Thickness (mm)
300	4.62
400	3.46
500	2.77
600	2.31
700	1.98
800	1.73
900	1.54
1000	1.38

Table 5.10 The thicknesses of the $\lambda/2$ Perspex used in modelling.

Figures 5.38 and 5.39 and Table 5.11 show the results of peak receive sensitivity as the SR thickness is varied in the same frequency range as was used in the transmitter models. The suggested SR thickness in Figure 5.39 is low until the frequency of 500kHz. This is because it is not until this frequency that a cavity resonance maxima is present in the SR thickness range from 0.02 to 1mm. This is clarified by comparing plots for 300kHz and 500kHz in Figure 5.40. The increase in suggested SR thickness between 750kHz and 800kHz can be explained in the same way as before. This is due again to a switch between cavity resonances as the operational frequency increases and the cavity wavelength reduces. An appreciation of the change in cavity response at different frequencies can be gained by examining Figure 5.40.

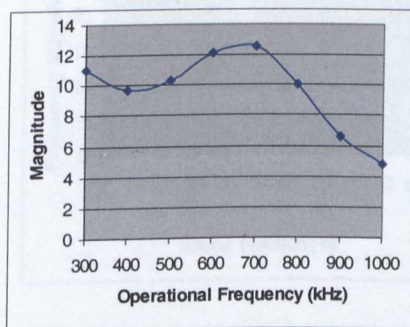


Figure 5.38 Theoretical peak reception performance at different receiver operational frequencies as the SR thickness was varied.

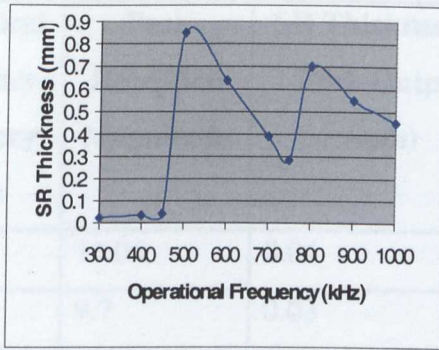


Figure 5.39 Theoretical silicone rubber thicknesses used to achieve the peak response magnitudes plotted in Figure 5.37.

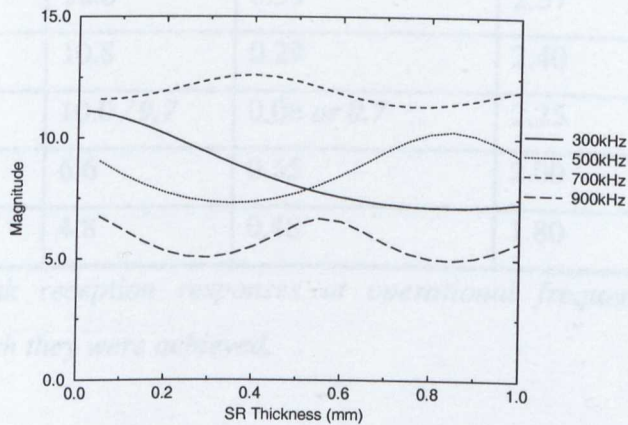


Figure 5.40 A selection of the theoretical SR thickness variation graphs that were modelled at different frequencies to produce the data plotted in Figures 5.38 and 5.39.

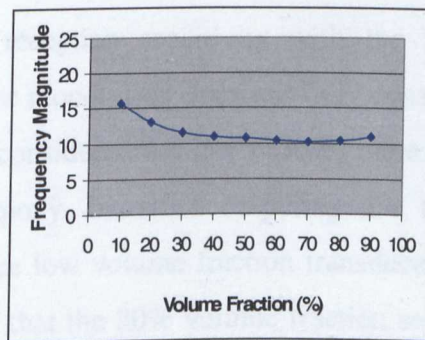


Figure 5.41 Theoretical performance variation of 600kHz receivers with no perspex attached as the SR thickness is varied and volume fraction increases.

Mechanical Resonance Frequency (kHz)	Peak Reception Magnitude	SR Thickness at Peak Output (mm)	Transducer Thickness (mm)
300	11.05	0.04	6.00
400	9.7	0.03	4.50
450	9.5	0.02	4.00
500	10.3	0.85	3.60
600	12.1	0.64	3.00
700	12.6	0.39	2.57
750	10.8	0.29	2.40
800	10.0 / 9.7	0.06 or 0.7	2.25
900	6.6	0.55	2.00
1000	4.8	0.48	1.80

Table 5.11 *Peak reception responses at operational frequency and the SR thicknesses at which they were achieved.*

The variation of the peak performance of a composite receiver as the transducer volume fraction is increased is presented in Figure 5.41. In this case the transducer had 600kHz mechanical frequency and had no perspex attached. As with Figure 5.35, each point represents the maximum receive magnitude for that volume fraction at 600kHz as the SR thickness is varied from 0.02 to 1mm. In this case there is a slight improvement in reception sensitivity with the lower volume fractions. Again, however, the linear model used does not fully consider the lateral effects. When the volume fractions considered are low (<30%) there is an increase in damping of the ceramic by the epoxy. Increased de-poling due to the amount of dicing that is required to produce low volume fraction transducers is also a practical factor. This leads to the belief that the 30% volume fraction selected for the receivers that have been employed throughout this Thesis is also suitable when designing receivers with the new matching layers attached.

d) Pitch-Catch Design Example

It is noted from Figures 5.35 and 5.40 that the use of 700kHz operational frequency for the transmitter and receiver would be an efficient frequency at which to operate in a pitch-catch system. The value of 600kHz that was selected for the prototype designs in the development of the air-coupled scanner introduced in Chapter 3 and used throughout this Thesis would also seem to be reasonable. As an example of the use of the design graphs presented here, the design of a 700kHz pitch-catch transducer pair is now given. It is assumed that the composite volume fractions used is 30% and 70% for the receiver and the transmitter respectively and that the attachment of $\lambda/2$ perspex to both transducers to simulate lens behaviour is employed.

When the operational frequency is decided the first thing that requires to be done is the manufacture of the transducers. The thicknesses of these are calculated for the electrical resonance for the transmitter and the mechanical resonance for the receiver and are given in Tables 5.9 and 5.11 respectively.

Transmitter thickness = 2.20mm

Receiver thickness = 2.57mm

The thickness of the Perspex required for half wavelength operation at 700 kHz can be found in Table 5.10.

Perspex thickness for $\lambda/2$ operation at 700kHz = 1.98mm.

The thicknesses of the matching layers can be calculated from the SR thicknesses given in Table 5.9 and 5.11 for the transmitter and receiver respectively by adding 0.2mm to the SR thickness to include MSR, SF and PF considerations.

Transmitter matching layer thickness = $0.74 + 0.2 =$ 0.94mm

Receiver matching layer thickness = $0.39 + 0.2 =$ 0.59mm

5.6.8 Summary

Empirical and theoretical methods have been used to design matching layers for operation in the pitch-catch air-coupled system. The accuracy of the linear matching layer model has been proven with comparison of modelled and experimental results. This has been done using both wideband and narrowband techniques and perspex plates have been used to simulate the inclusion of perspex lenses. With wideband testing, the frequency responses were measured and the resonant maxima and minima were noted to be in similar agreement with the cavity resonance theory. Tone burst excitation was also considered to investigate narrowband performance variation as the matching layer thickness was varied in both transmission and reception. Comparison of the theoretical plots of Figures 5.18 and 5.24 with the experimental results of Figures 5.22 and 5.28 lead to the belief that the modelled results are accurate. This would mean that matching layer thicknesses of 0.4mm and 0.86mm for transmitter and receiver respectively would provide the best improvement at 600kHz. This assumed that the transducers are 600kHz centre frequency and that $\lambda/2$ Perspex plates are attached. Using the matching layers designed, an improvement of 30dB was measured. It is now also believed that the design graphs provided could be used to design matching layers for other applications at different frequencies.

5.7 Conclusions

A novel concept in matching layer design for operation in air has been proposed. This takes into account the absence of a suitable material and the resulting energy entrapment within the transducer structure. Transducer cavity resonance maxima and minima dominate the responses, and the resonances within the transducer or a matching layer alone are insignificant. A new matching layer technology has also been developed that takes advantage of the very low specific acoustic impedances possible with porous materials. Microscopic and acoustic analyses of this technology enabled a linear model to be developed, and the accuracy of this has been verified experimentally. This model has been used to design matching layers for the transducers in the current air-coupled through transmission NDT system. These have been manufactured, and experiment has been used to substantiate the design.

CHAPTER 6

RESULTS AND EVALUATION OF **PROTOTYPE SYSTEMS**

Abstract

Prototype systems that have evolved as a result of the work throughout this Thesis were investigated by performing air-coupled through transmission C-scans of a number of realistic aerospace test samples. The results of this testing are presented within this Chapter. Both solid carbon fibre and honeycomb samples were scanned and the defects investigated included delaminations, inclusions, porosity and impact damage. The purpose of this evaluation was to establish the system limitations in terms of defect detection and resolution capability. Scan results of two of the samples were compared with water- coupled scans performed with an industrial scanner. Both single element and eight-channel parallel data acquisition were investigated and scanning was performed without recourse to signal averaging. The eight channel air-coupled system was also integrated with industrial water-jet scanning equipment and rapid scans were achieved, providing further evidence of the potential of the technology to improve scan rates.

6.1 Introduction

Assessment of the resolution and defect detection capability of the eight-channel prototype air-coupled system was achieved by performing through transmission C-scans of realistic aerospace test samples. The results of both laboratory and industrial testing and direct comparisons with water-coupled systems are provided and discussed in this Chapter. The principal aims of these investigations are to determine the limitations of the air-coupled system and to evaluate test capability compared with water-coupled industrial NDT systems.

6.2 Prototype Transducers

The transducer designs implemented for prototype evaluation and development closely conform to those that proved to be successful with the matching layer investigation of Chapter 5. The piezocomposite transducer design hypotheses explained in Chapter 4 are again taken into consideration. The significant parameters of the final designs are summarised below, with two final prototype transducer pairs (for transmit and receive) being used in the testing. One pair was used in the laboratory and the other was used with the industrial scanner. All of the important details are highlighted in **bold** and the parameter values that are different for the industrial scanner probes are given in ***bold italic*** typeface. The transmitters are named **Tx1** and **Tx2** for the laboratory and industrial tests respectively and the partnering receiver arrays are **Ry1** and **Ry2**.

Transmitters:

- **70% volume fraction** piezocomposite transmitter made with **PZT5H** and **CY1301/HY1300** (Ciba-Geigy) hard set epoxy.
- Electrical resonance frequency of **600kHz** – thickness of **2.56mm**.
- Dimensions: **30mm** (***60mm***) height by **30mm** width.
- Excitation signal is a **20 cycle, 600kHz** toneburst from a **HP signal generator**. Amplitude from the signal generator can be selected between **50mV** and **300mV** and this is amplified through an **ENI 50dB power amplifier**.
- Focusing is linear and concave with a **40mm** radius of curvature, set vertically as shown in Figure 3.32. The important dimension ‘**a**’ at the

low point of the curve was selected to be **2.3mm ($\lambda/2$)**. Material used is **Perspex**.

- Matching layer thickness is **0.39mm** and this is cured directly onto the front surface of the lens

Receiver Arrays:

- **30%** volume fraction piezocomposite receiver made with **PZT5A** and **CY1301/HY1300** (Ciba-Geigy) hard set epoxy.
- Mechanical resonance frequency of **600kHz**.
- Dimensions: **30mm (60mm)** height by **30mm** wide with array element pitch of **2mm (6mm)**.
- Focusing is linear and concave with a **40mm** radius of curvature, set vertically as shown in Figure 3.32, and the important dimension 'a' at the low point of the curve was selected to be **2.3mm ($\lambda/2$)**. Material used is **Perspex**.
- Matching layer thickness is **0.86mm** and this is cured directly onto the front surface of the lens

Note that both probes used for the transmitter and the receiver for the testing on the industrial scanner were larger than those used with the laboratory testing. This is because a larger array element pitch (and hence element active area) was selected in order to overcome the anticipated increased difficulty of the industrial environment. The array element isolation was produced in both cases by scribing into the positive electrode using the same dicing saw that was used to manufacture the composite structure. The composite was carefully designed and manufactured so that a whole number of ceramic pillars was used to produce a single array element. The number of pillars used for each element was maximised. This depended on the selected volume fraction, element pitch and various manufacturing constraints such as blade width, kerf loss and resulting pillar strength. For the 2mm array used in the laboratory, four pillars per element were possible and this structure is demonstrated in Figure 6.1. A 0.1mm thick blade was used to scribe the array pattern. This was also used to cut 1.0mm into the epoxy beneath, in an attempt to provide some additional mechanical isolation and

reduce element cross talk. Eight elements in the middle of this structure were used as the active elements.

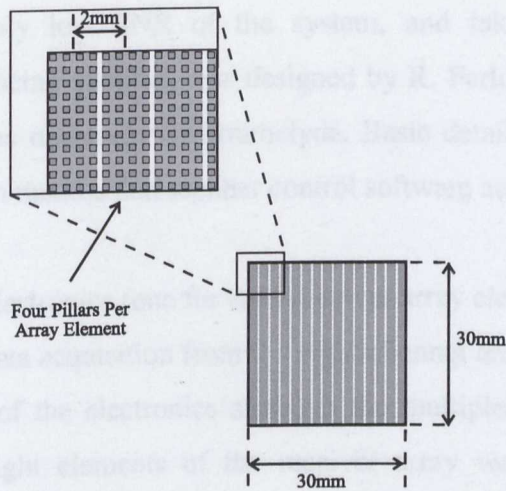


Figure 6.1 Schematic diagram of the array element pitch.

The transmitters in both cases were larger than the active section of the array aperture in order to provide an overlap. This was necessary because there is a reduction in signal strength at the vertical extremities of the transmitted beam relative to the rest of the beam. Beam profile measurements of the early prototype transmitters were used to determine the minimum required degree of overlap at the top and bottom of the active array aperture.

Each of the transmitters and the receiver arrays were housed in an aluminium casing. External input and output connections were achieved using BNC plugs. An example of one of the receiver arrays is given in Figure 6.2 below, and the reception electronics used will be explained in the next Section.

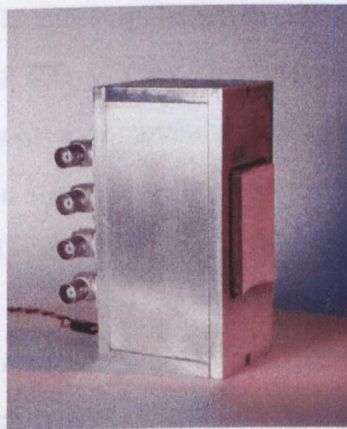


Figure 6.2 Photograph of eight element receiver array used for the industrial tests.

6.3 The Electronic Receive System

The reception electronics used during the course of this research in an attempt to overcome the inevitably low SNR of the system, and take full advantage of the narrowband approach being adopted, was designed by R. Farlow [19], a member of the Ultrasonics group at the university of Strathclyde. Basic details of this electronics, and also the data acquisition method and scanner control software are now presented.

Eight channels of the electronics (one for each receiver array element) were manufactured to enable the parallel data acquisition from the eight-channel array. Figure 3.32 illustrates the main components of the electronics although the multiplexers (Mux 1-8) were not required since only eight elements of the receiver array were utilised during initial investigations. The receive system can be separated into three main elements:

- a) Pre-Amplifiers.
- b) The Analogue Processing Units (APU)
- c) Parallel Data Acquisition.

Details of each of these elements will now be given:

a) The Pre-Amplifiers

Individual pre-amplifiers were used for each of the receiver array elements and these were housed within the transducer casing with short twisted pair wire connections to the inputs from the array elements to minimise the possibility of detecting electrical interference. The eight amplifier outputs were connected to eight BNC connections that were used for connection to the eight analogue processing units using coaxial cable. A bipolar amplifier originally developed for the Ministry of Defence (MOD) by Ferranti was used in the design of the pre-amplifiers. The pre-amplifiers that were designed possessed an ultra low input spectral noise density of $800\text{pV}/\sqrt{\text{Hz}}$. This was compared with the input spectral noise density of $4.2\text{nV}/\sqrt{\text{Hz}}$ with a commercial unit used with water-coupled systems, resulting in an improvement in signal to noise ratio (SNR) of a factor of 5.3. The input impedance of $7\text{k}\Omega$ is closely matched to the electrical impedances at mechanical resonance and was calculated by Farlow to provide a further improvement in SNR over the water-coupled amplifiers (which have an input impedance of 500Ω) of a factor of 7.6. The exact improvement in each case is determined by the exact electrical impedances at

mechanical resonance and therefore the extent of electrical match. The bandwidth of these amplifiers is 6MHz and the gain is 60dB.

b) *The Analogue Processing Unit (APU)*

The main functions of this stage are to reduce the bandwidth of the acquired signals by performing band pass filtering, and to provide an extra stage of gain. Again, there is one APU for each of the eight reception channels to enable parallel data acquisition. These units are housed in a metal casing. There are three variable parameters for each of the eight array elements and these are used first of all to realise the most efficient operation with a certain operational frequency and secondly to achieve consistent reception performance on all eight elements. These parameters are:

- Gain – Variable between factors of 0 and 500.
- Centre Frequency – Variable between 0.25MHz and 1.5MHz.
- Bandwidth – Variable between 10kHz and 35kHz.

Envelope detection is also performed on each of the eight channels and the main function of this is to simplify the digital data acquisition. Efficient operation of the band pass filters and the envelope detectors set a requirement that the transmitter excitation tone bursts should have a minimum duration of 36 μ s.

c) *Parallel Data Acquisition*

Data acquisition was performed using a commercially available computer card (produced by Keithley) that possesses a capability to store data in parallel from eight input channels. The data acquisition rate of this card is 1MHz. When storing on only one channel, or from several channels in series, the maximum acquisition rate of 1MHz can be utilised. When acquiring on eight channels in parallel however the acquisition rate is reduced to 125kHz. This is achieved using a sample and hold facility where consecutive samples are acquired on adjacent channels so the sampling rate on each channel is reduced by a factor of eight. This sample rate is adequate due to the fact that the envelopes of each signal are detected previously in the analogue processing units. Control of the data acquisition was achieved with a 'C' programme and a Lab Windows user interface, which enabled set-up, control and monitoring of the scan process using a computer.

6.4 Laboratory Testing

6.4.1 Initial Testing

Prior to testing scan capabilities, prototype transducers were first investigated in other ways. The beam profiles of the transmitter Tx1 were shown in Chapter 4, Figures 4.11 to 4.13. As noted before, it is evident from these results that the chosen design should possess adequate resolution to achieve the required 2mm defect detection. The sensitivities of the eight active elements of receiver array Ry1 with Tx1 transmitting were tested. The transducers were initially aligned in the absence of a sample, at a separation of 80mm, in order to achieve maximum receive sensitivity on all eight elements without the power amplifier and with 1 volt peak to peak transmitter excitation. A healthy carbon fibre sample was then introduced at the focal region in the middle of the air gap. The signal received on each element was measured after the transmitter excitation was increased to around 100 volts by reducing the signal generator output to 100mV and including the power amplifier. Minor adjustments to the amplification in the main amplifier were performed in each case in order to ensure equal sensitivity across the array aperture. Examples of the signals measured on each of the elements using a Le Croy digital storage oscilloscope may be seen in Figure 6.3. The SNR and the consistency of the amplitude that has been achieved in each case are adequate. The envelope detection that has been performed also means that the relatively low data acquisition rate of 125kHz for each channel (when acquiring in parallel) is sufficient, since only the magnitudes of the peak levels are stored when performing scans. Improvement in signal strength of 30dB was noted with the attachment of the matching layers.

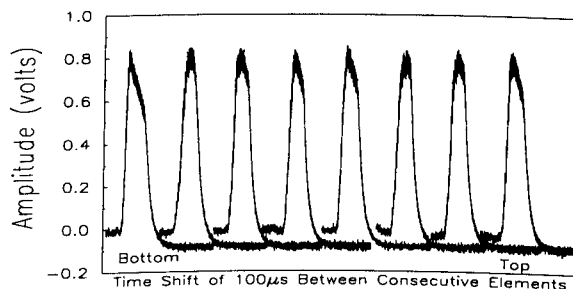


Figure 6.3 *Signals received on the eight elements of array Ry1 through a 3.7mm thick carbon fibre test sample with no averaging.*

6.4.2 Test and Scanning Capability

Laboratory scanning was performed using a tank that has three axes of linear manipulation capability (2m length, 1m width and 0.5m height), and one of angular manipulation (360°). The movement of these axes can be driven using stepper motors and the positions are adjusted and controlled with a computer that sends the appropriate number and width of pulses to the controller card that controls the coils of the motors. A photograph of this scanner is shown in Figure 6.4. The width and height axes were used to scan the position of the test sample through the middle of the fixed transmitter and array positions. Data acquisition was achieved using an intermittent mode, where the sample was moved to an acquisition position then stopped. The data was then acquired on all eight elements before moving one step. The width axis was always used as the primary axis and one step was chosen to be 1mm. At the end of each primary axis line the secondary axis height was adjusted by the height of the receiving array aperture (16mm) and then primary axis movement in the opposite direction was performed. This raster pattern continued until the full test area was scanned.

Figure 6.5 shows the system that was used in conjunction with the scanner to produce C-scans. One of the Lab Windows user interface windows showing eight received signals is displayed here. This was used to set the eight received amplitudes during set-up before commencing scanning, and it is also shown during scanning as an indication of the presence of a defect if the peak amplitude of any of the channels reduces. The peak values of each of the envelope signals are also shown in this window and it is only these values that are stored in a file for each element at each scan position. The manipulator that is shown holding the transducers is placed inside the tank and is used to adjust the height, separation and alignment of the transducers prior to scanning.

6.4.3 Test Samples

Although many test samples were investigated throughout the course of the prototype system investigations, the results with only eight of these are included. Five of these samples were so-called "solid carbon" systems in the sense that they were constructed from a single layer of carbon fibers. The other three were "double layered" systems in the sense that they were constructed from two layers of carbon fibers.

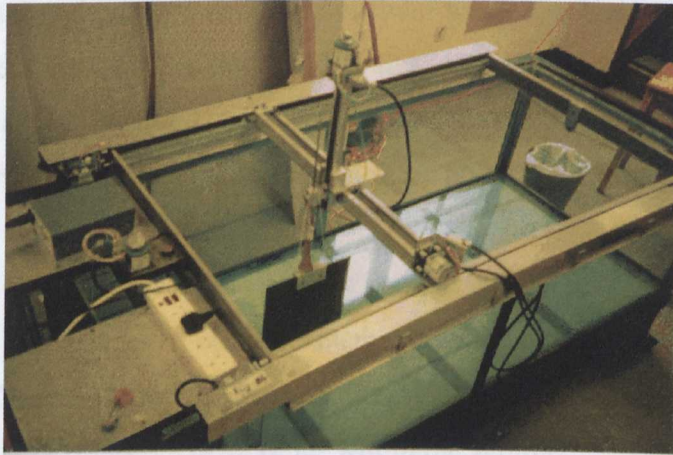


Figure 6.4 Photograph of the scanner used to perform C scans.

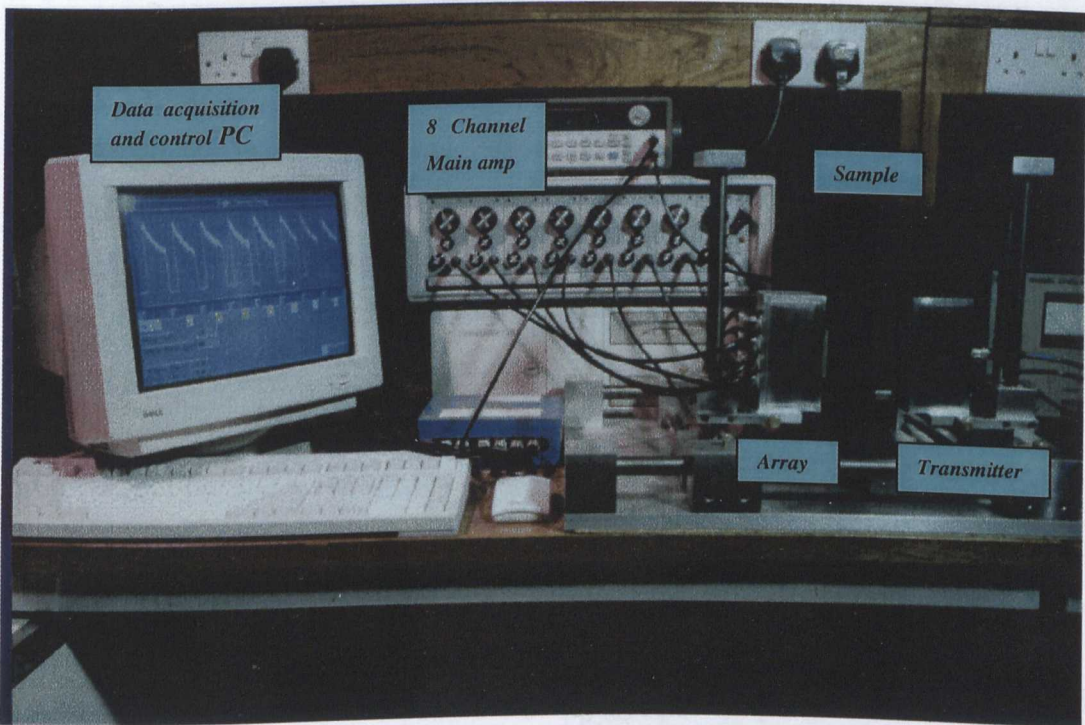
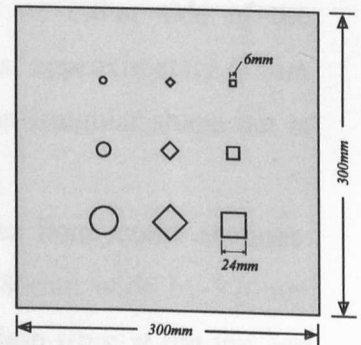


Figure 6.5 Photograph of the system used to produce C-scans and acquire data on the eight receiver channels.

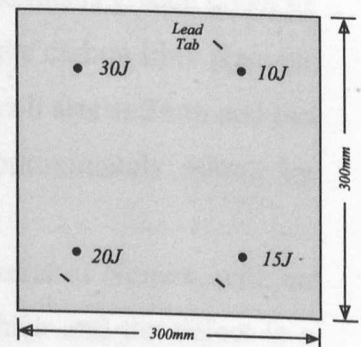
6.4.3 Test Samples

Although many test samples were investigated throughout the course of the prototype system investigations, the results with only eight of these are included. Five of these samples were solid carbon fibre and three of them were of a honeycomb construction, and details of these samples are described in the following. Three of the solid carbon fibre samples may be regarded as test cards for ultrasonic imaging systems in the aerospace industry and schematic diagrams of these are also included.

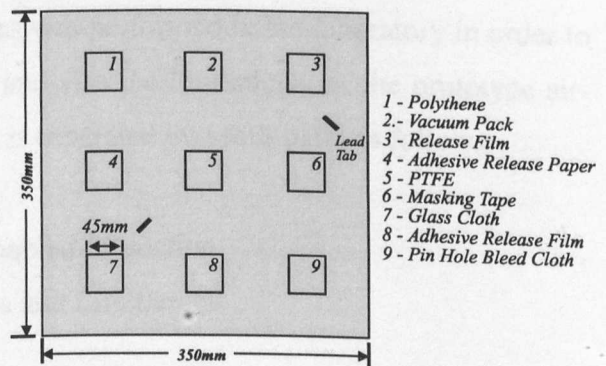
C1) A 3.7mm thick solid carbon fibre test sample with nine PTFE inclusions with shapes of circles, squares and diamonds, of sizes 6mm, 12mm and 24mm. Each of the inclusions was double layered and so trapped a layer of air within the sample.



C2) A 5.4mm thick solid carbon fibre test sample, subjected to a different level of impact close to each corner. The energies involved were 10, 15, 20, and 30 Joules. As with sample C1, there is almost no external evidence of the defects but the internal damage is extensive and typical of what might be expected. This sample also had three lead tabs with an approximate width of 2mm placed on one side. These are often used in the aerospace industry in order to easily match the orientation of the scan data with that of the sample.



C3) A 4.5mm thick carbon fibre test sample with nine 45mm square inclusions of different materials of a single layer. The materials included are typical of those that are encountered in the manufacturing process of a carbon fibre section.



C4) Two samples of carbon fibre (3.5mm thick and 200mm square) joined together in order to perform the scan. One of these samples possessed porosity and the other did not.

C5) Curved glass fibre reinforced polymer sample (4.5mm thick and 100mm by 150mm) with 12cm radius of curvature. This sample had been subjected to an impact of 20 joules.

H1) Total sample thickness of 10mm and a honeycomb material of Nomex, with average cell size of 4mm. The carbon fibre plate thickness on either side of the honeycomb is 0.8mm and two defects of induced delaminations, approximately 60mm by 15mm and 40mm by 15mm, are included. This sample is an irregular shape but is approximately 300mm wide by 270mm high.

H2) This sample contains both solid carbon fibre and Nomex honeycomb sections. Dimensions are irregular with approximate dimensions of a 180mm wide by 220mm high honeycomb section at the centre, with 45mm of solid carbon fibre at the top and sides. The total thickness of the honeycomb section is 11mm, and this is graded down to 3mm thick at the section of solid carbon fibre. The thickness of the carbon fibre plate on either side of the honeycomb is 1mm. The honeycomb average cell size is 3mm and the two defects are induced delamination of the honeycomb, approximately 40mm by 20mm and 20mm by 15mm.

H3) Total sample thickness of 50mm and a honeycomb material of Nomex, with an average cell size of 3mm. The carbon fibre plates are 4mm thick and the defect is a 10mm square inclusion. This sample is 150mm high by 180mm wide.

6.4.4 Scan Results

Inspection of the each of the above samples was performed in the laboratory in order to gain an appreciation of the test potential, and also the limitations, of the prototype air-coupled scanning system. The test process is separated into four parts as follows:

- a) Comparison with Water-Coupled Inspection
- b) Investigation of Capabilities and Limitations
- c) Honeycomb Inspection
- d) Lamb Wave Through Transmission Testing

a) **Comparison with Water-Coupled Inspection**

The carbon fibre samples C1 and C2 were scanned with both air and water-coupled scanning to give a comparison of the two approaches, and the results are given in Figures 6.6 to 6.9. Note that data thresholding of the scan data has been applied in each case. The water-coupled scans were performed using a submersed pulse-echo technique employed by British Aerospace and the C-scan plots may be seen in Figures 6.6 and 6.8. This technique is often used to scan smaller samples and has a defect detection advantage in that the energy must pass through the sample twice. The resolution of the detection of all of the defects is obvious. Note that the BAe scan data is represented by signal attenuation, where higher display values represent smaller received signal amplitudes.

Before performing the air-coupled scans, the alignment of the transducers was adjusted to receive maximum signals in the absence of a sample. Alignment also ensured that the system was focussed at the centre of the air gap. The samples were then introduced and the raster scans initiated. The results of these scans are shown in Figures 6.7 and 6.9. With Figure 6.7 the scan was performed with 11 passes of the sample along primary axis (moving horizontally in relation to the plot orientation) with steps of 1mm between each eight channel data acquisition. Vertical steps of 16mm were performed at the end of each primary axis pass (moving vertically from top down in relation to the plot orientation). Although the sharpness of the edge detection of the inclusions is degraded slightly compared to the water-coupled scan (Figure 6.6), the defective regions have been identified clearly. This was to be expected due to the fact that the vertical step size is 2mm (due to the array element pitch) as opposed to the 1mm used in the water-coupled scan. It is also important to note that it was not possible to achieve **exactly** the same peak response from all eight elements. Every effort was made to achieve parity between the elements by adjusting the gain and bandwidth of the eight main amplifiers (the result of which is shown in Figure 6.3). However, the peak amplitude levels of the eight channels are slightly different and this influences the sharpness of the defect edge detection.

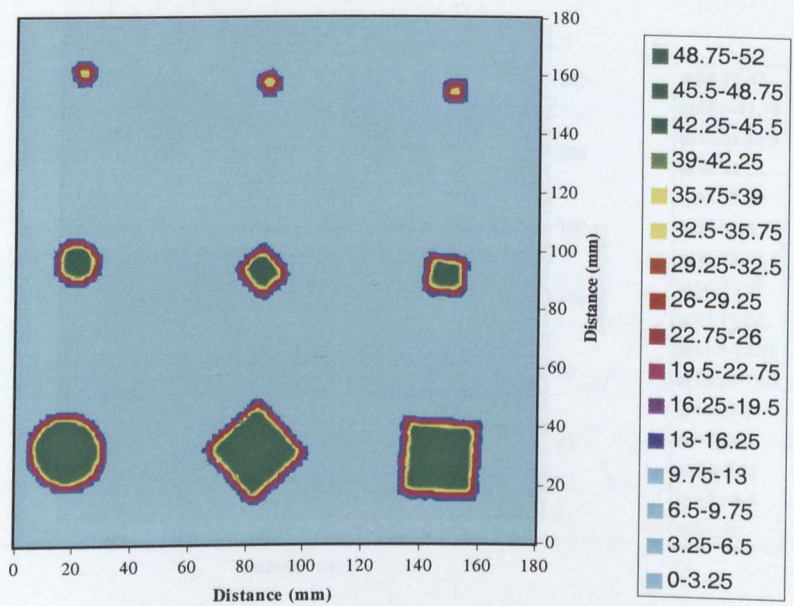


Figure 6.6 Water-coupled scan of carbon fibre sample C1 with 9 inclusions.

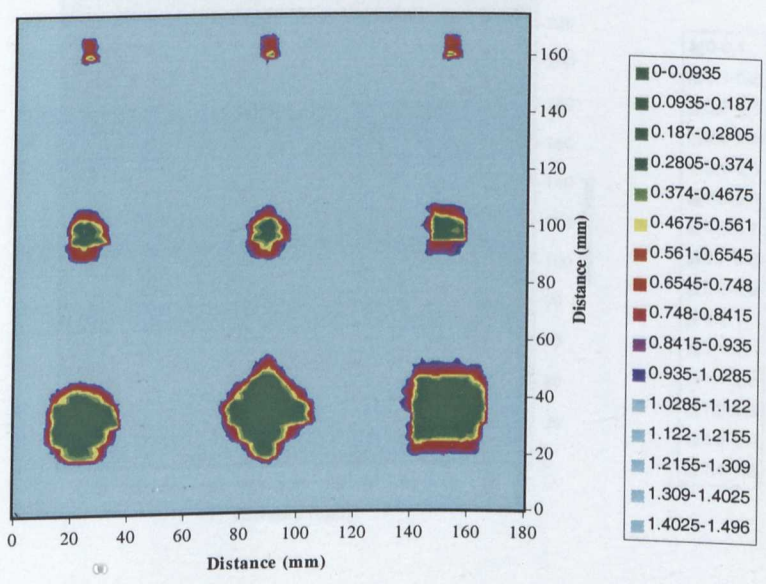


Figure 6.7 Air-coupled scan of carbon fibre sample C1 with 9 inclusions.

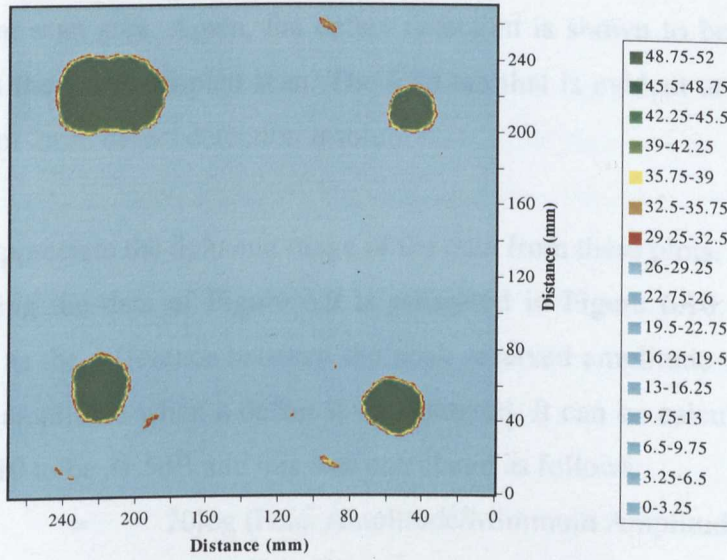


Figure 6.8 Water-coupled scan of carbon fibre sample C2 with 4 Impacts.

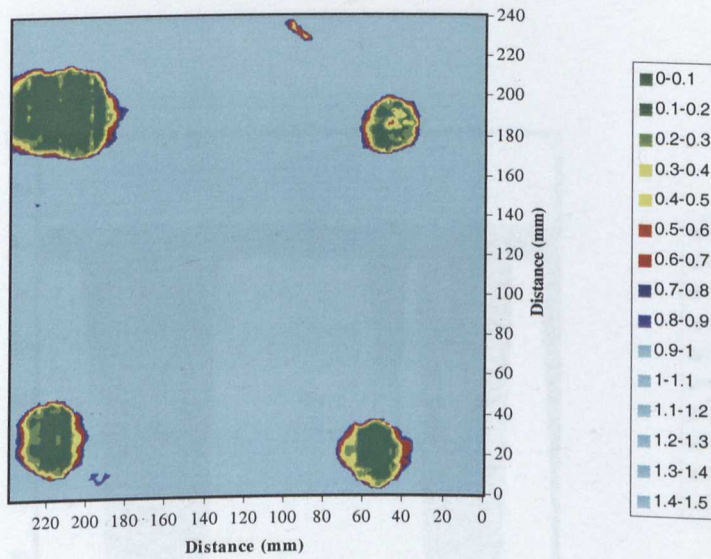


Figure 6.9 Air-coupled scan of carbon fibre sample C2 with 4 impacts.

Figure 6.10 Dynamic range of the air-coupled scan of carbon fibre sample C2.

The air-coupled plot data of sample C2 is shown in Figure 6.9. Scanning was performed in the same way as described for sample C1, except that here the primary axis is now displayed from top to bottom and 15 secondary axis steps of 16mm were required to cover the 240mm scan area. Again, the defect detection is shown to be adequate and comparable with the water-coupled scan. The lead tab that is evident at the top of the plot is evidence of 2mm defect detection resolution.

It is difficult to appreciate the dynamic range of the data from these plots. An alternative method of viewing the data of Figure 6.9 is presented in Figure 6.10. The dynamic range is defined as the difference between the peak received amplitude with no defect and the reduced amplitude when a defect is encountered. It can be calculated from the data in Figure 6.10 to be 31.5dB and this was calculated as follows:

$$\begin{aligned} \text{Dynamic range} &= 20\log(\text{Peak Amplitude}/\text{Minimum Amplitude}) \\ &= 20\log(83/2.2) = 31.5\text{dB} \end{aligned}$$

Similar measurements were made from the water-coupled data provided by BAe and the dynamic range was calculated at 25dB.

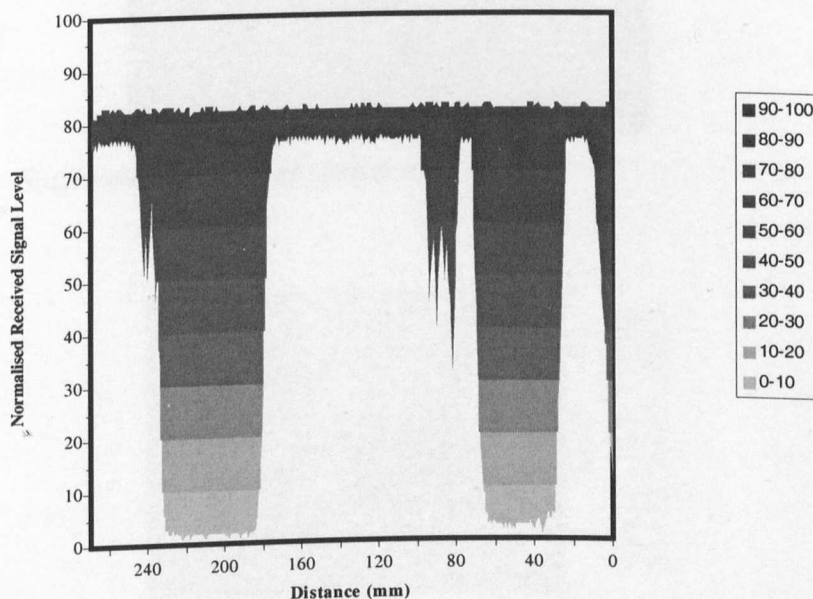


Figure 6.10 *Dynamic range of the air-coupled scan of carbon fibre sample C2.*

b) Investigation of Capabilities and Limitations

A number of other scans were performed in order to investigate other potential, as well as the limitations, of the system in the inspection of carbon fibre sections. Samples C1, C3, C4 and C5 were used for this purpose. Firstly, the resolution capability was investigated when the transmitter was turned through 90 degrees, and only a single element of the receiver was used. This was intended to improve the resolution by creating a point rather than a line focus. The carbon fibre sample C1 was scanned with the system in this orientation and the result is shown in Figure 6.11. In this case the sharpness of the defect edge detection is impressive. It is proposed that the rough pattern that can be distinguished in the areas between the inclusions is an indication of the fibres of the carbon fibre structure. The ripples that are observed around the inclusions are believed to be due to diffraction of the signal around the inclusions.

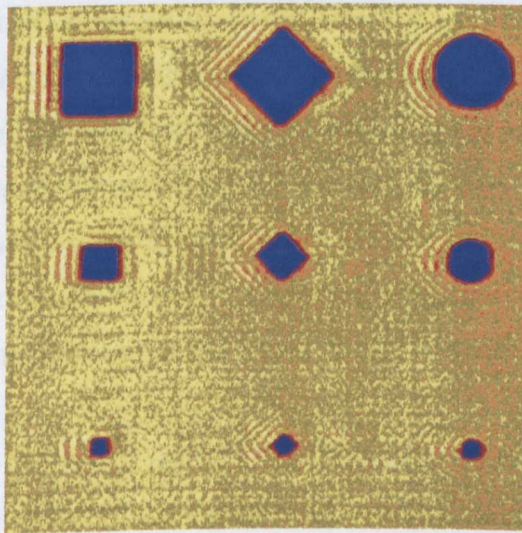


Figure 6.11 Single element scan of sample C1.

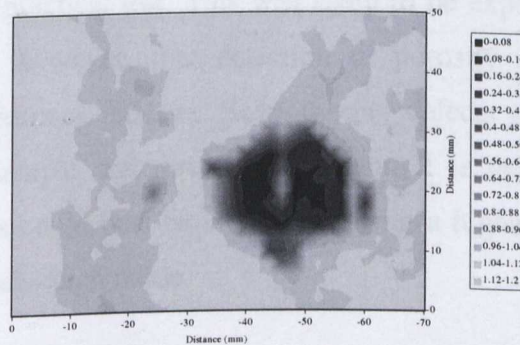


Figure 6.12 Single element scan of curved sample C5.

The scan of sample C5 in Figure 6.12 was included simply as an indication that successful scanning can be performed when the angle of incidence is not normal. This would be an important consideration in any practical system since slightly curved surfaces would be encountered frequently.

The scans shown in Figure 6.13 and 6.14 demonstrate limitations of the air-coupled system. Firstly, the scan of C3 shows that several of the material inclusions have not been detected adequately. The materials included are all materials that are involved in the manufacturing process of composite sections. However, the difficulty in this case is that the inclusions are each of a single layer and the pockets of air, present in sample C1, are not present. This means that any of these inclusions will only be detected if the materials themselves either attenuate or reflect the transmitted signals. The air-coupled system has limited detection capability (inclusions 2,3,5,7 and 9) due to the relatively low operational frequency. It should be noted, however, that it was pointed out by BAe that the water-jet system also had difficulty in detecting the same inclusions. It relied heavily on averaging and still only provided a rough outline. It is believed that some evidence of all the inclusions can be identified in the air-coupled scan. This is with prior knowledge of their existence, however. Improved detection would be possible with many averages but the practical potential would still be in doubt.

Figure 6.14 shows an attempt to identify the difference between two samples, where one had a problem with porosity and the other did not. It was known that the sample on the right had porosity, but no information was provided about any other defects. Some difference between the scans of the two samples is evident but there is clearly insufficient detail for a practical test. This was again to be expected, due to the lower frequency. It is noted, however, that detection of porosity is acknowledged as a difficulty within the aerospace industry. Several other defects were detected however, with four on the left sample and three on the right. It is believed that these were inclusions, although this could best be confirmed using a higher frequency contact or water-coupled test in pitch-catch mode.

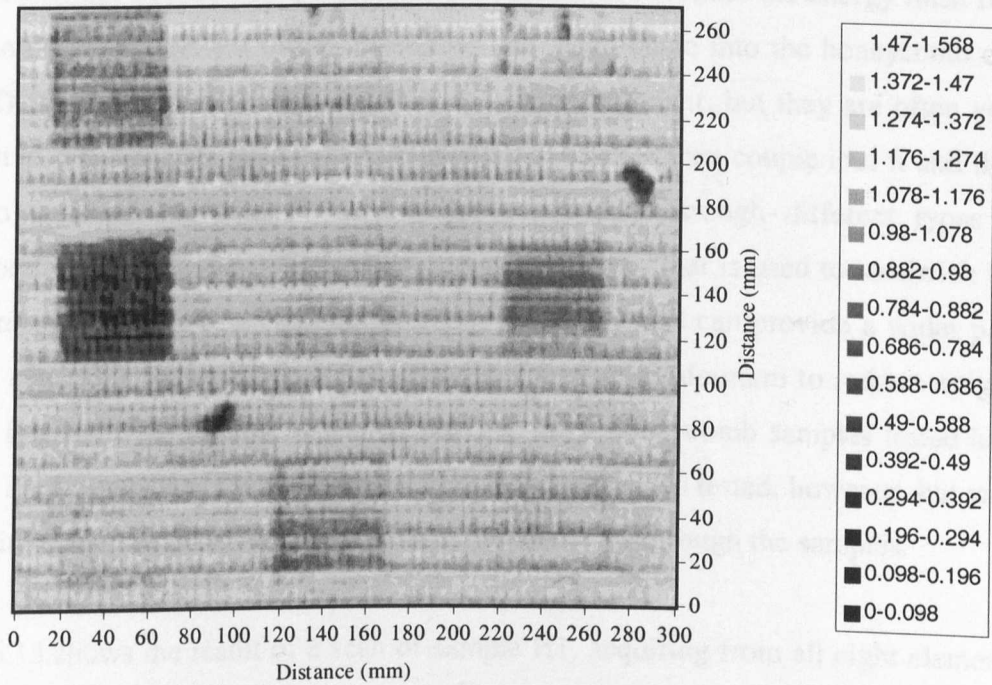


Figure 6.13 *Eight Channel scan of sample with 9 different inclusions (C3).*

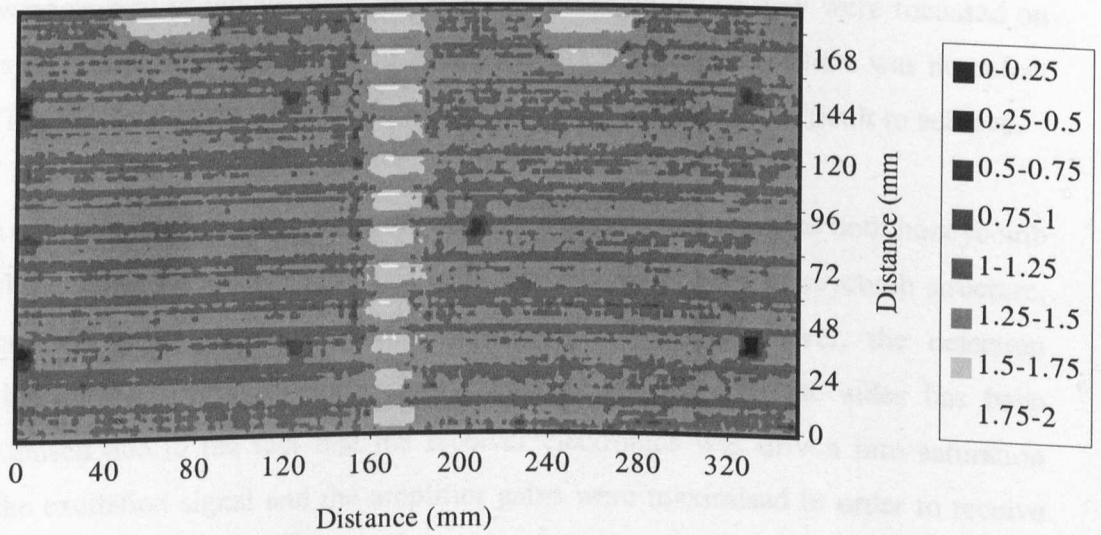


Figure 6.14 *Eight Channel Scan of sample with and without porosity (C4).*

c) **Honeycomb Inspection**

Honeycomb samples are considerably more difficult to penetrate than solid carbon fibre, whether air or water coupling is considered. This is because the energy must first enter the outer skin closest to the transmitter and then couple into the honeycomb cell walls. These walls are not only very thin, to minimise weight, but they are often very attenuative. The energy that remains at the other skin must then couple into it and then out into the load medium. The difficulty of scanning through different types of honeycomb is variable depending on the amount of epoxy that is used to sandwich the structure together. If a large amount of epoxy is present this can provide a wider path into the cell walls, however epoxy is sometimes kept to a minimum to reduce weight, making through transmission very difficult. The three honeycomb samples tested here were of the former type. Other honeycomb samples were also tested, however, but with less positive results due to reduced transmission of energy through the samples.

Figure 6.15 shows the result of a scan of sample H1, acquiring from all eight elements of the receiver, in 10 primary axis scans. The two delaminations at the bottom of the scan are visible but the clarity is uncertain. This is partly because of the difficulty of transmitting through the sample, and partly because of the difficulty in alignment of the transducers. This was because the tightness of the focus meant that, at any one time, there were several of the elements that received no signal since they were focussed on an area without a signal carrying cell wall behind it, even although there was no defect there. The result of this was that adequate signal to noise ratio was difficult to achieve.

Figure 6.16 demonstrates a problem of scanning a sample that contains both honeycomb and solid carbon fibre sections. In this case, the detection of the honeycomb structure, and the two delaminations at the bottom, are apparent. However, the detection capability in the section of solid carbon fibre at the top and the sides has been compromised due to the fact that the receiver electronics was driven into saturation since the excitation signal and the amplifier gains were maximised in order to receive through the honeycomb successfully. Note that, at the bottom of the honeycomb, there is an air gap, and the reception was again driven into saturation.

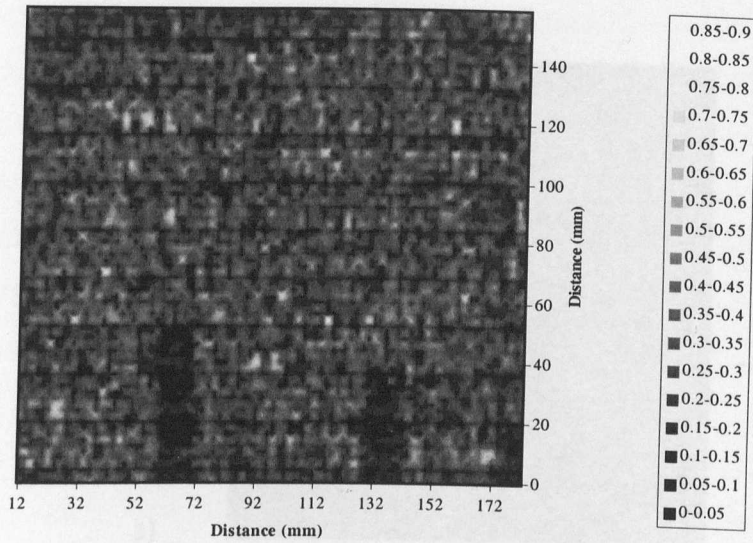


Figure 6.15 *Eight element scan of honeycomb test sample H1.*

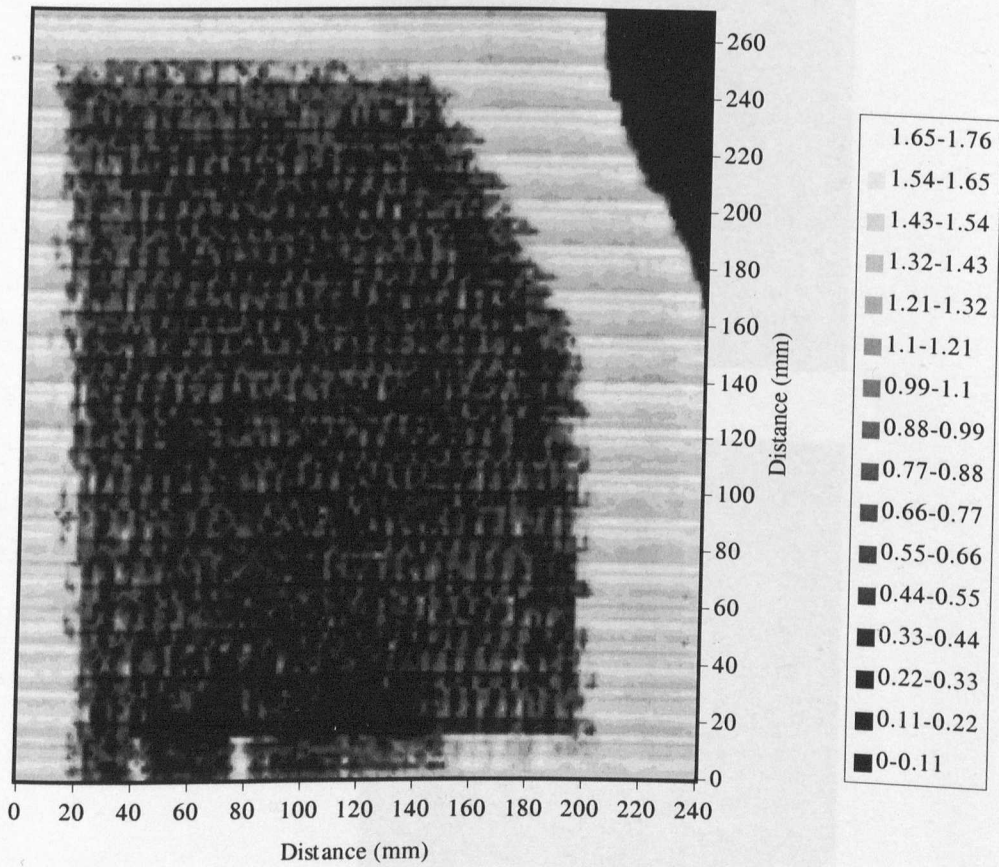


Figure 6.16 *Eight element scan of honeycomb test sample H2.*

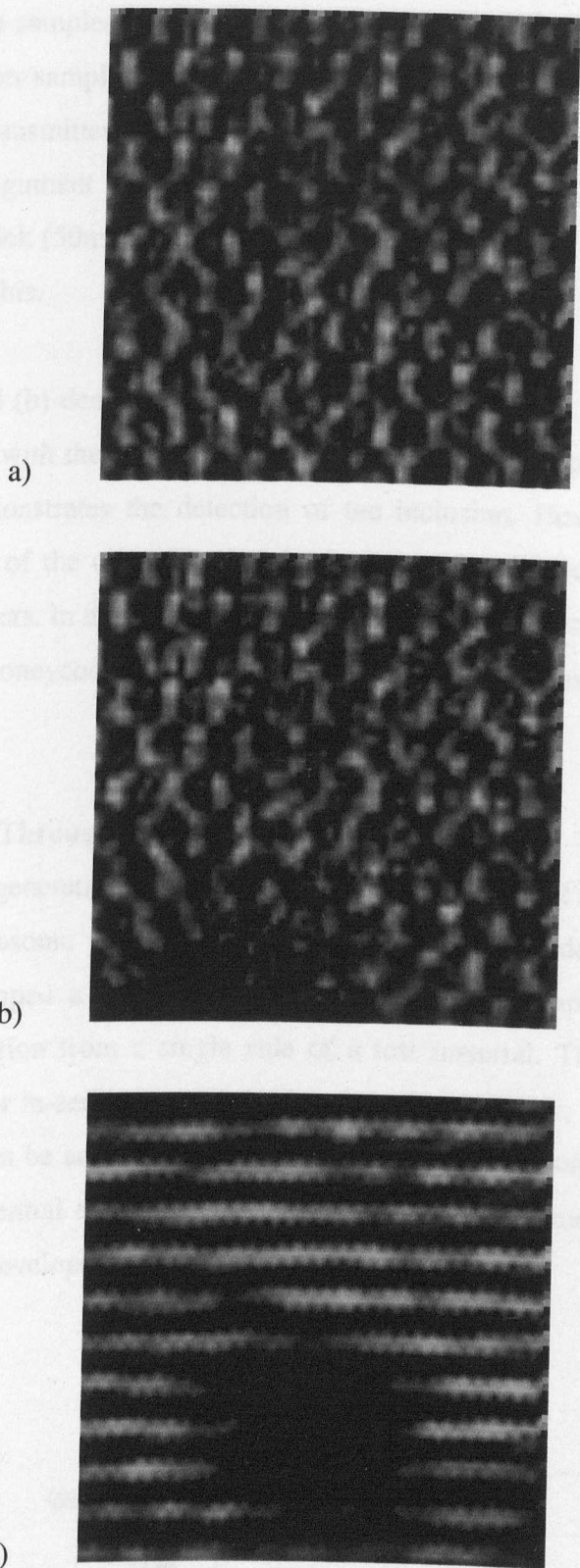


Figure 6.17 High resolution scans through sample H3 using one element. Scan area in each case was 30mm square.

In an attempt to show that the air-coupled system could be used to scan accurately through honeycomb samples and identify the honeycomb cell structure, several scans were made of another sample (H3). This adopted the same single-element technique as before, where the transmitter was turned through 90 degrees to improve the resolution. The difficulty of alignment was not so pronounced in this case and the plots of scans through this very thick (50mm) sample, that are shown in Figures 6.17 (a, b and c), are the consequence of this.

Figures 6.17 (a) and (b) demonstrate clearly that the honeycomb cell walls have been detected accurately, with the bottom of plot (b) showing the detection of the inclusion. Figure (c) also demonstrates the detection of the inclusion. However, this plot also shows the influence of the orientation of the honeycomb cell structure relative to the focus of the transducers. In this case the sample had been turned through 90 degrees and the detection of the honeycomb cell walls was constant on some passes and non-existent on others.

d) Lamb Wave Through Transmission Testing

It is understood that generation of Lamb wave modes within a test sample can improve the coupling of ultrasonic energy into and from a sample under test. Farlow and Hayward [28] developed a single sided air-coupled system employing Lamb wave generation and reception from a single side of a test material. This could provide a valuable capability for in-service testing in the aerospace industry, when only one side of the test material can be accessed. In light of this work it was considered worthwhile to investigate the potential enhancements of using Lamb waves modes in the through transmission system developed here.

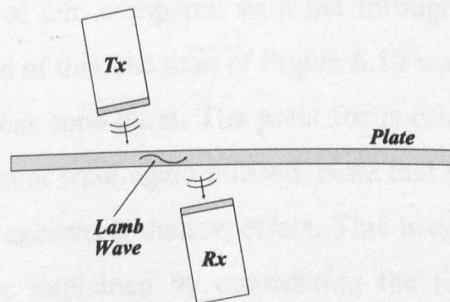


Figure 6.18 *Lamb wave through transmission scanning of a carbon fibre plate.*

Through transmission Lamb wave methods were investigated with a solid carbon fibre sample, and the transducer arrangement shown in Figure 6.18 was used to achieve this. Sample C1 was scanned with this orientation and the result of this scan is given in Figure 6.19. The angles of the transducer, relative to the sample, were selected by adjusting the angles until the received signal was maximised. This was measured to be in the region of nine degrees off normal incidence and was achieved when the correct angles were reached. These angles promoted generation and reception of a Lamb wave mode based on the operational frequency and the thickness. The Lamb wave mode that was generated was believed to be the fundamental asymmetrical mode (a_0). At the frequency under consideration, the a_0 mode has a significantly greater out of plane displacement than the fundamental symmetrical mode (s_0), and is therefore much easier to generate and detect.

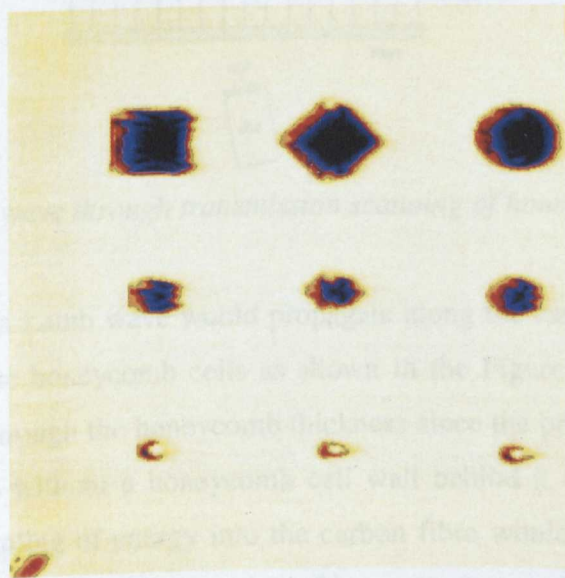


Figure 6.19 *Lamb wave scan of sample C1 using a 10 volt excitation signal.*

It was found that, at the correct angles, the increase in the received signal amplitude was measured to be a factor of ten, compared with the through transmission longitudinal method. As a consequence of this, the scan of Figure 6.19 was achieved using excitation with a 10 volts peak to peak tone burst. The point focus orientation of the transducers, and a single receiver element were again utilised. Note that the detection of each of the inclusions in this sample exhibits a shadow effect. This is consistent with testing using Lamb waves, and can be explained by considering the top of the largest diamond inclusion. As this point passes between the transducers, either transmission or reception

will be affected (depending on the direction of travel) and the received signal is reduced. There would then be some time, depending on the lateral separation of the transducers, when neither of the transducers is affected. After this time the other transducer is affected as it passes over the inclusion and the received signal is reduced.

Next, it was interesting to consider how scanning of a honeycomb section would be affected by adopting a similar Lamb wave approach. It was proposed that the transducers could be set to the angles and positions for Lamb wave generation in the first carbon fibre skin of the honeycomb, as demonstrated in Figure 6.20.

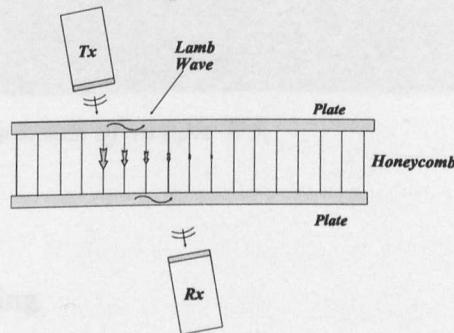


Figure 6.20 *Lamb wave through transmission scanning of honeycomb sample.*

It is believed that this Lamb wave would propagate along the carbon fibre, and energy would couple into the honeycomb cells as shown in the Figure. This would improve coupling of energy through the honeycomb thickness since the problem of focussing on a part of the sample without a honeycomb cell wall behind it would no longer be a factor. Also, the coupling of energy into the carbon fibre would also be enhanced, as was demonstrated in Figure 6.19. Scanning of honeycomb sample H3 was investigated with the arrangement in Figure 6.20 and the result is given in Figure 6.21. The scan area here was 30mm square and the defect detected in the middle is an inclusion. The optimum angles were found to be in the region of 10 degrees from normal for both the transmitter and the receiver. The Lamb wave mode was again believed to be the a_0 mode, however the increase in the received signal, relative to the through transmission longitudinal method, was less in this case, and was only about a factor of 2. This could have been due to the fact that the energy must first couple into the honeycomb cell walls. It is believed that the energy in the honeycomb would not have been a Lamb wave. This longitudinal energy would then have been incident at normal incidence to

the other carbon fibre layer and the generation of the Lamb wave in this layer would have been limited.

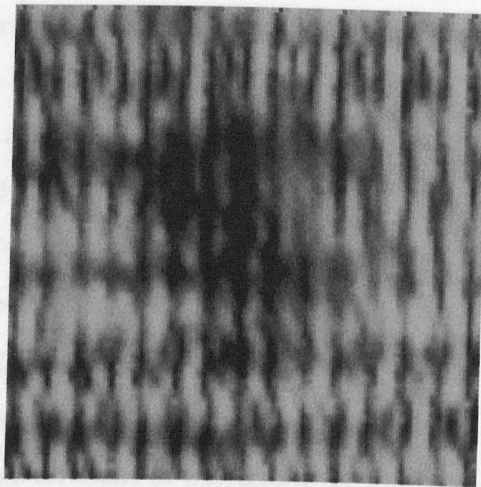


Figure 6.21 *Lamb wave scans of sample H3.*

6.5 Industrial Scanning

6.5.1 Introduction

An eight-channel prototype system was integrated with an industrial scanner at a British Aerospace test facility at Warton to provide an insight into the commercial viability of the air-coupled work. This environment introduced several additional complications and these are highlighted below. The influence on performance and/or the proposed solutions to these considerations are explained where appropriate.

1) Scanning was to be performed at speeds of up to 0.5m/s

The potential air currents could influence the ultrasonic beam. Testing at speed was performed and was not found to pose too great a problem. This could have been due to the fact that the air gaps were quite small at 40mm.

2) Additional electrical noise that is inherent to the industrial environment

The connections to and from the pre-amplifiers were made more robust with thicker earth and signal wires.

3) Data acquisition software

This had to be integrated with the commercial scanner control software so that continuous scanning could be performed without a requirement to stop before acquiring data. This combination of the laboratory data acquisition software

with the industrial scanner control software was completed in co-operation with John Smith of BAe.

4) The receiving array (and hence the pre-amplifiers) were separated from the main amplifiers by 12m

This introduced a requirement for the pre-amplifiers to drive 12m of coaxial cable. Buffer line drivers (Burr-Brown-OPA633) were added to each of the pre-amplifiers by Roger Farlow. These buffers have high input ($1.5\text{M}\Omega$) and low output (5Ω) impedances, and thus provide high output currents (100mA) to drive the long 50Ω coaxial cable load.

5) Different transmitter excitation hardware

Instead of the very efficient power amplifier that was used in the laboratory, a new PC based pulser (by Matec) was used at BAe. This proved to be much less effective than the power amplifier and had an influence on the success of the industrial scanning. Efforts are on going in an attempt to resolve this and produce more representative scans with the industrial scanner.

6) Transducer probe alignment difficulties

Alignment of the transducers is of paramount importance, particularly when receiving on all eight elements. The alignment capability on the industrial scanner, although modified for the air-coupled probes, was never as robust or repeatable as the laboratory manipulator. Finding a solution to this is another aspect that could significantly improve the test capability of the air-coupled system in the industrial environment.

6.5.2 Industrial Scanning Results

Two solid carbon fibre test samples were scanned in air using the industrial scanner. One of these was sample C2 with impact damage that was also investigated in the laboratory and the other was a larger carbon fibre test sample (C6) with eight inclusions of various sizes that were neither visible nor indicated on the surface. This was 600mm by 600mm in size.

Sample C2 was scanned first and the result of this is given in Figure 6.22(a). The industrial system software has been used to display the scan data. This scan took approximately 20 seconds to produce, as opposed to over 3 hours with the laboratory

scanner. However, the resolution of the result is obviously worse than the scan in the laboratory. This can be attributed to three factors:

- Array element size is three times larger at 6mm, compared to 2mm.
- Difficulty in setting and maintaining alignment throughout the scan.
- Non-ideal transmitter excitation.

It is encouraging, however, that all of the defects were detected with resolution that meets industrial requirements.

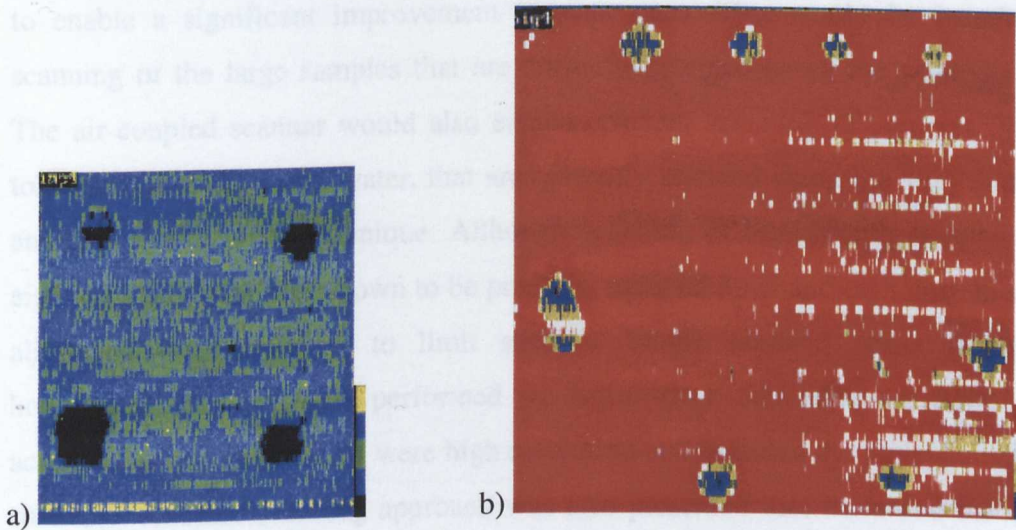


Figure 6.22 Eight channel *air-coupled scans* of Sample C2 (a) and Sample C6 (b) performed with the industrial scanner.

Sample C6 was scanned with the air-coupled system without prior knowledge about the integrity of the sample. It was concluded from the scan data in Figure 6.22(b), therefore, that the sample contained inclusions, or some other defects such as impact damage, in the positions noted. The size of this scan area is 480mm vertically (10 passes of the 48mm array active area). As before, scan resolution is reduced compared to what may have been achieved with the laboratory scanner but nevertheless believed to be adequate. It would be the case in a real test situation that these defects could be characterised in more detail using a high frequency hand-held probe in contact with the sample and in pulse-echo test mode. Also, it is expected that better results could have been achieved if the power amplifier and better probe manipulation devices were used.

6.6 Conclusions

The potential of the eight element, air-coupled system has been assessed under both laboratory and industrial conditions. It is believed that adequate resolution and defect detection capability has been demonstrated for several realistic test samples with different defects. Comparisons with scans performed in water have also been presented as practical evidence of the possibility to produce an air-coupled alternative to the water-coupled systems currently utilised. The array approach adopted has been shown to enable a significant improvement in scan rates. This would be beneficial with scanning of the large samples that are currently scanned using the water-jet systems. The air-coupled scanner would also enable efficient scanning of samples that cannot tolerate any contact with water, that are currently scanned using the very cumbersome and slow roller probe technique. Although scanning of honeycomb samples with the eight-element array was shown to be possible, reduced SNR and difficulty in setting up alignment were believed to limit success. Single element scans through thick honeycomb samples were performed to demonstrate that adequate SNR could be achieved in air. These scans were high resolution and detected the honeycomb cell wall structure. Another scanning approach was also presented that increased the energy of the through transmitted signal by generating Lamb wave modes within the sample.

CHAPTER 7

CONCLUSIONS AND SUGGESTIONS FOR FURTHER WORK

7.1 Conclusions

7.1.1 General Overview

The development of an array based air-coupled scanning system to perform non-destructive testing in the aerospace industry has been completed successfully. This technology has provided the potential to perform testing on certain large samples substantially more quickly than the currently utilised water-jet systems that are limited in their number of elements and therefore sample area coverage. Importantly, this will also provide an efficient method of scanning samples that cannot tolerate contact with water to any extent and that are currently tested with the very slow and inefficient dry contact roller probe techniques. In order to achieve this, a number of developments have had to be made, and the most important of these can be summarised as follows:

- Careful comparison of the available air-coupled transducer technologies revealed that the most appropriate choice is piezocomposite transducers.
- A novel matching layer has been developed.
- A linear mathematical model for this matching layer was produced.
- A new air-coupled transducer design concept was proposed due to the cavity resonance within the transducer as a result of energy entrapment.

Interest in the technology has already been expressed from several potential industrial users and work is in progress to provide a commercial product. It should also be noted that the success of the air-coupled system that has been developed could open

possibilities for other systems that do not currently use ultrasound due to the historical difficulties that are well known with air-coupled operation.

7.1.2 The Scanning System

A narrowband, relatively low frequency approach was selected to improve SNR of the system. This not only increased the energy contained within the transmitted signal but also enabled band pass filtering to be performed in reception. The system constraints caused by the signals reverberating within the propagation channel were also identified and incorporated within the design. Transmitter material limitations were realised and taken into account when it was determined that a minimum PRT of 1msec would have to be imposed. For this reason it was also concluded that, in order to realise the required improvement in the inspection rate, there would have to be an element of parallel acquisition and that signal averaging could not be performed. Available data acquisition hardware meant that initial prototypes should concentrate on the development of an eight-channel array that received data in parallel on all eight elements. It was also noted however that a system utilising a 32-element receiver array could be produced by introducing an element of multiplexing.

7.1.3 Selection of the Transducers

Piezocomposite transducers, designed specifically for operation in a pitch-catch air-coupled application, were adopted to provide adequate sensitivity and robustness for the proposed application. This was concluded after comparison with electrostatic transducers with the following results with regard to the piezocomposites:

- Higher sensitivity with lower pitch-catch insertion loss for improved SNR.
- Preferable robustness for the industrial environment.
- Simpler and better focusing capabilities.

7.1.4 The Matching Layer

Development of a novel matching layer was completed in order to reduce the impact of the large acoustic impedance mismatches between the transducers and the air load. This utilised porous filters that have very low impedance properties due to the presence of a

large percentage of air within them. The operational frequencies of the transducer/matching layer combinations were adjusted by coupling the filters with silicone rubber of a particular thickness. The required thicknesses were determined after developing a linear model based on a study of microscopic and acoustic properties of the constituent parts and then again after in the final matching layer. The model was verified experimentally and then used to study the performance as the thickness of the silicone rubber phase was varied for both transmitter and receiver. In the absence of ideal matching it was concluded that the matching layer and transducer act as a single cavity due to the high percentage of energy that is trapped within the structure. This also lead to the belief that the thickness of the low point of the lens should be set to half wavelength thickness. Finally, in order to provide the potential for others to adopt the technology for their own air-coupled application, a set of design guidelines with appropriate Graphs and Tables is supplied.

7.1.5 Results

Resolution and test capability has been shown to be adequate for many real test samples. This was demonstrated by comparison with scans performed using a water-coupled system. Specifically, two solid carbon fibre samples, one with test inclusions of various shapes and sizes and one with impact damages of various energy were compared. The air-coupled tests were accomplished by acquiring data in parallel from eight receiver array elements and therefore an improvement in scan rates of a factor of eight was achieved. Two phases of amplification was performed with each element. One of these was performed with dedicated preamplifiers for each element, housed within the transducer casing. The other was a main amplifier for each element. Bandpass filtering was performed on each element and envelope detection simplified data acquisition. The majority of prototype testing was performed in a scientific laboratory environment however realistic tests were also performed on an industrial scanner. In the laboratory, scans were performed under computer control with a specifically developed Lab Windows user interface. This enabled scan set-up and control, and inspection of the eight signal envelopes as the data was acquired for each point in the scan. A capability to scan honeycomb test samples with the air-coupled system was also demonstrated however the difficulty of setting up simultaneous reception on all eight-array elements

was acknowledged. Analysis of the transmitter prototype beam profile supported the belief that adequate resolution had been achieved. A technique of scanning test samples of solid carbon fibre or honeycomb was discussed and demonstrated. This involved setting the angles of incidence to promote generation of a Lamb wave mode in the carbon fibre or the skin of the honeycomb.

7.2 Suggestions for Further Work

7.2.1 Potential Future Developments

The work presented within this Thesis has achieved the initial goals, although it must be recognised that there are still areas where potential improvements could be realised. This Section gives recommendations about the areas where improvement could be found and how these could best be achieved. Suggestions about other potential air-coupled systems that could benefit from the improved sensitivity that has been provided with the new matching layers and techniques are also given.

It has recently been proposed that the development of high power transmitters could be achieved by stacking layers of transducers. The layers within the 'Stack' are connected mechanically in series and electrically in parallel resulting in an operational frequency that is produced with the combination of all the layers acting as a cavity. Initial theoretical and experimental work suggests that the pressure output is directly proportional to the number of layers used. Efforts are on going within the University of Strathclyde to optimise this technique for sonar applications at low frequencies (30kHz) and are soon to be considered for air-coupled frequencies as used within this Thesis (600kHz). The advantage for this work of the improved transmitter power output that could be achieved is evident. This technique can be manufactured using the 1-3 piezocomposite arrangement used here and so benefit in a similar way from a reduction in acoustic impedance when matching to low impedance media. Other composite arrangements such as 2-2 and 3-1 are also under consideration with the primary goal of simplifying manufacture but these would have the added benefit of enabling efficient heat dissipation with less damage to the transducer at high voltage excitation. The manufacturing complexity of even a single composite layer compared with monolithic ceramic transducers is accepted. In the future, this could be partially overcome using injection moulding techniques. At present however this technology is not widely available is also very expensive. To date, the question of electrical matching the load and source impedances to the receive and transmit transducers respectively has not been analysed in detail. It is possible, however, that electrically matching of the reception and transmission electronics to the mechanical and electrical impedances of transducers could improve system efficiency.

It is recommended that a more robust and repeatable array manufacturing technique should be devised. This would have to provide an alternative to the fragile array element connections that have been developed for the purpose of prototype development here. If this is achieved then it could be possible to extend the array to the 32 element size suggested in Chapter 3. The importance of the transducer alignment must be appreciated however, and an accurate 3D manipulator for both probes would have to be utilised. Improved alignment capability would also increase the potential to scan through honeycomb samples. The integration of the technology with industrial scanners should also be continued and full-scale commercialisation is believed to be a realistic possibility. In doing this the scan technique of coupling the Lamb wave mode with the through transmission longitudinal wave, to scan sections with both honeycomb and solid carbon fibre sections, should be studied further.

More detailed investigation into the lens designs could reveal potential system improvements. This could be achieved using finite element modelling. The most suitable radius of curvature could be found to achieve improved resolution. Different lens materials could also be investigated and could result in better acoustic matching.

7.2.2 Further Matching Layer Investigations

Only one filter type has been investigated in the manufacture of the matching layers so far. The filter is obviously a critical factor in the success of the matching layer, however it is also has a major influence in the frequency performance. Only the thickness of the SR phase has been investigated to control the operational frequency of the matched transducers. If different filter types were considered there would be greater flexibility in design and there could be better acoustic match for a wider range of frequencies. There are also filters available with a range of different materials and porosity so improved matching could also be a possibility.

The thickness of the matching layers is very important in achieving efficient cavity resonances. Although every effort was made in the manufacture of the matching layers to achieve constant and accurate thickness, it is believed that there is still room for

improvement. Although the modification of the SR phase in contact with the filter during curing was identified and is believed to have a significant influence on the performance, no effort has gone into investigating the exact nature of why and how this happens. For example, it is unclear how the exact temperature of the surrounding air or the pressure used to set the required thickness affects the performance. Although every effort was made to keep these parameters as consistent as possible throughout the matching layer investigations, it would help future developments if there was a greater understanding of the curing process. Also, if the new matching layer technique is ever to be used commercially, the change in performance with time would have to be investigated.

In producing the Design graphs presented in Section 5.6.7, it became clear that an operational frequency of around 750kHz would be favoured. From these results it would be worthwhile investigating a pitch-catch transducer pair operating at 750kHz. If successful, this could offer improved defect detection capability.

The improved match to air with the new matching layer technology could also be utilised with other air-coupled applications. A parallel and complimentary body of work within the Ultrasonics group at the University of Strathclyde also investigated the use of air-coupled ultrasound for pitch-catch NDT applications. Where the system developed within this Thesis adopted a double sided scanning approach, which required access to both sides of the test piece, and so must be performed in pre-production tests, the other system used a single sided approach suitable for in-service testing. This utilised the generation of Lamb waves by setting the transducers at the correct angles and operating in a pitch-catch mode. This system would also benefit from the attachment of the matching layers in the same way as the through transmission system and is currently being developed further to produce a hand held battery operated system for convenient in service testing.

REFERENCES

1. Steinchen W, Yang L, Kupfer G and Mackel P, "Non-Destructive testing of aerospace composite materials using digital shearography", Proc Inst Mech Engrs, Vol 212, Part G, 1998, pp 21-30.
2. Gieske JH, "Aviation focused eddy current and ultrasonic scanner assessment", Materials Evaluation, July 1995, pp 820-826.
3. Dewhurst RJ, Ruhua H and Shan Q, "Defect visualisation in carbon fibre composite using laser ultrasound", Materials Evaluation, August 1993, pp935-940.
4. Willsher SJ, Smith RA, "Multi-Element ultrasonic scanning of in-service airframes", Insight, Vol 40, No 3, 1998, pp154-159.
5. Lethiecq M, Pejot C, Berson M and Guillement P, "An Ultrasonic array based system for real time inspection of carbon epoxy composite plates", NDT&E International, Vol 24, No 6, 1994, pp311-315.
6. Non-destructive Testing Handbook, Vol 7, American Society for Non-destructive Testing, 1991, pp222-224.
7. Taylor K J, "The approach to ultrasonic inspection of carbon fibre reinforced plastic production components within British Aerospace (Military Aircraft) Ltd.", Internal BAe. Report. 1990.
8. Tretout H, Guillois F, Bajou D and Violette D, "Investigation of acoustic pressure fields in advanced water squirters – application to ultrasonic inspection of composite materials", Non Destructive Testing, Proceedings of the 4th European Conf., Vol 3, 1987.
9. Tretout H., Maurer A David M., and Juengling K and Pepin P, "Advanced water squirter systems for composite materials inspection and application in industrial quality control", 11th World Conference on NDT, Vol 11, 1985.
10. Violette D., Blanc-Benon P., Juve D., Tretout H. and Mol R, "Simulation numerique de la propagation d'ondes acoustiques dans un systeme de controle non destructif en immersion locale", Revue D'Acoustique, No 81, 1987.
11. Light GM, Cervantes RA and Harvey DP, "Development of pulse echo ultrasonic squirter for detection of first layer delamination in composite structures", Rev of Progress in QNDE, Vol 8A &8B, 1989, pp929-936.

12. Torgersen R, "Developments in jet couplant techniques for ultrasonic NDE of aerospace components", *Materials Evaluation*, Vol 41, 1983, pp520.
13. Panametrics Automated Systems (promotional video).
14. Meccasonics Ltd. Guide to Products and Services.
15. Ultrasonic Sciences Ltd., "USL systems for automated inspection of large CFC structures", Data Sheets.
16. Buckley J and Loertscher H, "Frequency considerations in air-coupled ultrasonic inspection", *Insight*, Vol. 41 No. 11, Nov.1999.
17. Wells PNT, "Biomedical Ultrasound", Academic Press, 1977.
18. Hayward G, "Time and frequency domain modelling of the piezoelectric transducer", PhD thesis.
19. Farlow R and Hayward G, "Real time ultrasonic techniques suitable for implementing non-contact NDT systems employing piezoceramic composite transducers", *Insight*, Vol 36, No. 12, December 1994, pp 926-935.
20. Bass HE, Sutherland LC, Piercy J and Evans L, *Absorption of Sound by the Atmosphere*, Physical Acoustics Vol XVII, Editors Mason WP and Thurston RN, Academic Press Inc. (London) Ltd, 1984.
21. Hayward G and Gorfu Y, "Performance assessment of ultrasonic NDT through an intermediate airgap", Final report MOD contract 2065/058.
22. Reilly D and Hayward G, "Through air transmission for ultrasonic non-destructive testing", *IEEE US Symp*, 1991, pp763-766.
23. Rivera O and Vitale V, "Airborne ultrasonic scanning", *Materials Evaluation*, Vol 46, 1988, pp 614-615.
24. Rogovsky AJ, "Development and application of ultrasonic dry contact and air contact c-scan systems for non-destructive evaluation of aerospace composites", *Materials Evaluation*, December 1991, pp 1491-1497.
25. Chimenti DE and Furtunko CM, "Characterisation of composite prepreg with gas-coupled ultrasonics", *Ultrasonics*, Vol 32(4), 1994, pp261-264.
26. Hayward G and Hossack J, "Unidimensional modelling of 1-3 composite transducers", *JASA*, Vol 88(2), 1990, pp618-629.

27. Hayward G and Gachagan A, "An evaluation of 1-3 connectivity composite transducers for air-coupled ultrasonic applications", *JASA*, Vol 99(4), 1996, pp 2148-2157.
28. Farlow R and Hayward G, "An automated ultrasonic NDT scanner employing advanced air-coupled 1-3 connectivity composite transducers", *Insight*, Vol 38, No. 1, Jan 1996, pp 41-50.
29. Edwards C, Al-Kassim A and Palmer SB, "Laser ultrasound for the study of thin sheets", *Review of progress in Quantitative NDE*, Vol 12a, Plenum Press, New York, 1993, pp538-548.
30. McKie ADW and Addison RC, "Rapid Inspection of composites using laser based ultrasonics", *Review of progress in QNDE*, Vol 12a, Plenum Press, New York, 1993, pp507-516.
31. Gururaja TR, Schulze WA, Cross LE, Newnham RE, Auld BA and Wang YJ, "Piezoelectric composite materials for ultrasonic transducer applications. Part I: Resonant modes of vibration of PZT rod polymer composites", *IEEE Trans UFFC*, Vol 32(4), 1985, pp 481-498.
32. Gururaja TR, Schulze WA, Cross LE, Newnham RE, "Piezoelectric composite materials for ultrasonic transducer applications. Part II: Evaluation of ultrasonic medical applications", *IEEE Trans UFFC*, Vol 32(4), 1985, pp 499-513.
33. Smith WA, Shaulov A and Auld BA, "Tailoring the properties of composite piezoelectric materials for medical ultrasonic transducers" *IEEE US Symp*, 1985, pp642-647.
34. Hossack J and Hayward G, "Finite element analysis of 1-3 composite transducers", *IEEE Trans. UFFC*, Vol 38(6), 1991, pp 618-629.
35. Hayward G and Bennett J, "Assessing the influence of pillar aspect ratio on the behavior of 1-3 connectivity composite transducers", *IEEE Trans. UFFC*, Vol 43(1), 1996, pp 98-108.
36. Smith WA and Auld BA, "Modelling 1-3 composite piezoelectric: thickness mode oscillations", *IEEE Trans. UFFC*, Vol 38, 1990, pp 40-47.

37. Hayward G, Gachagan A, Hamilton R, Hutchins DA and Write WMD, "Ceramic epoxy composite transducers for non-contacting ultrasonic applications", Proceedings of the Society of Photo-Optical Instrumentation Engineers, Vol 1733, 1992, pp 49-56.
38. Hayward G, "The influence of pulser parameters on the transmission response of piezoelectric transducers", Ultrasonics 23, 1985, pp 103-112.
39. Hayward G, "Using a block diagram approach for the evaluation of electrical loading effects on piezoelectric reception", Ultrasonics 24, 1986, pp 156-163.
40. Galbraith W and Hayward G, "Development of a PVDF membrane hydrophone for use in air-coupled ultrasonic transducer calibration", IEEE Trans on UFFC, 1998, pp 1-10.
41. Mason WP, Physical Acoustics, Vol 1, New York Academic, 1964.
42. Kino GS, "Acoustic Wave Devices, Imaging and Analogue Signal Processing", 1987, Prentice-Hall, Inc., pp 554-556.
43. Smith WA, "Optimising electromechanical coupling in piezocomposites using polymers with negative Poisson's ratio", IEEE US Symp, 1991, pp661-666.
44. Hayward G, Bennett J, Hamilton R, "A theoretical study on the influence on some constituent material properties on the behaviour of 1-3 connectivity composite transducers", JASA, 1996.
45. Turnbull DH and Foster FS, "Fabrication and characterisation of transducer elements in two-dimensional arrays for medical imaging", IEEE UFFC, Vol 39 No4, 1992, pp464-475.
46. Hall DDN, Hayward G, Gorfu Y, "Theoretical and experimental evaluation of a two-dimensional composite matrix array", IEEE UFFC, Vol 40 No 6, 1993, pp 704-709.
47. Matsuzawa K, "Condenser microphones with plastic diaphragms for airborne ultrasonics", J. Phys. Soc Japan, 13,1958, pp1533-1544.
48. Carr H and Wykes C, "Diagnostic measurements in capacitive transducers", Ultrasonics, Vol.31, No.1, 1993, pp13-20.
49. Hietanen J, Mattilla P, Stor-Pellinen J, Tsuzuki F, Väätäjä H, Sasaki K and Lukkala M, "Factors affecting the sensitivity of electrostatic ultrasonic transducers", Meas. Sci. Technol., 4, 1993, 1138-1142.

50. Rafiq M and Wykes C, "The performance of capacitive ultrasonic transducers using V-grooved backplates", *Meas. Sci. Technol.*, 2, 1991, pp 168-174.
51. Warren JE and Brezezinski AM, "Capacitance microphone dynamic membrane deflections", *JASA*, Vol.52 (3), 1972, pp711-719.
52. Mattila P, Tsuzuki F, Väättäjä H and Sasaki K, "Electroacoustic model for electrostatic ultrasonic transducers with v-grooved backplates", *IEEE Trans UFFC*, Vol42 (1), 1995, pp1-7.
53. Hietanen J, Stor-Pellinen J, Lukkala M, Mattilla P, Tsuzuki F and Sasaki K, "A Helmholtz resonator model for an electrostatic ultrasonic air transducer with a V-grooved backplate", *Sensors and Actuators A*, 39, 1993, pp 129-132.
54. Hietanen J, Ignatius J and Stor-Pellinen J, "Electrostatic solutions for a capacitive ultrasonic air transducer with a uniformly -grooved backplate", *Sensors and Actuators A*, 45, 1994, pp 95-98.
55. Adamowski JC, Silva ECN, Simon C, Buiocchi F and Higuti RT, "Finite element modelling of an ultrasonic capacitive transducer", *IEEE US Symp 1994, Cannes*, pp1261-1264.
56. Hutchins DA, Wright WMD and Schindel DW, "Ultrasonic measurements in polymeric materials using air-coupled capacitance transducers", *JASA*, Vol 96(3), 1994, pp1634-1642.
57. Schindel DW, Hutchins DA, "Applications of micro-machined capacitance transducers in air-coupled ultrasonics and non-destructive evaluation", *IEEE Trans UFFC*, Vol42 (1), 1995, pp 51-57.
58. Schindel DW, Hutchins DA, Zou I and Sayer K, "The design and characterisation of micro-machined air-coupled capacitance transducers", *IEEE Trans UFFC*, Vol42 (1), 1995, pp 42-50.
59. Anderson MJ, Hill JA, Fortunko CM, Dogan NS and Moore RD, "Broadband electrostatic transducers: modelling and experiments", *JASA*, Vol97 (1), 1995, pp262-272.
60. Haller MI and Khuri Yakub BT, "A surface micromachined electrostatic ultrasonic air transducer", *IEEE Trans UFFC*, Vol.43 (1), Jan. 1996, pp1-6.
61. Mason W P, "Electromechanical transducers and wave filters", New York, D. A Nostrand Company, 1942, pp163-165, 193-195.

62. Ladabaum I, Khuri Yakub BT, Spoliansky D, , Haller MI, "Micromachined ultrasonic transducers (MUTs)", IEEE US Symp, Seattle, 1995, pp 501-504.
63. Hutchins DA, Bashford AG, Wright WMD and Schindel DW, "Advances in wide bandwidth air-coupled capacitance transducers", IEEE US Symp, Seattle, 1995, pp981-984.
64. Higuchi K, Suzuki K and Tanigawa H, "Ultrasonic phased array transducer for acoustic imaging in air", IEEE US Symp, 1996, pp559-562.
65. Munro WSH and Wykes C, "Arrays for airborne 100kHz ultrasound", Ultrasonics, Vol 32 (1), 1994, pp57-64.
66. Saakus HP, Klicker KA and Newman RE, "PZT epoxy piezoelectric transducers: a simplified fabrication process", Material Res. Bull., Vol 16, 1980, pp667-680.
67. Hutchins DA and Hayward G, "Radiated fields of ultrasonic transducers", Physical Acoustics, Vol XIX, Academic Press, 1990, pp1-80.
68. Gachagan A, Hayward G, Kelly SP and Galbraith W, "Characterisation of air-coupled transducers", IEEE Trans on UFFC, Vol 43 (4), 1996, pp 687-689.
69. Smith RA and Bacon DR, "A multiple frequency hydrophone calibration technique ", JASA, Vol 85 (5), 1990, pp2231-2243.
70. Fox JD, Kuhri-Yakub and Kino GS, High frequency acoustic wave measurements in air", IEEE US Symp, 1983, pp581-584.
71. Yano T, Tone M and Fukumoto A, "Range finding and surface characterisation using high-frequency air transducers", IEEE Trans on UFFC, Vol 34, 1987, pp232-236.
72. Haller MI and Khuri-Yakub BT, "Micromachined 1-3 composites for ultrasonic air transducers", Rev Sci Instrum, Vol 65(6), 1994, pp2095-2098.
73. Jackson MN, Ph.D. Thesis, University of Strathclyde Glasgow, 1984.
74. Kossoff G, "The effects of backing and matching on the performance of piezoelectric ceramic transducers", IEEE Trans on Sonics and Ultrasonics, Vol SU-13, No1, 1966, pp20-30.
75. Lewis GK, "A matrix technique for analysing the performance of multilayered front matched and backed piezoelectric ceramic transducers", Acoustic Imaging, 8,1980, pp 395-416, Plenum New York.

76. Khuri-Yakub BT, Kim JH, Parent P, and Kino GS, "A new design for air transducers", IEEE Ultrasonics Symposium, 1988, pp 503-506.
77. Schiller S, Hsieh CK, Chou CH, and Khuri-Yakub BT, "Novel high frequency air transducers", Review of prog QNDE, Vol 9, 1990, pp 795-798.
78. Fletcher NH and Thwaites S, "Multi-horn matching plate for ultrasonic transducers", Ultrasonics, Vol 30(2), 1992, pp67-75.
79. Biot MA, " Theory of propagation of elastic waves in a fluid-saturated porous solid. I. Low-frequency range." JASA, Vol 28(2), pp 168-178, 1956.
80. Biot MA, " Theory of propagation of elastic waves in a fluid-saturated porous solid. I. Higher-frequency range." JASA, Vol 28(2), pp 179-191, 1956.
81. Kinsler LE and Frey AR, "Fundamentals of Acoustics", John Wiley and Sons, New York, 1982.
82. Brodeur P H, Hall M S and Esworthy C "Sound dispersion and attenuation in the thickness direction of paper materials," JASA, Vol 94(4), pp 2215-2225, 1990.
83. McSkimin H J "Ultrasonic methods for measuring the mechanical properties of liquids and solids" Physical Acoustics. Ed. W. P. Mason. Vol I part A. Academic Press, 1964.
84. Sides DJ, Attenborough and KA Mulholland "Applications of a general acoustic propagation theory to fibrous absorbents", J Sound and Vib, Vol 19 (1), pp49-64, 1971.
85. Hannant DJ "Handbook of Composites", Vol IV, Fabrication of composites, North Holland.
86. Callister WD, "Material science and engineering", John Wiley and Sons, 1985.
87. Gomez TE, Elvira and Riera E, "Generation of the slow wave to characterise air-filled porous fabrics" J Appl. Phys., Vol78, no 4, pp 2843-2845, Aug 1995.
88. Maurice RDA, "Convolution and Fourier Transforms for communications engineers", Pentech Press, London, 1976.
89. Blitz J and Simpson G, "Ultrasonic methods of non-destructive testing", Chapman and Hall, London, 1996.

APPENDIX A

AIR-COUPLED MATCHING LAYER MATERIALS AND MANUFACTURING METHOD

The air-coupled matching layers that have been manufactured, tested and developed within this Thesis have adopted a very specific manufacturing technique and materials. This Appendix aims to provide the necessary information for reproduction of the technology by interested readers.

The two materials types that are used to produce the new matching layers are as follows:

- Silicone (or RTV-Room Temperature Vulcanised) Rubber.
- Micro-porous Membrane Filters.

There are many variations of these two materials with similar properties, but the model that has been developed within this work is specific to the following types:

- Cellulose Nitrate membrane filters made by Whatman. They are discs with 50 or 100 mm diameter. Thickness is 0.12mm and a pour size is 0.45 μ m.
- Bartoline Multi-Purpose Silicone Sealant.

The combination of these two materials is explained in Figure A1 below.

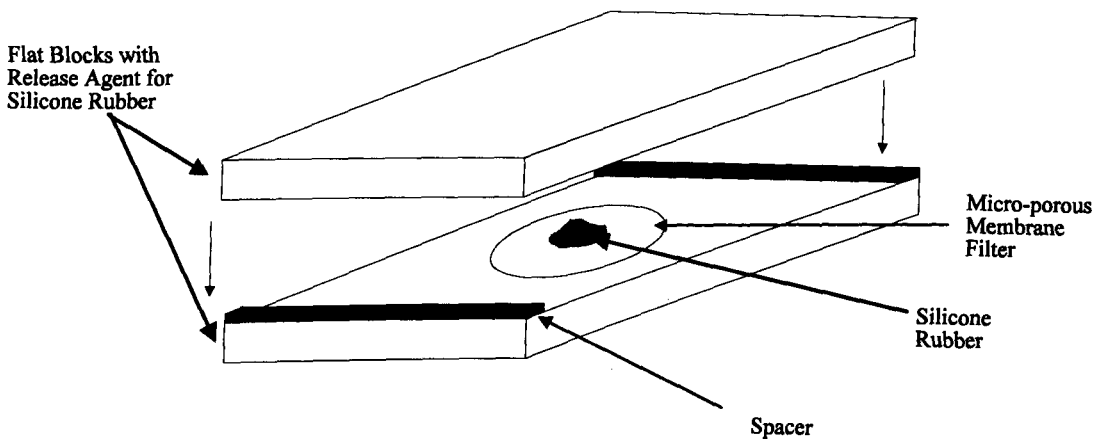


Figure A1 Manufacture of the ultrasonic matching layer.

Two blocks of perspex of a size at least 20mm larger than the required finished matching layer area in length and width dimensions are prepared. Preparation involves coating with a silicone rubber release agent to enable removal of the matching layer once cured. The filter is placed on the lower block and an excess quantity of RTV rubber is squeezed onto the top face. A second block is then brought into contact with two spacers of the desired matching layer thickness. These spacers were made up using various brass shim pieces of different thicknesses. A torque wrench is used to control the pressure that is applied to the second block till it makes contact with the spacers, although this is variable depending on the thickness of the matching layer required and the amount of silicone rubber that is deposited. Pressure can vary from 10 to 30 pounds per square inch. This is then left to allow the rubber to cure in contact with the filter. Curing of the RTV occurs at room temperature and curing time can vary between around 12 hours and 48 hours depending on the thickness of the matching layer with the thickest made to date at 1mm taking around 48 hours and the thinnest at 0.2mm taking 12hours.

A diagram of a matching layer once the rubber has cured is presented in Figure A2.

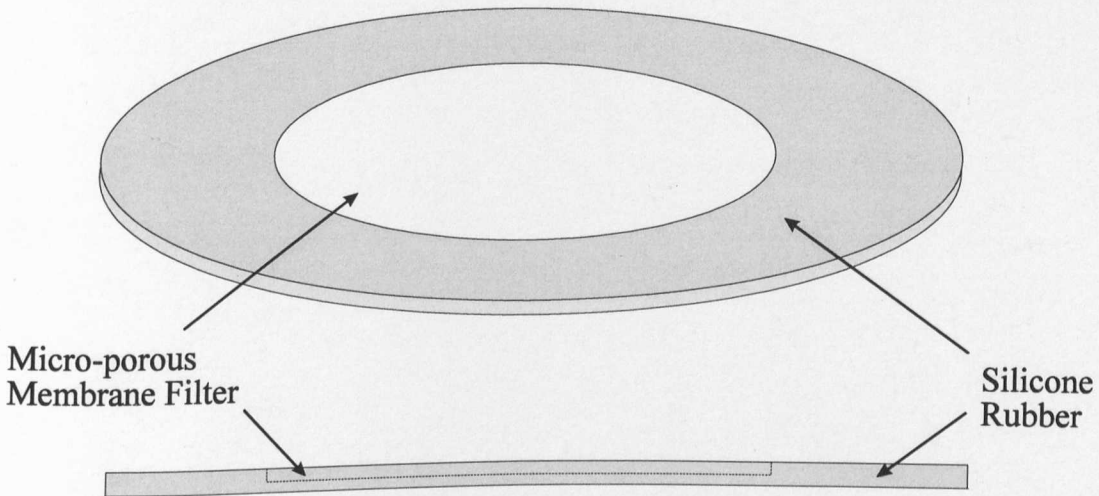


Figure A2 Structure of a matching layer after curing of the silicone rubber.

This can then be attached to a transducer using a suitable adhesive with the filter at the outer face in contact with the air load and the rubber in contact with the transducer, lens, or inner matching layer. One adhesive that has been tested successfully is Flowable Silicone Rubber manufactured by RS.

An alternative technique is to cure the rubber in a sandwich between the transducer (or an inner matching layer) and the filter, thus using the adhesion of the rubber itself for attachment to the transducer. Attachment of the matching layer temporarily using coupling fluid has also been investigated and has proven to be acceptable for short term investigations in a laboratory environment although this is not a suitable long-term solution.